

Max Planck Institute for Colloids and Interfaces

Molecular Fundamentals of Foam Fractionation

Dissertation

zur Erlangung des akademischen Grades

"doctor rerum naturalium"

(Dr. rer. nat.)

in der Wissenschaftsdisziplin „Physikalische Chemie“

eingereicht an der

Mathematisch-Naturwissenschaftlichen Fakultät

der Universität Potsdam

von

Vamseekrishna Ulaganathan

geboren am 16. December 1985 in Tirupathi, India

Published online at the
Institutional Repository of the University of Potsdam:
URN urn:nbn:de:kobv:517-opus4-94263
<http://nbn-resolving.de/urn:nbn:de:kobv:517-opus4-94263>

Abstract

Foam fractionation of surfactant and protein solutions is a process dedicated to separate surface active molecules from each other due to their differences in surface activities. The process is based on forming bubbles in a certain mixed solution followed by detachment and rising of bubbles through a certain volume of this solution, and consequently on the formation of a foam layer on top of the solution column. Therefore, systematic analysis of this whole process comprises of at first investigations dedicated to the formation and growth of single bubbles in solutions, which is equivalent to the main principles of the well-known bubble pressure tensiometry. The second stage of the fractionation process includes the detachment of a single bubble from a pore or capillary tip and its rising in a respective aqueous solution. The third and final stage of the process is the formation and stabilization of the foam created by these bubbles, which contains the adsorption layers formed at the growing bubble surface, carried up and gets modified during the bubble rising and finally ends up as part of the foam layer.

Bubble pressure tensiometry and bubble profile analysis tensiometry experiments were performed with protein solutions at different bulk concentrations, solution pH and ionic strength in order to describe the process of accumulation of protein and surfactant molecules at the bubble surface. The results obtained from the two complementary methods allow understanding the mechanism of adsorption, which is mainly governed by the diffusional transport of the adsorbing protein molecules to the bubble surface. This mechanism is the same as generally discussed for surfactant molecules. However, interesting peculiarities have been observed for protein adsorption kinetics at sufficiently short adsorption times. First of all, at short adsorption times the surface tension remains constant for a while before it decreases as expected due to the adsorption of proteins at the surface. This time interval is called induction time and it becomes shorter with increasing protein bulk concentration. Moreover, under special conditions, the surface tension does not stay constant but even increases over a certain period of time. This so-called negative surface pressure was observed for β -casein (BCS) and β -Lactoglobulin (BLG) and discussed for the first time in terms of changes in the surface conformation of the adsorbing protein molecules. Usually, a negative surface pressure would correspond to a negative adsorption, which is of course impossible for the studied protein solutions. The phenomenon, which amounts to some mN/m, was rather explained by simultaneous changes in the molar area required by the adsorbed proteins and the non-ideality of entropy of the interfacial layer. It is a transient phenomenon and exists only under dynamic conditions.

The experiments dedicated to the local velocity of rising air bubbles in solutions were performed in a broad range of BLG concentration, pH and ionic strength. Additionally, rising bubble experiments were done for surfactant solutions in order to validate the functionality of the instrument. It turns out that the velocity of a rising bubble is much more sensitive to adsorbing molecules than classical dynamic surface tension measurements. At very low BLG or surfactant concentrations, for example, the measured local velocity profile of an air bubble is changing dramatically in time scales of seconds while dynamic surface tensions still do not show any measurable changes at this time scale. The solution's pH and ionic strength are important parameters that govern the measured rising velocity for protein solutions. A general theoretical description of rising bubbles in surfactant and protein solutions is not available at present due to the complex situation of the adsorption process at a bubble surface in a liquid flow field with simultaneous Marangoni effects. However, instead of modelling the complete velocity profile, new theoretical work has been started to evaluate the maximum values in the profile as characteristic parameter for dynamic adsorption layers at the bubble surface more quantitatively.

The studies with protein-surfactant mixtures demonstrate in an impressive way that the complexes formed by the two compounds change the surface activity as compared to the original native protein molecules and therefore lead to a completely different retardation behavior of rising bubbles. Changes in the velocity profile can be interpreted qualitatively in terms of increased or decreased surface activity of the formed protein-surfactant complexes. It was also observed that the pH and ionic strength of a protein solution have strong effects on the surface activity of the protein molecules, which however, could be different on the rising bubble velocity and the equilibrium adsorption isotherms. These differences are not fully understood yet but give rise to discussions about the structure of protein adsorption layer under dynamic conditions or in the equilibrium state.

The third main stage of the discussed process of fractionation is the formation and characterization of protein foams from BLG solutions at different pH and ionic strength. Of course a minimum BLG concentration is required to form foams. This minimum protein concentration is a function again of solution pH and ionic strength, i.e. of the surface activity of the protein molecules. Although at the isoelectric point, at about pH 5 for BLG, the hydrophobicity and hence the surface activity should be the highest, the concentration and ionic strength effects on the rising velocity profile as well as on the foamability and foam stability do not show a maximum. This is another remarkable argument for the fact that the interfacial structure and behavior of BLG layers under dynamic conditions and at equilibrium

are rather different. These differences are probably caused by the time required for BLG molecules to adapt respective conformations once they are adsorbed at the surface.

All bubble studies described in this work refer to stages of the foam fractionation process. Experiments with different systems, mainly surfactant and protein solutions, were performed in order to form foams and finally recover a solution representing the foamed material. As foam consists to a large extent of foam lamella – two adsorption layers with a liquid core – the concentration in a foamate taken from foaming experiments should be enriched in the stabilizing molecules. For determining the concentration of the foamate, again the very sensitive bubble rising velocity profile method was applied, which works for any type of surface active materials. This also includes technical surfactants or protein isolates for which an accurate composition is unknown.

List of papers and contributions

Included in this thesis

1. Ulaganathan, V., Fainerman, V. B., Gochev, G., Aksenenko, E. V., Gunes, D. Z., Gehin-Delval, C., & Miller, R. (2014). **Evidence of negative surface pressure induced by β -lactoglobulin and β -casein at water/air interface.** *Food Hydrocolloids*, 34, 10-14.
2. Ulaganathan, V., Krzan, M., Lotfi, M., Dukhin, S. S., Kovalchuk, V. I., Javadi, A., ... & Miller, R. (2014). **Influence of β -lactoglobulin and its surfactant mixtures on velocity of the rising bubbles.** *Colloids and Surfaces A: Physicochemical and Engineering Aspects*, 460, 361-368.
3. Ulaganathan, V., Gochev, G., Gehin-Delval, C., Leser, M. E., Miller, R. (2015). **Effect of pH and electrolyte concentration on rising air bubbles in β -lactoglobulin solutions.** Submitted to *Colloids and Surfaces A: Physicochemical and Engineering Aspects*.
4. Ulaganathan, V., Retzlaff I., Won J.Y, Gochev G., Gehin-Delval , Leser, M.E., Noskov B.A., Miller R. (2015). **β -Lactoglobulin Adsorption Layers at the Water/Air Surface: 1. Kinetics of Adsorption, Effect of pH and Ionic Strength.** Submitted to *Colloids and Surfaces A: Physicochemical and Engineering Aspects*.

Not included in this thesis

1. Won, J. Y., Krägel, J., Gochev, G., Ulaganathan, V., Javadi, A., Makievski, A. V., & Miller, R. (2014). **Bubble–bubble interaction in aqueous β -Lactoglobulin solutions.** *Food Hydrocolloids*, 34, 15-21.
2. Lotfi, M., Bastani, D., Ulaganathan, V., Miller, R., & Javadi, A. (2014). **Bubble in flow field: A new experimental protocol for investigating dynamic adsorption layers by using capillary pressure tensiometry.** *Colloids and Surfaces A: Physicochemical and Engineering Aspects*, 460, 369-376.
3. Ulaganathan, V., Bergenstahl, B., Krägel, J., & Miller, R. (2012). **Adsorption and shear rheology of β -lactoglobulin/SDS mixtures at water/hexane and water/MCT interfaces.** *Colloids and Surfaces A: Physicochemical and Engineering Aspects*, 413, 136-141.

4. Javadi, A., Mucic, N., Karbaschi, M., Won, J. Y., Lotfi, M., Dan, A., & Miller, R. (2013). **Characterization methods for liquid interfacial layers**. *The European Physical Journal Special Topics*, 222(1), 7-29.
5. Mucic, N., Gochev, G., Won, J., Ulaganathan, V., Fauser, H., Javadi, A., ... & Miller, R. (2015). **Adsorption of equimolar aqueous sodium dodecyl sulphate/dodecyl trimethylammonium bromide mixtures at solution/air and solution/oil interfaces**. *Colloid and Polymer Science*, DOI: 10.1007/s00396-015-3735-0.
6. Ulaganathan, V., Bergenstahl, B., Krägel, J., & Miller, R. (2012).. **Adsorption and shear rheology of β -lactoglobulin/SDS mixtures at water/hexane and water/MCT interfaces** *Colloids and Surfaces A: Physicochemical and Engineering Aspects*, 413, 136-141.
7. Javadi, A., Krägel, J., Karbaschi, M., Won, J. Y., Dan, A., Makievski, A. V., Loglio, G., Liggieri, L., Ravera, F., Kovalchuk, N.M., Lotfi, M., Ulaganathan, V., Kovalchuk, V.I., & Miller, R., (2013). **Capillary pressure experiments with single drops**. In *Colloid and Interface Chemistry for Nanotechnology* (pp. 271-312). CRC Press.

Table of Contents

ABSTRACT	II
LIST OF PAPERS AND CONTRIBUTIONS	V
TABLE OF CONTENTS.....	VII
1. INTRODUCTION.....	1
REFERENCES.....	2
2. TARGET OF THIS PHD THESIS	3
3. BACKGROUND	5
3.1. THERMODYNAMICS OF ADSORPTION.....	5
3.1.1. Equations of state for surfactant adsorption	5
3.1.2. Equations of state for protein adsorption	7
3.1.3. Equations of state for surfactant mixtures.....	10
3.1.4. Equations of state for protein-surfactant mixtures.	12
3.2. KINETICS OF ADSORPTION	15
3.2.1. Diffusion controlled adsorption	15
3.2.2. Kinetic controlled adsorption kinetics.....	16
3.2.3. Adsorption kinetics for mixed solutions.....	17
3.3. SINGLE BUBBLE RISING IN SURFACTANT SOLUTION	18
3.5. FOAM STABILIZATION	21
3.5.1 Thin Liquid films	21
3.5.2. Foam drainage	24
3.5.3. Ostwald ripening or coarsening.	26
3.5.4. Attempts to correlate foam stability.....	27
3.6. FLOATATION.....	29
3.7. REFERENCES.....	30
4. MATERIAL & METHODS.....	40
4.1. MATERIALS	40
4.1.1. Surfactants.....	40
4.1.2. Proteins	41
4.2. EXPERIMENTAL METHODS.....	42
4.2.1. Maximum bubble pressure tensiometer	42
4.2.2. Bubble and drop profile analysis tensiometry	44
4.2.3. Rising bubble setup	49
4.2.4. Foam stability setup	52
4.2.5. Foam fractionation setup	54
4.2.6. References	56
5. RESULTS AND DISCUSSION	58
5.1. EVIDENCE OF NEGATIVE SURFACE PRESSURE INDUCED BY β -LACTOGLOBULIN AND β -CASEIN AT WATER/AIR INTERFACE.....	59
5.1.1. Summary.....	59
5.1.2. References	61
5.2. INFLUENCE OF B-LACTOGLOBULIN AND ITS SURFACTANT MIXTURES ON VELOCITY OF THE RISING BUBBLES	62

5.2.1. Summary.....	62
5.2.2. References	64
5.3 EFFECT OF pH AND IONIC STRENGTH ON STATIC AND VELOCITY OF RISING BUBBLES IN β -LACTOGLOBULIN SOLUTIONS	65
5.3.1. Introduction.....	65
5.3.2. Materials and methods.....	66
5.3.3. Results	66
5.3.4. Discussion	71
5.3.5. Conclusion.....	73
5.3.6. References	74
5.4. ADSORPTION KINETICS OF B-LACTOGLOBULIN AT THE SURFACE OF STATIC BUBBLE FOR VARYING pH AND SALT CONCENTRATION	77
5.4.1. Introduction.....	77
5.4.2. Materials and Methods.....	78
5.4.3. Results and discussion.....	79
5.4.4. Conclusions	89
5.4.5. References	91
5.5. FOAM STABILITY OF β -LACTOGLOBULIN SOLUTIONS	95
5.5.1. Introduction.....	95
5.5.2. Materials & methods.....	95
5.5.3. Results	95
5.5.4. Discussion	100
5.5.5. References	103
5.6. FOAM FRACTIONATION OF PROTEINS AND SURFACTANTS	106
5.6.1. Introduction.....	106
5.6.2. Materials & methods.....	106
5.6.3. Results	107
5.6.4. Discussion	112
5.6.5. Conclusions	114
5.6.6. References	114
6. GENERAL CONCLUSIONS AND OUTLOOK.....	116
REFERENCES.....	120
7. ACKNOWLEDGMENTS	121
8. APPENDICES.....	122
8.1.....	122
8.2.....	123

1. Introduction

Separation methods are typically based on rather complex processes, depending on the differences in properties of components to be separated. Flotation is one of the most popular separation techniques which exploits adsorptive properties of components. The bubbles are formed and agitated in a liquid where particles are attached and floated up into a froth layer at the top of the flotation tank [1]. These particles are either the target or the waste components of the original material. To design very selective attachments of one or the other type of particles, the respective flotation collectors are added. These collectors modify the surface properties of particles to enable them to attach at bubble surfaces. This floatation process, however, is of macroscopic character as the particle sizes are in the order of micrometer. Similar techniques are also applied to sub-micrometer particles, as it is described for micro-flotation technologies. It was discussed in [2] that the mechanisms of a selective attachment of particles is changed. When passing to separation processes on a molecular level, the mechanisms again change significantly as it is the case in the so-called foam fractionation [3]. Foam fractionation is a separation process based on the molecular adsorption of surface active materials at the air-water interface. Thereby, the surface active molecules in an aqueous solution can be harvested by producing air bubbles and separating the foam produced.

The foam fractionation technique is used for instance in waste water treatment, cleaning of aquariums etc. This is a very environmental friendly technique and also very cost-effective.

Due to the great economic and ecologic potential the application of this separation technology is very favorable as it does not need any chemical methods nor consumes large amounts of energy. Therefore, foam fractionation found its importance among researchers working in various technology fields.

The aim of this thesis is to understand the physico-chemical factors that would enhance the enrichment of surface active material in foam fractionation processes. Emphasis is made on proteins as they are surface active components frequently found in many food systems. Three stages in the process of foam fractionation are defined and discussed in the presented thesis. At first the dynamics of adsorption of the compounds to be separated has to be investigated systematically. This is required in order to know the time scales at which the single components adsorb at certain bulk concentrations. The second stage is translating the knowledge to the behavior of rising bubbles with surface layers modified by the adsorbing species under very dynamic conditions. These bubbles carry the material to a foam layer at

the top of the fractionation column. For an efficient “harvest” of the material accumulated in the foam, investigations on the stability of these foams are required. A most efficient “harvesting” is established when we reach a stable foam formed by thinnest foam films so that the surface-to-area ratio is maximum.

These three stages are investigated in this PhD thesis mainly for the protein β -lactoglobulin but also for other surface active compounds. As proteins change their interfacial properties when the concentration, solution pH and ionic strength are modified, the presented work looks particularly into the impact of these solution properties.

References

1. Lu, S., Pugh, R. J., & Forsberg, E. (2005). Interfacial separation of particles (Vol. 20). Elsevier Science, ISBN: 9780444516060
2. S.S. Dukhin, G. Kretschmar and R. Miller, Dynamics of Adsorption at Liquid Interfaces: Theory, Experiment, Application, D. Möbius and R. Miller (Editors), in Studies in Interface Science, Vol. 1, Chapter 10, Elsevier, Amsterdam, 1995, ISBN 0-444-88117-4
3. P. Stevenson and X.L. Li, Foam Fractionation: Principles and Process Design, CRC, 2014, ISBN: 978-1466558519.

2. Target of this PhD thesis

The main target of this PhD thesis is to determine the key factors that influence the process of foam fractionation. To determine these factors one needs to consider all the steps involved in a foam fractionation process. In case of a foam generated by sparging air bubbles through a capillary or porous material into the solution containing surface active material, three steps can be broadly classified.

1. Formation and detachment of bubbles at the capillary orifice
2. Rising of gas bubbles in aqueous solutions of proteins, surfactants and their mixtures
3. Accumulation of gas bubbles in form of a foam at the top layer of the solution column

The adsorption of the surface active material such as surfactants or proteins or their mixtures would occur during the lifetime of a bubble in all locations of the entire process: bubble formation and growth, bubble detachment, bubble rising, assembling of bubbles in a foam layer and interacting with neighbor bubbles. All these items are of dynamic character and any equilibrium characteristics of the adsorbing species provide only basic knowledge and serve as a kind of baseline.

For some of the defined stages in the lifetime of a bubble well elaborated theories exist, such as for bubbles formed and growing at the tip of a circular orifice (capillary). The well-understood maximum bubble pressure and bubble profile tensiometry methods will therefore be applied in this thesis to understand the kinetics of adsorption of the selected proteins and surfactants at bubble surfaces.

For the stage of bubbles rising in aqueous solutions well-elaborated experimental protocols exist. However, the situation at the bubble surface is rather complex and comprises of an adsorption flux to and a desorption flux from the surface caused by the drag force which carries the adsorbed molecules along the bubble surface towards to rear part of the rising bubble. This leads to a surface tension gradient which in turn generates a Marangoni flow directed opposite to the liquid flow around the rising bubble. Due to missing theories, which exist only for bubbles with a completely mobile and completely immobile surface, only qualitative interpretations will be possible.

A similar complicated situation exists in the understanding of the foam stability during foam formation (foamability) and in the ready foam. Only for single foam lamellae quantitative models for their rupture exist. However, there is neither a link to properties of the stabilizing

adsorption layers nor to the behavior of a real foam consisting of many single foam films interconnected with each other available so far. Therefore, the aim of this work is to provide additional experimental data for refinement of existing models and development of new theories in the near future.

Due to the large impact of solvent conditions on the surface properties of BLG as the main protein compound studied here, data will be presented on the effects of the protein concentration, the solution pH and ionic strength as well as of added ionic and non-ionic surfactants. These data comprise the adsorption dynamics of BLG, the equilibrium adsorption behavior, the local velocity profiles for air bubbles of a well-defined size, and the foamability and foam stability of BLG solutions.

In a final section, several practical tests are performed to demonstrate the enrichment of selected surface active compounds in a foam layer produced in a foam fractionation column.

3. Background

This section provides a theoretical background for various phenomena involved in the foam formation. First, the thermodynamic fundamentals of adsorption in general and the state-of-art theories for particular systems are discussed, such as of protein and surfactant solutions, as well as of their mixtures. Then, the principles of adsorption dynamics are presented. These two levels of modeling are required to understand the formation process of adsorption layers at the solution-air surface. Subsequently, the main knowledge on rising bubbles in solutions, and on foam films and foams is summarized. For all discussed topics typical examples are presented and characteristic parameters discussed.

3.1. Thermodynamics of adsorption

So to understand the adsorption behavior and influence of various parameters, an accurate description of the thermodynamics of adsorption layers at interfaces is the vital prerequisite for any equilibrium or non-equilibrium processes going on at the surface of liquids. The thermodynamic analysis of adsorption layers at interfaces is provided by the equation of state which expresses the surface pressure as a function of surface layer composition, and the adsorption isotherm, which determines the dependence of adsorption of each dissolved component on their bulk concentrations. From these equations, the surface tension (pressure) isotherm can also be calculated and compared with experimental data.

3.1.1. Equations of state for surfactant adsorption

The Langmuir model [1] describes the adsorbed amount Γ , per unit area as follows,

$$\Gamma = \Gamma_{\infty} \frac{bc}{1 + bc} \quad (1)$$

and the corresponding Szyszkowski-Langmuir equation of state has the form

$$\gamma_0 - \gamma = \Pi = -RT\Gamma_{\infty} \ln\left(1 - \frac{\Gamma}{\Gamma_{\infty}}\right) = RT\Gamma_{\infty} \ln(1 + bc) \quad (2)$$

Here γ_0 is the interfacial tension in absence of surfactant, c is the surfactant bulk concentration, Π is the surface pressure $\gamma_0 - \gamma$, R and T are the gas law constant and absolute

temperature, respectively, Γ_∞ is the maximum adsorption, and b is the adsorption constant with the dimension of a reciprocal concentration.

The description of experimental data by the Langmuir adsorption isotherm or the corresponding von Szyszkowski surface tension equation often shows significant deviations. These equations can be derived for a surface layer model where the molecules of the surfactant and the solvent from which the molecules adsorb obey two conditions:

- (i) no interaction between adsorbed molecules
- (ii) equal molar areas at the interface.

In a number of cases, deviations from the Langmuir behavior can be explained by an invalidity of the former condition, for example by the presence of interactions between adsorbed molecules or differences in the molecular areas. The adsorption isotherm and equation of state for adsorption layers proposed by Frumkin [2] describe the adsorption of low molecular weight surfactants rather well, provided the systems under investigation deviate only slightly from an ideal (Langmuir) behavior.

$$bc = \frac{\theta}{1-\theta} \exp(-2a\theta) \quad (3)$$

$$\Pi = -\frac{RT}{\omega_0} [\ln(1-\theta) + \alpha \theta^2] \quad (4)$$

$\theta = \omega \cdot \Gamma$ is the surface coverage by surfactant molecules, and a is the interaction constant. The molar area of a surfactant ω is often assumed to be constant. It was shown, however, that it can better be presented by a linear dependence on surface pressure Π [3, 4]

$$\omega = \omega_0 (1 - \varepsilon \Pi \theta), \quad (5)$$

where ω_0 is the molar area at zero surface pressure, and ε is the two-dimensional relative surface layer compressibility coefficient, which characterises the intrinsic compressibility of the molecules in the surface layer. This intrinsic compressibility, for example, reflects the change of the tilt angle of the molecules upon surface layer compression, accompanied by an increase in the thickness of the surface layer [5]. For any set of model parameters α , ω_0 , b and ε , one can solve Eq. (3) at any value of c . From this solution $\theta = \theta(c)$ the values of Π and Γ_s are calculated via Eqs. (4) and (5).

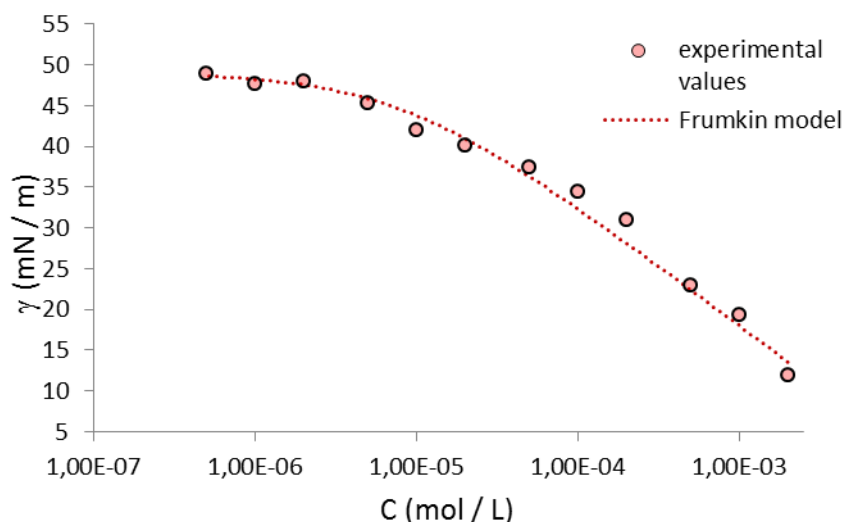


Figure 3.1. The equilibrium interfacial tension isotherm comprising of interfacial tension values at the water/hexane interface corresponding to concentration of SDS after the equilibrium has been reached (shown as points) and the dotted line indicates the calculated Frumkin model [6].

There are other models such as the re-orientation model [7] which assumes that for some surfactants the molecules in the adsorption layer can change their orientation upon increasing the surface coverage to that with smaller molar area.

3.1.2. Equations of state for protein adsorption

In case of proteins initially the Langmuir model was attempted to describe its thermodynamic state of equilibrium but the problem arises with the assumption of reversibility of its adsorption which contradicts the protein adsorption. Later this problem was addressed by Schaaf and Talbot where they have considered irreversibility of protein adsorption [8]. Attempts have been made to describe protein adsorption by several authors, such as van Eijk and Cohen Stuart. [9] and Fainerman and Miller [10] where for the protein adsorption it has been assumed to have different adsorption states or molecular conformations at the interface.

Varying from a maximum molar area (ω_{\max}) to a minimum molar area (ω_{\min}), protein molecules can adsorb in a number of states, which is described by the following equation of state for the surface layer [11]

$$-\frac{\Pi\omega_0}{RT} = \ln(1 - \theta_p) + \theta_p(1 - \omega_0 / \omega_p) + \alpha_p\theta_p^2 \quad (6)$$

where α_p is the intermolecular interaction parameter, ω_0 is the molar area of the solvent, or the area occupied by one segment of the protein molecule. The quantity

$$\Gamma_P = \sum_{i=1}^n \Gamma_{Pi} \quad (7)$$

is the total adsorption of proteins in all n states, and

$$\theta_p = \omega_p \Gamma_P = \sum_{i=1}^n \omega_i \Gamma_{Pi} \quad (8)$$

is the total surface coverage by protein molecules. Here ω_p is the average molar area of the adsorbed protein, $\omega_i = \omega_1 + (i - 1)\omega_0$ ($1 \leq i \leq n$) is the molar area in state i , assuming $\omega_1 = \omega_{\min}$, $\omega_{\max} = \omega_1 + (n - 1)\omega_0$. The equations for the adsorption isotherm for each state (j) of the adsorbed protein are:

$$b_{pj}c_p = \frac{\omega_p \Gamma_{Pj}}{(1 - \theta_p)^{\omega_j / \omega_p}} \exp\left[-2\alpha_p (\omega_j / \omega_p) \theta_p\right] \quad (9)$$

where c_p is the protein bulk concentration and b_{pj} is the equilibrium adsorption constant for the protein in the j^{th} state. When we assume that the values of all b_{pi} are equal to each other, i.e. $b_{pj} = b_p$ for any j (and therefore the adsorption constant for the protein molecule as a whole is $\sum b_p = nb_p$), from Eq. (9) we can calculate the distribution function of various adsorption states:

$$\Gamma_{Pj} = \Gamma_P \frac{(1 - \theta_p)^{\frac{\omega_j - \omega_1}{\omega_p}} \exp\left[2\alpha_p \theta_p \frac{\omega_j - \omega_1}{\omega_p}\right]}{\sum_{i=1}^n (1 - \theta_p)^{\frac{\omega_i - \omega_1}{\omega_p}} \exp\left[2\alpha_p \theta_p \frac{\omega_i - \omega_1}{\omega_p}\right]} \quad (10)$$

The model given by Eqs. (6)- (10) describes the evolution of states of protein molecules with increasing adsorption. The plot below shows the fitting of the above mentioned model by assuming the values of parameters (see Table 1.1) and the Fig. 3.1 and 3.2 taken from reference [6].

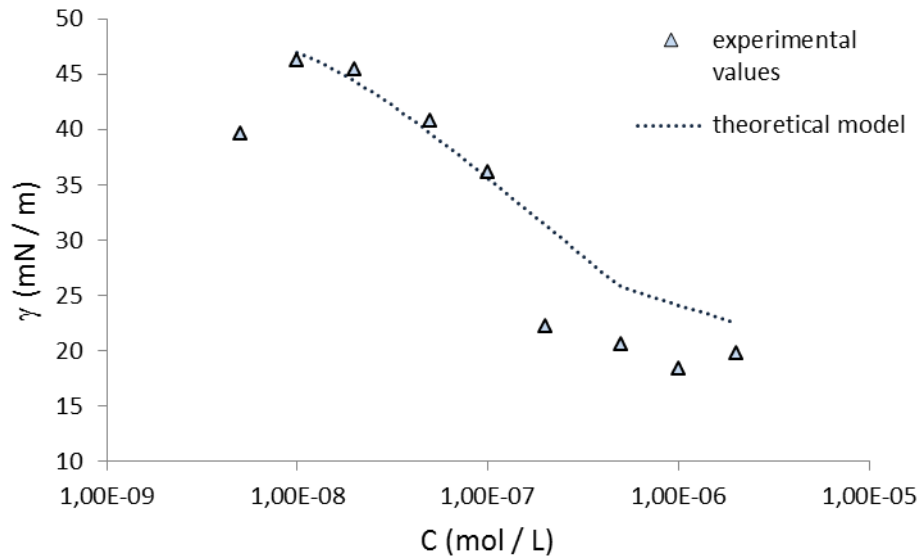


Figure 3.2. The equilibrium interfacial tension isotherm comprising of interfacial tension values at the water/hexane interface as a function of the BLG concentration after the equilibrium has been reached (shown as points) and the dotted line indicate the calculations with the theoretical model [8].

The theoretical model does not fit well at the higher β -LG concentrations ($> 2 \times 10^{-7} \text{M}$), where the experimental values show much lower surface tensions. One reason could be that there is a chance of formation of multiple layers at these concentrations

SDS			β -LG				
ω_s (m^2/mol)	a_s	b_s (m^3/mol)	ω_0 (m^2/mol)	ω_{\min} (m^2/mol)	ω_{\max} (m^2/mol)	a_p	b_p (m^3/mol)
$3.80 \times 10^{+5}$	0	$1.25 \times 10^{+2}$	$3.50 \times 10^{+5}$	$5.50 \times 10^{+6}$	$9.00 \times 10^{+6}$	0.4	$1.00 \times 10^{+4}$

Table 1.1. Parameters obtained by fitting the single components (SDS and β -LG) with the respective theoretical models described above with isotherms shown in figure 1 and 2; taken from [8]

3.1.3. Equations of state for surfactant mixtures

The theoretical models for the equation of state for adsorption layers of surfactant mixtures have been proposed and reviewed for example in [12-15]; which are developed from the models presented for single surfactants as discussed in the previous report. So the properties of mixed surfactant adsorption layers have been derived from those of single surfactants considering the non-ideality of mixing at the interface due to different molar areas.

A rigorous model for surfactant mixtures could be derived from the Frumkin adsorption model for single surfactants. So the equation of state and adsorption isotherm for mixtures of two non-ionic surfactants ($i=1, 2$) is given by [13]

$$\Pi = -\frac{RT}{\omega_0} \left[\ln(1 - \theta_1 - \theta_2) + \theta_1 \left(1 - \frac{1}{n_1} \right) + \theta_2 \left(1 - \frac{1}{n_2} \right) + a_1 \theta_1^2 + a_2 \theta_2^2 + 2a_{12} \theta_1 \theta_2 \right] \quad (11)$$

$$b_1 c_1 = \frac{\theta_1}{(1 - \theta_1 - \theta_2)^{n_1}} \exp(-2a_1 \theta_1 - 2a_{12} \theta_2) \exp[(1 - n_1)(a_1 \theta_1^2 + a_2 \theta_2^2 + 2a_{12} \theta_1 \theta_2)] \quad (12)$$

$$b_2 c_2 = \frac{\theta_2}{(1 - \theta_1 - \theta_2)^{n_2}} \exp(-2a_2 \theta_2 - 2a_{12} \theta_1) \exp[(1 - n_2)(a_1 \theta_1^2 + a_2 \theta_2^2 + 2a_{12} \theta_1 \theta_2)] \quad (13)$$

where

$$\omega = \frac{\omega_1 \Gamma_1 + \omega_2 \Gamma_2}{\Gamma_1 + \Gamma_2} \quad (14)$$

The parameter a_{12} defines the interaction between the surfactant species 1 and 2. This addresses the non-ideality of interfacial mixing and, therefore, this parameter depends on the kind of surfactants used. The value for a_{12} can be taken as equal to $a_{12} = (a_1 + a_2)/2$, which is the average of the values of the two single compounds.

Examples for the surface tension isotherms of mixed surfactants are given in Fig. 3.3 and 3.4. Fig. 3.3 shows experimental data for the very weak surface active butanol and the famous anionic surfactant SDS. The solid lines correspond to the model for surfactant mixtures as given by Eqs. (11) – (14). Fig. 3.4. shows a second example where SDS is mixed with the extremely strong surface active surfactant $C_{10}EO_5$. Again the solid lines are the calculated dependencies and they show an excellent agreement between experiment and theory.

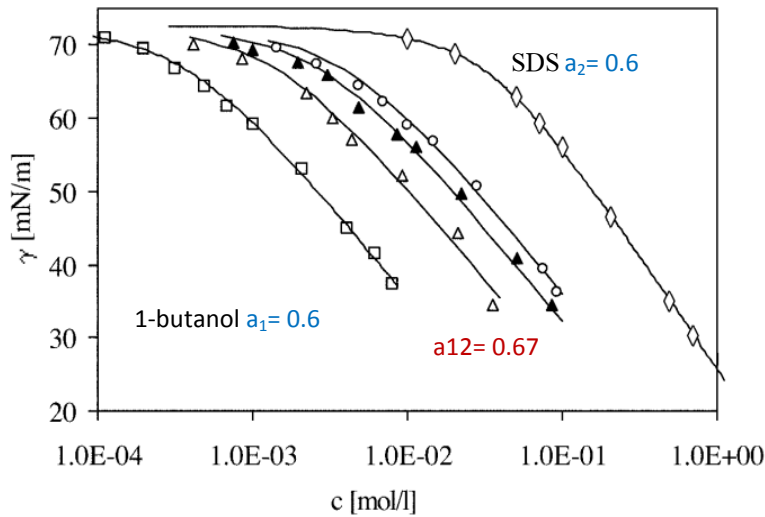


Fig 3.3. Surface tension isotherms of 1-butanol and SDS mixtures at air/water interface showing ideality (taken from [16]). SDS (\diamond) and 1-butanol (\square) and their mixtures with ratio, $x = 1:2.89$ (\triangle), $1:6.81$ (\blacktriangle) and $1:10.63$ (\circ)

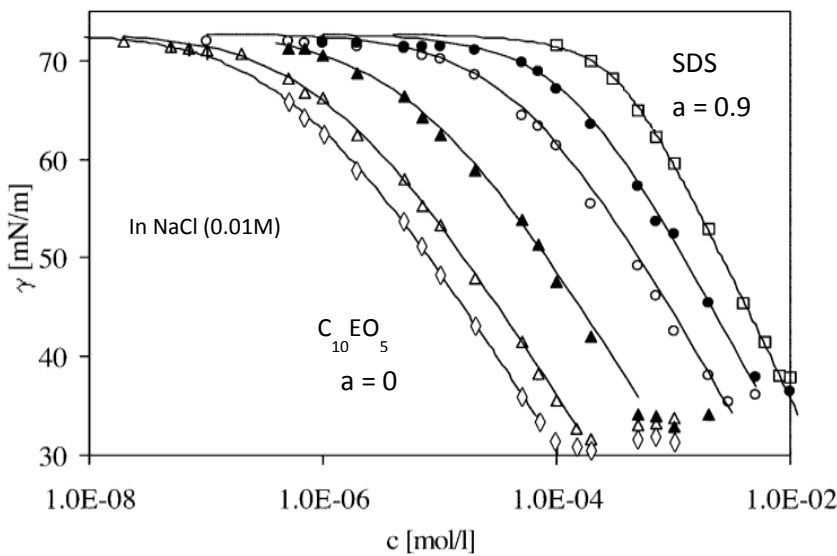


Figure 3.4. Surface tension isotherms of SDS and $C_{10}EO_5$ and its mixtures showing non-ideality (taken from [17]). SDS (\square), $C_{10}EO_5$ (\diamond) and its mixtures with ratios $x= 1:1$ (\triangle), $1:10$ (\blacktriangle), $1:100$ (\circ) and $1:500$ (\bullet)

While for the butanol/SDS system the arithmetic mean value for the coefficient a_{12} reflects the experiments very well but in the case of SDS and $C_{10}EO_5$ mixtures the mutual interaction $a_{12} > (a_1 + a_2)/2$ and, therefore, the value of a_{12} is uncertain and specific for the surfactant mixtures [16]. Thus, the thermodynamic models give a great insight and also quantify the interaction between two species at the interface.

Stubenrauch et al. have studied the adsorption, surface rheology and thin film stability of ionic and nonionic surfactants and their mixtures [18-21] and have shown so-called synergetic effects in the foamability and foam stability [22]. Here they consider the diffusive relaxation time of the surfactant which is an important parameter as bubbles are need to be quickly stabilized by adsorption coverage of quickly adsorbing surfactants to prevent coalescence. This has shown to stabilize the foam films and eventually the foams [22-24]. It was noted, however, that these conclusions are valid only for the studied systems and it was not possible to generalize the interrelations.

3.1.4. Equations of state for protein-surfactant mixtures.

With the approximation $\omega_0 \cong \omega_s$, the following equation of state for a protein/non-ionic surfactant mixture was derived in [25]

$$-\frac{\Pi\omega_0^*}{RT} = \ln(1 - \theta_p - \theta_s) + \theta_p(1 - \omega_0 / \omega_p) + a_p\theta_p^2 + a_s\theta_s^2 + 2a_{ps}\theta_p\theta_s \quad (15)$$

The parameter a_{ps} describes the interaction between the protein and surfactant molecules. A small difference between ω_0 and ω_s can be accounted for by introducing a mean molecular area

$$\omega_0^* = \frac{\omega_0\theta_p + \omega_{s0}\theta_s}{\theta_p + \theta_s} \quad (16)$$

Note, in contrast to the model developed earlier as Eq. (4), the Eq. (6) involves the parameter ω_{s0} rather than ω_s . For the protein adsorbed in state $j = 1$ and the surfactant, the adsorption isotherms read

$$b_{p1}c_p = \frac{\omega_p\Gamma_{p1}}{(1 - \theta_p - \theta_s)^{\omega_1/\omega_p}} \exp[-2\alpha_p(\omega_1/\omega_p)\theta_p - 2\alpha_{ps}\theta_s] \quad (17)$$

$$b_s c_s = \frac{\theta_s}{(1 - \theta_p - \theta_s)} \exp[-2\alpha_s\theta_s - 2\alpha_{ps}\theta_p] \quad (18)$$

where the subscripts S and P refer to parameters characteristic for the individual surfactant and protein, respectively. The distribution of protein adsorptions over the states j is given by the expression:

$$\Gamma_{Pj} = \Gamma_P \frac{(1 - \theta_P - \theta_S)^{\frac{\omega_j - \omega_1}{\omega_P}} \exp[2\alpha_P \theta_P (\omega_j - \omega_1) / \omega_P]}{\sum_{i=1}^n (1 - \theta_P - \theta_S)^{\frac{\omega_i - \omega_1}{\omega_P}} \exp[2\alpha_P \theta_P (\omega_i - \omega_1) / \omega_P]} \quad (19)$$

The total adsorption of protein molecules and the total surface coverage by protein molecules are obtained from Eq. (9). The theoretical description for a protein-surfactant mixture can be managed in the following way: given the known values of T , ω_0 , ω_{\min} , ω_{\max} , a_P , b_P , ε , ω_{S0} , a_S and b_S for the individual components and α_{PS} as single additional parameter for the protein-surfactant mixture, the dependencies of the parameters ω_P , Γ_P , Γ_S , θ_P , θ_S and Π as a function of the concentrations c_S and c_P can be calculated.

The behaviour of protein- ionic surfactant mixtures is essentially different from that of protein-non-ionic surfactant mixtures. When a protein molecule with m ionized groups at a concentration of c_P interacts with ionic surfactant molecules of concentration c_S , Coulomb forces cause the formation of complexes. These complexes are determined by the average activity of ions $(c_P^m c_S)^{1/(1+m)}$ participating in the reaction. The respective equation of state of the surface layer, however, is similar to mixed non-ionic surfactant-protein solutions [26]

$$-\frac{\Pi \omega_0^*}{RT} = \ln(1 - \theta_{PS} - \theta_S) + \theta_{PS}(1 - \omega_0 / \omega) + a_{PS} \theta_{PS}^2 + a_S \theta_S^2 + 2a_{SPS} \theta_{PS} \theta_S \quad (20)$$

The corresponding adsorption isotherms for protein-surfactant complexes in state $j=1$ (similar isotherms can be obtained for any of the possible i states) and for the free surfactant not bound to the protein read

$$b_{PS} (c_P^m c_S)^{1/(1+m)} = b_{PS} c_P^{m/(1+m)} c_S^{1/(1+m)} = \frac{\omega \Gamma_1}{(1 - \theta_{PS} - \theta_S)^{\omega_1/\omega}} \exp[-2a_{PS} (\omega_1/\omega) \theta_{PS} - 2a_{SPS} \theta_S] \quad (21)$$

$$b_S (c_S c_C)^{1/2} = \frac{\theta_S}{(1 - \theta_{PS} - \theta_S)} \exp[-2a_S \theta_S - 2a_{SPS} \theta_{PS}] \quad (22)$$

Here $\theta_{PS} = \omega \Gamma$ is the coverage of the interface by adsorbed protein-surfactant complexes, c_C is the surfactant counter-ion concentration, and a_{SPS} is the parameter which describes the interaction of the non-associated surfactant with the protein-surfactant complexes. The subscript PS refers to the protein/surfactant complex, and the subscript S to the free surfactant.

Fig. 3.5 presents an example for a mixed BLG-SDS adsorption layer formed at the aqueous solution-hexane interface for a fixed BLG concentration. The dotted line corresponds

to a calculated isotherm using the equations (20) to (22) and the parameter values summarized in Table 1.2.

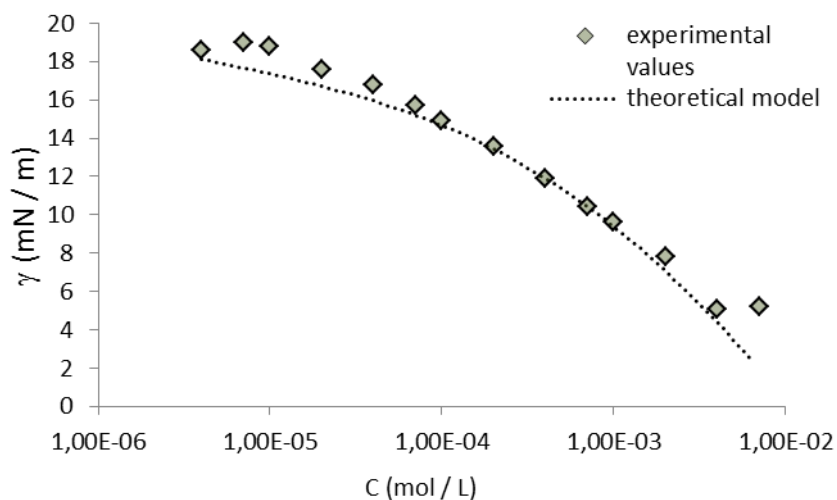


Figure 3.5. Interfacial tension γ as a function of the SDS concentration for mixtures of BLG (β -lactoglobulin) and SDS at a fixed BLG concentration of 10^{-6} M at water/MCT(medium chain triglyceride) interface [6].

SDS			BLG					
ω_s (m^2/mol)	a_s	b_s (m^3/mol)	ω_0 (m^2/mol)	ω_{min} (m^2/mol)	ω_{max} (m^2/mol)	a_{ps}	b_{ps} (m^3/mol)	a_{sps}
$3.80 \times 10^{+5}$	0	$1.25 \times 10^{+2}$	$3.50 \times 10^{+5}$	$5.50 \times 10^{+6}$	$9.00 \times 10^{+6}$	0.6	$1.25 \times 10^{+4}$	1

Table 1.2. Parameters obtained by fitting the mixtures of (SDS and β -LG with the respective theoretical models described above with isotherms shown in Figure 3.5; taken from [6]

In this case the best fit was obtained for $a_s < a_p < a_{ps} < a_{sps}$ [6]. So here the domination of surfactant at higher concentration at the interface is shown in the equilibrium surface tension values. The good quality of fitting supports the applicability of the given thermodynamic model to this protein-surfactant mixture.

3.2. Kinetics of adsorption

The majority of scientists working on adsorption kinetics agree that most surfactant molecules adsorb in diffusion controlled way. This physical model is based on the assumption made by Ward and Tordai in 1946 [27] that surfactant molecules have at first to be transported by diffusion close to the surface from where they can adsorb easily, i.e. change into the adsorbed state. This so-called diffusion controlled adsorption kinetics model induces that the transition of a surfactant molecule from the solution into the adsorbed state at the surface or vice versa is very fast as compared to the transport in the solution bulk by diffusion. We first discuss this main adsorption mechanism, and then also elaborate briefly the alternative one which is called kinetic controlled adsorption. In this mechanism the diffusional transport is very fast as compared to the interfacial transfer step. In the end of this paragraph models are described for mixtures of surfactants or proteins.

3.2.1. Diffusion controlled adsorption

Assuming the adsorption process is diffusion controlled, the kinetics is given by the integral equation derived by Ward and Tordai for a flat interface [27]

$$\Gamma(t) = \sqrt{\frac{4D}{\pi}} \left[c_0 \sqrt{t} - \int_0^{\sqrt{t}} c_s(t-\tau) d\sqrt{\tau} \right] \quad (11)$$

where D is diffusion coefficient of the surfactant molecule, c_0 is the bulk concentration of surfactant, τ is a dummy integration variable and c_s is the concentration in the sub-surface layer related to adsorption via the corresponding adsorption isotherm. This equation can be modified for the case of adsorption at a spherical surface of radius r [28]

$$\Gamma(t) = \sqrt{\frac{4D}{\pi}} \left[c_0 \sqrt{t} - \int_0^{\sqrt{t}} c_s(t-\tau) d\sqrt{\tau} \right] \pm \frac{D}{r} \left[c_0 t - \int_0^t c_s(t-\tau) d\tau \right] \quad (12)$$

The plus in Eq. (12) corresponds to adsorption from outside the droplet. It is obvious from Eq. (11), the adsorption of surfactant molecules depends on the bulk concentration c_0 . Once $\Gamma(t)$ has been obtained, the corresponding dynamic interfacial tension is calculated via the corresponding equation of state, for example via Eq. (2).

To describe the pseudo-equilibrium state of adsorption it can be stated as equilibrium in dynamic surface tension observed in experimental time and it depends on the bulk concentrations as discussed above and the choice of instrument and the detailed information

of these instrumental techniques will be provided in the forth-coming paragraph. One example of experimental evidence where human serum albumin was studied by applying trapezoidal compression and relaxation of surface layer where one and the same surface tension value as perturbations before and after the harmonic cycles of compression-relaxation was obtained showing the attainment of a pseudo-equilibrium state [29].

One example of where the kinetics of adsorption for β -lactoglobulin was compared with two different models can be found in [30]. Here it was assumed that globular protein molecules can adsorb in two configurations ‘head on’ and ‘side on’. The two kinetic models were applied: the quasi-equilibrium dynamic adsorption model with an instantaneous transition between the two assumed configurations, and the re-orientation kinetic model where it was assumed that the transition step has a finite rate constant.

Comparing with experimental data the re-orientation kinetic model fitted best to the results indicating a finite time interval required for the transition between the two adsorption states. A more precise theoretical model would require several considerations of all states of proteins each having different rate constant but for now this approximation serves as the best for globular proteins [30].

3.2.2. Kinetic controlled adsorption kinetics

When the diffusion transport in the solution bulk is negligible, i.e. when the diffusion is very fast as compared to the transition step of a molecule from the solution to the adsorbed state, then we speak about a kinetic controlled adsorption. Such a situation is easily established by an efficient stirring of the solution or by the establishment of convection in the bulk by other means. For this case, Baret [31] proposed various rate equations as boundary condition at the surface, instead of an equilibrium equation of state. For this purpose Baret used equations which approach to well-known adsorption models when the adsorption equilibrium is reached. For example, Eq. (13) described the Langmuir adsorption mechanism

$$\frac{d\Gamma}{dt} = k_{ad}c_0 \left[1 - \frac{\Gamma}{\Gamma_\infty} \right] - k_{des} \frac{\Gamma}{\Gamma_\infty} \quad (13)$$

where k_{ad} and k_{des} are the rate constants of adsorption and desorption, respectively, and the parameter Γ_∞ corresponds to the maximum number of adsorbed molecules at the interface. For long adsorption times, $d\Gamma/dt$ tends to zero and we obtain a relation which has the form of a Langmuir isotherm

$$\Gamma = \Gamma_{\infty} \frac{c_0}{k_{des} / k_{ad} + c_0} \quad (14)$$

When the surface coverage $\Gamma/\Gamma_{\infty} \ll 1$, the relation (13) can be simplified to

$$\frac{d\Gamma}{dt} = k_{ad}c_0 - k_{des} \frac{\Gamma}{\Gamma_{\infty}} \quad (15)$$

which in equilibrium corresponds to a linear Henry isotherm.

It was also Baret [31] who combined the two general models of a diffusion and kinetic controlled adsorption, leading to a model in which both the transport by diffusion and the transition between the solution and adsorbed states are relevant. For this purpose, he replaced the bulk concentration c_0 by the surfactant's sub-surface concentration $c_s(t)$. For the Langmuir mechanism this reads

$$\frac{d\Gamma}{dt} = k_{ad}c_s(t) \left[1 - \frac{\Gamma}{\Gamma_{\infty}} \right] - k_{des} \frac{\Gamma}{\Gamma_{\infty}} \quad (16)$$

When we combine Eqs. (11) or (12) with Eq. (16) we obtain such a mixed diffusion-kinetic-controlled adsorption, as it was discussed in detail also in [32].

3.2.3. Adsorption kinetics for mixed solutions

It was shown in [33] that the adsorption of surfactant mixtures can theoretically be described by a set of Ward & Tordai equations. For each component i one of these integral equations is required

$$\Gamma_i(t) = \sqrt{\frac{4D_i}{\pi}} \left[c_{i0} \sqrt{t} - \int_0^{\sqrt{t}} c_{is}(t-\tau) d\sqrt{\tau} \right] \quad (17)$$

The equations, however, are not independent but linked to each other via a generalized equation of state or adsorption isotherm. Such a relationship includes all adsorbed amount $\Gamma_i(t)$ and sub-surface concentrations $c_{is}(t)$. Supposed we use a generalized Langmuir adsorption model, this relationship is non-linear and provides some complication for a quantitative analysis [34]. For solutions containing a protein and a surfactant, the situation is even more complicated and first quantitative simulations at flat and curved surfaces with a constant area are yet in development.

In summary, we can conclude that there are theoretical models for describing quantitatively the adsorption of surfactants, proteins and their mixtures at the solution-air surface. However, we have to confess that for the adsorption at liquid surfaces not in a mechanical equilibrium,

i.e. at the surface of growing drops/bubbles or even of rising bubbles, there are still enormous problems for a quantitative analysis of experimental data. Fluid dynamics simulations combined with thermodynamic and transport models will probably soon allow such quantitative simulations, as it was shown in an example by Dieter-Kissling et al. [35] for a growing drop of a surfactant solution.

3.3. Single bubble rising in surfactant solution

The bubble rising in liquid media is one of the important steps in the floatation process as it involves the adsorption-desorption kinetics to and from the bubble surface which differs from that of static bubbles. In pure water the bubble accelerates to some distance and reaches a constant velocity called terminal velocity depending on its size. In surfactant solution the convective-diffusion kinetics which involves adsorption and desorption exchange with the sub-surface is accompanied by the hydrodynamics of the liquid layer around the bubble. In 1947 Frumkin and Levich have described the adsorption layer of such rising bubbles having a concentration gradient on its surface [36]. The physico-chemical nature of this phenomenon was much more elaborated by Levich in 1962 [37]. The movement of the bubble induces a concentration gradient decreasing from the top pole where the surface coverage is highest towards the bottom one. It causes a surface tension gradient along the bubble surface, which retards the mobility and increases the total drag force exerted on it. A stagnant cap is formed at the bottom pole once the bubble reaches a steady state in motion. Hence such layer is termed as dynamic adsorption layer (DAL) as it differs from that at a stationary bubble surface [38-50]. The understanding of the dynamics of such system has been extended by Derjaguin and Dukhin in the 1960's, who have described the heterogeneity of DAL for lower surface coverage due to the weakly retarded surface [50]. The theory of stagnant cap formation and its angular dependence was developed further by Sadhal *et al.* [51] and latest developments in DAL theory were addressed by He *et al.* [52] for the case of low Reynolds numbers.

A shape deformation occurs for bubbles rising in pure liquids ($\gamma = \text{const}$) which depends on its size. According to the Laplace law the smaller the radius the higher the capillary pressure inside the bubble which resists to deformations. At high surfactant concentrations the deformation is smaller as the bubble surface is immobile and acts as a rigid sphere. Velocity profiles and shape oscillations have been extensively studied by Krzan *et al.* [53-55] for bubbles of various sizes and times of bubble formation in different surfactant

solutions. The time of formation of a bubble and the bubble diameter could be controlled by the size of the capillary and the flow rate.

Fig. 3.6 shows the local velocity profiles (U_L vs. L) for rising bubbles in water (the experimental setup has been mentioned in the previous section and in several papers [53-55]) and in n-butanol solutions of different concentrations, where U_L is the local velocity of a rising bubble and L is the distance from the capillary. At a bubble diameter of $d_b = 1.5$ mm and a time of bubble formation of 1.6 s, after a certain rising time, the terminal velocity, $U_T = 34.8 \pm 0.2$ cm/s for water and $U_T = 15$ cm/s for n-butanol concentrations higher than 32 mM are attained which agrees with a model described in [56]. Further increase in the concentration has negligible effects on the terminal velocity and it is the rigidity of the surface which makes the bubbles to behave as solid spheres. The local velocity profiles for concentrations lower than 32 mM exhibit a maximum followed by a monotonic decrease of U_L until a certain U_T -value is attained. Increase of the surfactant concentration leads to decrease in the height of the maximum and its position is shifted towards shorter distances. This maximum gives evidence that a stationary non-uniform distribution of surface coverage at the gas/solution interface is not established, while beyond a certain concentration this does happen right after detachment of the bubble which consequently rises with a terminal velocity [40, 54 & 55].

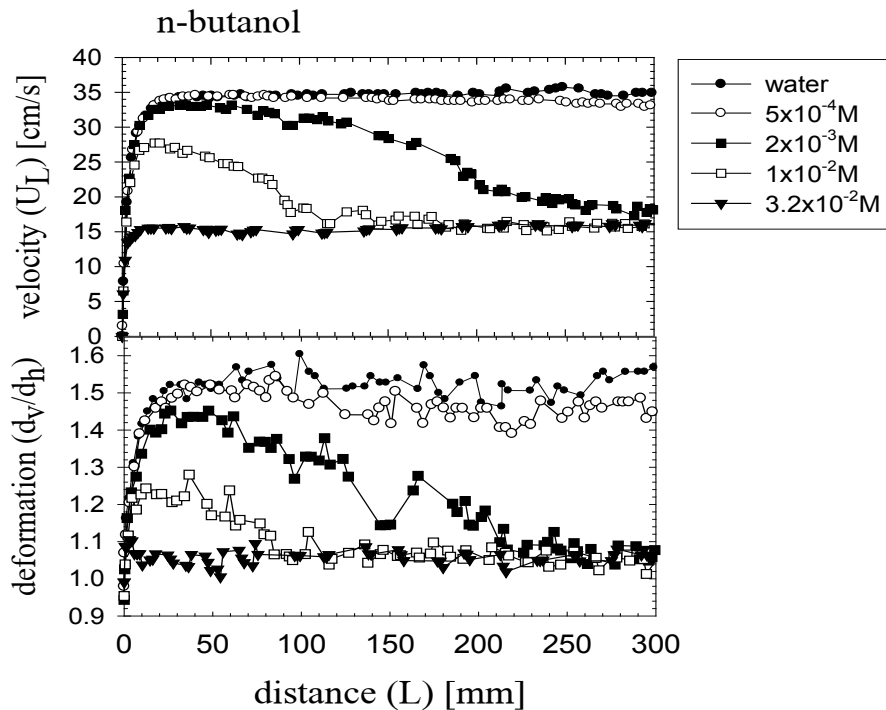


Figure 3.6. Deformation ratio and local velocity profiles for rising bubbles in water and n-butanol solutions (redrawn from Ref. [55]).

The adsorption at the leading pole and desorption from the bottom pole of the bubble occur during the bubble motion and due to interfacial convection the adsorbed surfactants are pushed toward the bottom pole generating a surface tension gradient. If Γ_{top} , Γ_{bottom} and Γ_{eq} are the surface concentrations at the top and bottom poles, and in the equilibrium state, respectively, then for a stationary bubble the condition is $\Gamma_{\text{top}} = \Gamma_{\text{bottom}} = \Gamma_{\text{eq}}$, whereas for a rising bubble this would be $\Gamma_{\text{top}} < \Gamma_{\text{eq}} < \Gamma_{\text{bottom}}$. Therefore, the bubble deceleration can be explained by a Marangoni stress which should affect the drag force exerted on the bubble surface [36, 50, 52, 57].

Though, there is no technique to measure the surface tension or to detect the adsorbed amount on the rising bubble, by assuming the DAL theory we could assume that adsorption reaches an steady-state when the terminal velocity attains to that of a rigid layer.

3.4. Foam generation

Foams are dispersions of a gas phase into a liquid phase which are stabilized by adsorbed material at the bubbles surfaces. There are different ways employed to disperse the gas into liquid such as using a rotor to agitate the solution, passing the liquid and gas through packed beads or porous material which is mainly employed in petroleum industries. A simple method used commonly in laboratories is passing the gas through a capillary or glass filter plate. The current focus in this work would be to that of foams generated through sintered glass filters. The bubble size distribution of the foam produced in this way depends on the pore size of the frit, gas flow rate and physico-chemical parameters of the solution such as bulk concentration of surfactant, viscosity of solution, etc. [58]

Once the bubble detaches from the capillary orifice (frit pore) it travels through the solution at a certain velocity depending on the properties of the solution. Two broadly classified regimes of foam formation could be described which depends on the gas flow rate, namely a “static regime” and “dynamic regime”. We have a static regime when the gas flow rate has a Reynolds number less than 100. The Reynolds number of gas flow is given by the following equation,

$$\text{Re} = \frac{2q\rho_l}{\pi r\eta_l} \quad (18)$$

Here q is the gas flow rate, ρ_l and η_l are density and viscosity of air and r is the radius of the capillary pore size [58].

So in case of a static regime the bubble radius r can be expressed here as follows,

$$r = \sqrt[3]{\frac{3\gamma r_p}{2\rho_2 g}} \quad (19)$$

where ρ_2 is density of the liquid, γ is the surface tension and r_p is radius of pore. So the bubble size depends on the surface tension and the density of the liquid [58, 59].

In case of a dynamic regime, the bubble volume V is expressed as follows,

$$V = K \left[\frac{q\eta_2}{\rho_2 g} \right]^{3/4} \quad (20)$$

where η_2 is viscosity of the liquid, and K is a constant. From equation (20) it could be noted that the surface tension of solution has no impact on it [34]. It has been also mentioned that depending on the material of the porous plate i.e. whether it is hydrophilic or hydrophobic, the size of the bubbles vary [58, 59].

3.5. Foam stabilization

The stability of foam is a collective stability of the thin liquid films that are formed between the bubble surfaces. The interstitial liquid is drained through the plateau borders, which brings the bubble surfaces closer to form a film. As the drainage progresses the foam gets dryer from the top to the bottom which eventually influences the foam stability.

3.5.1 Thin Liquid films

Thin liquid films (TLF) are important elements of every dispersed systems under dynamic and static conditions, and can be described as a liquid layer between two interfaces, where the specific additional interactions (DLVO forces - (Derjaguin and Landau, 1941; Verwey and Overbeek, 1948)) start to play an essential role for their stability [60, 61]. Thus, the main differences of TLF from the bulk phase are due to these specific interactions, which occur for liquid films thinner than ca. 100 nm. Due to the type of the interfaces and interrelated to that specific DLVO forces, thin liquid films can be divided into two groups [62];

- a) symmetrical films, which possess two identical interfaces (e.g. foam films, emulsion films) - interactions are homogenous
- b) asymmetrical films, formed between two different interfaces (e.g. wetting films) - heterogeneous interactions.

As the state and stability of liquid films which eventually affect the stability of foam systems, is based on the analysis of the surface forces acting across thin liquid films, it is worth to pay a little more attention to this phenomenon.

For the two surfaces in a fluid phase, separated by an interlayer with sufficient large thickness h , that the middle parts of the layer retain the properties of the bulk phase, changes in the interlayer do not change the system's free energy. But, the situation is different at some sufficiently small h , where the surface zones close to the interfaces begin to overlap and then, the properties of the liquid interlayer become different from those of the bulk phase. In general, to maintain the thermodynamic equilibrium, opposing forces (named “disjoining pressure” - Π), proportional to the interlayer area must be applied to the interfaces. Thus, the equilibrium is fulfilled for the following condition

$$\Pi(h) = P_f(h) - P_o = \Delta P_f \quad (21)$$

where P_f is the pressure exerted by the dispersed phases on the interlayer, and P_o is the pressure in the bulk liquid phase. On the other hand, the overlap of the transition regions results in the appearance of excess Gibbs free energy of the interlayer induced by the overlapping, and in terms of Gibbs free energy (G) can be presented as [58, 62]

$$\Pi(h) = -\frac{1}{A} \left[\frac{\partial G}{\partial h} \right]_{T,P,\mu_i} \quad (22)$$

where T and P are the temperature and the pressure in the system, containing the thin film, and μ_i is the chemical potential of the i -th component of the system. According to the established tradition the total disjoining pressure in a thin film is considered as an additive sum of different independent components, each defined by mechanisms of different physical nature [63]

$$\Pi = \Pi_{vW} + \Pi_{el} + \Pi_{non-DLVO} \quad (23)$$

The subscripts in Eq. (23) indicate the following contributions: vW for van der Waals forces, el for electrostatic double layer forces, and $non-DLVO$ refers to components not accounted for in the classical DLVO theory. Generally if $\Pi > 0$ then Π acts towards disjoining of the interfaces and for $\Pi < 0$ the film becomes thinner [58, 64].

The individual thin films are the key elements to understand foam stability which involves various factors. The foam film or lamella which is formed between two contacting bubbles will thin due to drainage. Three foam lamellae meet at 120° angle forming a junction called *plateau border*. This creates suction due to the high capillary pressure in the plateau border induced by the small radius of curvature according to the Laplace equation. The liquid between the films is sucked into these borders causing film drainage. This in turn would induce Marangoni stresses due to a surfactant concentration gradient which could stabilize the

film; therefore the surfactant coverage and the dilational elasticity of the film interfaces are considered very important [58].

The Fig. 3.7. shows a plot where the drainage of the films causing thinning and the potential energy at the surfaces during the thinning which could be attractive or repulsive. Initial drainage is caused due to Plateau borders suction and gravity and after which van der Waals forces act on it until it reaches a configuration called Common Black Film (CBF). The films here are primarily stabilized by electrostatic forces. Further thinning occurs due to evaporation at a spot on the film and causes further drainage where it reaches the Newton Black Film (NBF) configuration. In case of non-ionic surfactants it occurs as if there are no electrostatic forces acting. This is often a stable configuration where the stability is determined by entropic confinement forces after which films rupture. All this would depend on the bulk concentration and the type of surfactant used [65].

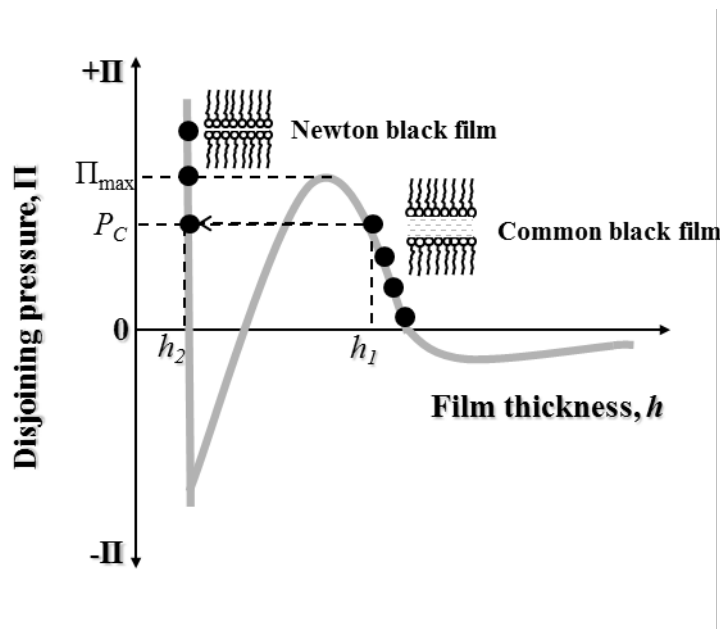


Figure 3.7. Disjoining pressure vs. film thickness isotherm $\Pi(h)$ for symmetric thin liquid films. The arrow indicates the transition between common and Newton black films by overlapping the barrier of the repulsive interaction forces Π_{\max}

Radke et al. have studied extensively the behavior of TLF with β -casein (BCS) and bovine serum albumin (BSA) [66]. The thickness of the adsorbed layer was measured with ellipsometry which was largest for the proteins at the isoelectric point (IEP) due to the formation of multilayers in the absence of electrostatic repulsion. It was noted that BCS films were more stable to applied pressure as compared to BSA due to the compressibility of BCS molecules at the interface. The aging at the interface created more stable films while drainage

and thickness was less uniform with formation of dimples trapped in the films which is possibly due to the existence of aggregates. The elasticity of the protein film interfaces arises due to intermolecular interactions and network formation which is unique for each protein under given conditions [66].

Wilde et al. have studied mixtures of BSA and Tween 20 and found that the drainage of films formed by BSA was slow and the surface was rigid as compared to Tween 20 stabilized films. In mixtures at ratios where Tween 20 dominates the interface (obtained from surface pressure data) the fluidity increased. Further work was dedicated to understand the protein- protein interaction, for which ethanol and sucrose was added. The ethanol acts as denaturant of protein and provides poor solvent condition which had negative effect on the film stability. Sucrose, on the other hand, had a positive effect as it increased hydration around the protein and decreased aggregation which facilitated more adsorption of protein at the interface [67]. Alahverdijeva et al. found correlation between the adsorption isotherms of lysozyme and its mixtures with C₁₀DMPO and SDS to the TLF thickness and foam stability. While individual lysozyme has not formed stable films, its mixtures with surfactants formed stable films. Kotsmar et al. have studied TLF thickness of BCS and C₁₂DMPO mixed solutions which correlates with adsorption studies and agrees with the DLVO theory [68].

3.5.2. Foam drainage

Due to the high density difference and the resulting buoyancy the bubbles gather quickly at the liquid's top during foam formation. The liquid in between is flowing downwards between the bubbles which induces a shear and dilational stress on the bubble surface which is counterbalanced by the Marangoni flow caused by a surface concentration gradient. Four plateau borders intersect each other at a 109⁰ angle forming a channel through which liquid flows [65].

To obtain the equation for drainage of liquid in foams, the drainage of the films is neglected and only liquid drainage in the Plateau borders is considered. So if we consider single vertical Plateau borders with a cross section $A(x,t)$ drainage depends on the downward vertical coordinate x and time t . For incompressible liquids we get the following equation of continuity,

$$\frac{\partial}{\partial t} A(x,t) + \frac{\partial}{\partial x} [A(x,t)u(x,t)] = 0 \quad (24)$$

Here $A = C^2 r^2$ is an elementary geometry parameter with $C = \sqrt{(\sqrt{3} - \pi/2)}$ and the velocity u is the average velocity over the cross section of the Plateau border. The Young-Laplace law for the liquid surface is given by,

$$p_l = p_g - \frac{\gamma}{r} \quad (25)$$

At the Plateau border the dissipative force due to flow is given by $-f\eta_1 u / A$, where f is a numerical factor (~ 49 for Plateau borders based on a shape of the given cross-section), η_1 is the viscosity of the liquid. Therefore, the dissipation balanced by gravity ρg , and the pressure gradient $-\partial p_l / \partial x$, could be written as,

$$\rho g - \frac{\partial}{\partial x} p_l - \frac{\eta_1 f u}{A} = 0 \quad (26)$$

From equations (24) and (26) we can derive u as a function of A ,

$$\frac{\partial A}{\partial t} + \frac{\partial}{\partial t} \left(\frac{\rho g}{f\eta_1} A^2 - \frac{C\gamma}{2f\eta_1} \sqrt{A} \frac{\partial A}{\partial x} \right) = 0 \quad (27)$$

Until now we assumed the Plateau border to be vertical but now if we consider giving it an angle θ with respect to the x -coordinate then $x_\theta = x / \cos \theta$. The gravitational force acting on the liquid would be $\rho g \cos \theta$. Therefore, eq. (27) becomes,

$$\frac{\partial A}{\partial t} + \frac{\cos^2 \theta}{f\eta_1} \frac{\partial}{\partial t} \left(\rho g A^2 - \frac{C\gamma}{2} \sqrt{A} \frac{\partial A}{\partial x} \right) = 0 \quad (28)$$

By approximating $\cos^2 \theta$ to $1/3$ which is valid for a cubic structure, and by introducing dimensionless variables, such as $\xi = x/x_0$, $\tau = t/t_0$, $\alpha = A/x_0^2$ with $x_0 = \sqrt{C\gamma/\rho g}$ and $t_0 = \eta^* / \sqrt{C\gamma\rho g}$ ($\eta^* = 3f\eta_1$), equation (28) simplifies to,

$$\frac{\partial \alpha}{\partial \tau} + \frac{\partial}{\partial \xi} \left(\alpha^2 - \frac{\sqrt{\alpha}}{2} \frac{\partial \alpha}{\partial \xi} \right) = 0 \quad (29)$$

The equation (26) is termed as foam drainage equation by Verbist et al. [69] which was first derived from Goldfarb et al. [70].

Foam drainage varies with surfactant. For protein foams the interface was rigid, whereas foams stabilized by small-surfactant molecules show significant interfacial mobility [71, 72]. Koehler et al. did measurements of the flow velocity profiles across a single Plateau border. A significant consequence is that bubble size and liquid volume fraction in a foam affect the relative importance of surface rheology on the drainage behavior [71].

The surface shear viscosity of the adsorbed layer has been studied by direct methods like the rotational viscometer and non-invasive or indirect methods where the mobility of liquid draining through plateau borders is translated into surface viscosity. Inconsistencies between reported values were reviewed by Stevenson et al., for the surface shear viscosity of SDS solutions [74]. The values obtained from observations of drainage in Plateau borders and thin films [71, 74-76] are seen to be approximately 100 times lower than those obtained by three independent but approximately mutually consistent direct invasive measurements [77-79]. It was thought that since SDS is a soluble surfactant its resistance to shear deformation at the surface is governed by a three-dimensional layer in the vicinity of the surface which entirely depends on the experimental conditions [73]. It might, however, also be that particularly the specificity of SDS lead to the observed inconsistencies, as this surfactant contains always dodecanol as an admix due to the hydrolysis of SDS in aqueous solution.

Durand et al. have shown theoretically that the Gibbs elasticity of the interface and the surface diffusion coefficient may play an important role in determining the drainage rate [80]. Stevenson et al. found the apparent shear viscosity between the plateau borders which was decreasing when the airflow rate was increased [81]. Elizalde et al. have studied the drainage rates for different food proteins and found correlation to an empirical drainage model [82].

3.5.3. Ostwald ripening or coarsening.

Ostwald ripening is the process where the gas diffuses from the bubbles of smaller size to that of larger or to the atmosphere due to pressure differences. So the resting foam while it drains its liquid between the Plateau borders would also change its bubble size distribution due to this phenomenon. It is a destabilizing factor for the foams as the gas is diffused out through the permeable adsorption layers and liquid films. It has been accounted that the desorption rate of adsorbed material contributes to the diffusion of the gas. Hence particles are known to stabilize foams against coarsening as they require high energy to desorb [65] which surfactants do not offer [83]. Murray et al. describe that surfactant molecules which have generally higher desorption rates would not provide complete packing on the bubble surface to prevent gas molecules from diffusing through the surface. For proteins though they form highly elastic layers at the interface by crosslinking, there is always an 'empty gap' through which gas molecules would diffuse [84].

Wierenga et al. wrote a detailed review about foams stabilized by proteins where a section is devoted to Ostwald ripening [85]. The dissolution of gas from smaller bubbles to larger

bubbles or to the atmosphere has been studied with different proteins like BCS, BLG and glycinin. It was found that the dissolution of gas was the same for all the proteins independent of the dilation elasticity. It was concluded that either the proteins desorb (which is very slow) or the protein layer ‘buckles’ when the bubble shrinks creating gaps for gas diffusion [85].

3.5.4. Attempts to correlate foam stability

As the foams are formed under dynamic conditions when the gaseous phase is dispersed into the aqueous phase; various factors influence their formation and life time. The adsorption coverage by surfactants on the bubble surface stabilizes them against coalescence and rupture of the films between them. However, the adsorption coverage of the bubble surface is quite different to that obtained from surface tension measurements performed at static conditions. Rheological properties of adsorption layers are crucial for estimating the foam stability. Nguyen stated “In particular, the rheological properties of adsorption layers, like surface elasticity, surface dilational, and shear viscosities are important for the investigation of liquid foams” [86]. For example the surface shear viscosity of surfactants was considered by some authors such as Brown et al., [87, 88] and Shah et al [89] as stabilizing effect for foams. The effect of interfacial properties on the foam behavior with food systems was also reviewed by Wilde et al [90].

It has been experimentally shown that foam stability depends on surface dilational elasticity and viscosity. In other words, higher dilational elasticities correspond to a higher foam stability which was shown for fatty acids by Malysa et al [91, 92] and for other surfactants in [93, 94].

Coke et al. have shown for β -lactoglobulin and Tween 20 mixtures that there is progressive displacement of protein by the Tween 20 surfactant at the surface. This was confirmed by surface tension studies, transitions in the drainage characteristics, thickness of free foam films, and surface mobility studies with a fluorescent-labeled β -lactoglobulin photobleaching method. The results indicated that maintenance of the viscoelastic properties of the surface is of great importance for foam stability of systems comprising mixtures of protein and surfactant [95].

Kim and Kinsella have shown a relationship between viscoelasticity of interfacial films and foam stability of Bovine Serum Albumin [96]. Martin et al., have done studies on foam stability with BLG, BCS, gelatin etc., and found good correlation with shear and dilation rheology [97]. For mixed polyelectrolyte/surfactant systems we have similar results [98, 99].

The stability of foams with various proteins and nano particles in food systems was extensively reviewed by Murray et al [84].

Some workers have shown an increase in foam stability of protein solutions by inducing structural changes. For example Horiuchi et al. have found a correlation between foam stability and molecular structures which was established by five kinds of proteins as hydrolysed pepsin [100]. Here they estimated the hydrophobic regions inside the protein core and those on the surface of the protein hydrolysates. A close correlation was found between hydrophobic regions on the protein surface and their foam stability.

Kim et al. studied film properties and foam stability of glycinin by progressive succinylation and found that the foam stability was best for 25% succinylated protein and further succinylation again reduced the foam stability [101]. Sarker et al. showed the enhancement of foam stability by formation of Wheat Arabinoxylan-Protein crosslinks with Bovine serum albumin (BSA) and Tween 20 systems and found effects of bulk viscosity which increased the foam stability [102].

In contradicting to the above studies Ipsen et al. have found that hydrolysates of β -lactoglobulin had better foaming properties but lower interfacial viscoelasticities as compared to the intact protein [103]. Another surprising effect noticed by Husband et al. with β -casein was that de-phosphorylation caused reduction in emulsion stability but had no effect on foam stability. The poor emulsion stability was supported by thin film thickness measurement which shows reduced thickness for dephosphorylated β -casein due to less electrostatic repulsion [104]. Whereas Le Floch-Fouere et al. have demonstrated that Lysozyme and Ovalbumin show synergism in adsorption layers probably due to electrostatic interactions as net charges of these proteins are opposite to each other. This synergism was confirmed by surface pressure, IRRAS and ellipsometry measurements, however, the foam properties of mixtures showed no synergism and were corresponding to that of ovalbumin alone, whereas lysozyme did not contribute to the foam behavior [105].

Kinsella et al. have shown that whey protein isolates obtained from acid treated milk have lower foaming ability while the centrifuged and filtered samples have increased foamability. The conclusion was drawn that larger protein aggregates and partly insoluble particles contribute to better foam destabilization [106].

3.6. Flotation

Flotation is the oldest separation technique which is based on adsorption phenomena. In the late 19th century during the industrial revolution this technique was employed in a large scale for separating minerals. The ore containing minerals of economic interest is crushed and a slurry is made into which gas bubbles are introduced. The hydrophobic mineral particles adhere to the bubble surface and these particle laden bubbles gather on top as a froth which is collected. To make this process effective certain chemical additives are necessary which could be classified as follows,

1. Collector – A reagent which would modify the wetting properties of target particles and thereby improving its adhesion to bubble surface
2. Frother – a surface active agent which stabilizes the air bubbles and therefore the froth.
3. Depressant – a reagent which would prevent the unwanted particles to be carried into the froth [107, 108].

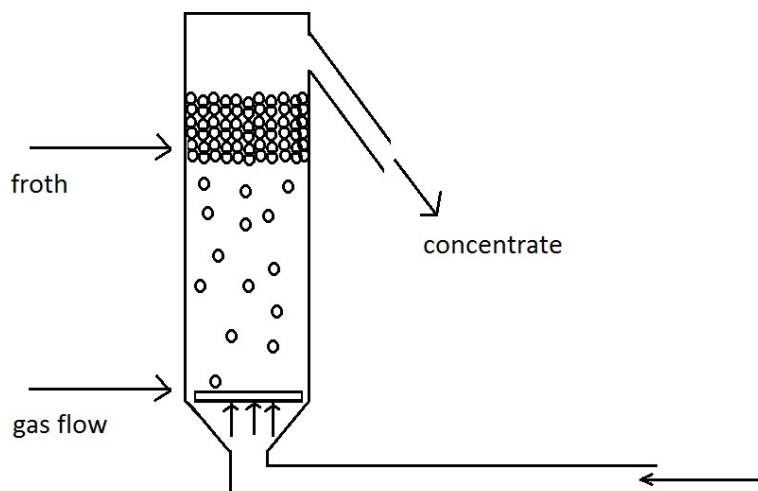


Figure 3.8. Schematic representation of a flotation process.

The above Fig. 3.8 shows a simplified representation of a flotation process. Here the gas bubbles are sparged into the flotation column from the bottom of the aqueous media. The particle suspension is agitated with inlet of gas bubbles carrying the attached material to the top. The froth is formed and pushed through the outlet which is then gathered for further purification processes [107].

The initial phase of development of this technique was mainly a trial and error based even though the concepts of wetting and hydrophobicity were known. Later most of the research focus was on physicochemical aspects of flotation. Most of the eminent colloidal scientists

such as W. Hardy, I. Langmuir, O. Bartsch and Wo. Ostwald studied the adsorption of floatation reagents to the mineral surfaces. The properties of the film between a hydrophilic surface and an air bubble was studied by Derjaguin. The concept of disjoining pressure between the surfaces of thin liquid films was also introduced by then [108].

For an effective floatation process the particles of interest should attach with sufficient energy to the bubble surface. The agitation in the highly dynamic process of floatation should not act against the attachment of particles. Therefore, the optimum conditions at which the particles can be carried to the bubble surface and get strongly attached to it are crucial.

The size of the particle play an important role as for larger particles a stronger effect of gravity results and would settle them down in the liquid phase. Therefore, particle sizes of few micrometers are generally preferred. The most important factor would be the wetting properties of the particles which is given by the three phase contact angle θ . The following equation gives us the energy, E required to remove an attached particle from the bubble surface.

$$E = \pi r^2 \gamma_{lg} (1 \pm \cos \theta)^2 \quad (30)$$

Here r is the radius of the particle, and γ_{lg} is the surface tension of the air/water interface. From the above equation we could see that the adsorption energy of a particle is maximum when the contact angle of the particles, θ is 90° [107,109].

3.7. References

1. Langmuir, I. (1917). The constitution and fundamental properties of solids and liquids. II. Liquids. 1. Journal of the American Chemical Society, 39(9), 1848-1906.
2. Frumkin, A. N. (1925). Electrocapillary curve of higher aliphatic acids and the state equation of the surface layer. Zeitschrift für Physikalische Chemie, 116, 466.
3. Fainerman, V. B., Miller, R., & Kovalchuk, V. I. (2003). Influence of the two-dimensional compressibility on the surface pressure isotherm and dilational elasticity of dodecyldimethylphosphine oxide. The Journal of Physical Chemistry B, 107(25), 6119-6121.
4. Fainerman, V. B., Kovalchuk, V. I., Aksenenko, E. V., Michel, M., Leser, M. E., & Miller, R. (2004). Models of two-dimensional solution assuming the internal compressibility of adsorbed molecules: a comparative analysis. The Journal of Physical Chemistry B, 108(36), 13700-13705.

5. Fainerman, V. B., Miller, R., & Kovalchuk, V. I. (2002). Influence of the compressibility of adsorbed layers on the surface dilational elasticity. *Langmuir*, 18(20), 7748-7752.
6. Ulaganathan, V., Bergenstahl, B., Krägel, J., & Miller, R. (2012). Adsorption and shear rheology of β -lactoglobulin/SDS mixtures at water/hexane and water/MCT interfaces. *Colloids and Surfaces A: Physicochemical and Engineering Aspects*, 413, 136-141.
7. Fainerman, V. B., Lylyk, S. V., Aksenenko, E. V., Makievski, A. V., Petkov, J. T., Yorke, J., & Miller, R. (2009). Adsorption layer characteristics of Triton surfactants: 1. Surface tension and adsorption isotherms. *Colloids and Surfaces A: Physicochemical and Engineering Aspects*, 334(1), 1-7.
8. Schaaf, P., & Talbot, J. (1989). Kinetics of random sequential adsorption. *Physical review letters*, 62(2), 175.
9. van Eijk, M. C., & Cohen Stuart, M. A. (1997). Polymer adsorption kinetics: Effects of supply rate. *Langmuir*, 13(20), 5447-5450.
10. Möbius, D., & Miller, R. (Eds.). (1998). *Proteins at liquid interfaces* (Vol. 7). Elsevier.
11. Miller, R., Fainerman, V. B., Makievski, A. V., Krägel, J., Grigoriev, D. O., Kazakov, V. N., & Sinyachenko, O. V. (2000). Dynamics of protein and mixed protein/surfactant adsorption layers at the water/fluid interface. *Advances in Colloid and Interface Science*, 86(1), 39-82.
12. Lucassen-Reynders, E. H. (Ed.). (1981). *Anionic surfactants: Physical chemistry of surfactant action*. M. Dekker.
13. Fainerman, V. B., Lucassen-Reynders, E. H., & Miller, R. (1998). Adsorption of surfactants and proteins at fluid interfaces. *Colloids and Surfaces A: Physicochemical and Engineering Aspects*, 143(2), 141-165.
14. Mulqueen, M., & Blankshtein, D. (1999). Prediction of equilibrium surface tension and surface adsorption of aqueous surfactant mixtures containing ionic surfactants. *Langmuir*, 15(26), 8832-8848.
15. Mulqueen, M., Stebe, K. J., & Blankshtein, D. (2001). Dynamic interfacial adsorption in aqueous surfactant mixtures: Theoretical study. *Langmuir*, 17(17), 5196-5207.
16. Fainerman, V. B., & Miller, R. (2001). Simple method to estimate surface tension of mixed surfactant solutions. *The Journal of Physical Chemistry B*, 105(46), 11432-11438.
17. Wüstneck, R., Miller, R., Kriwanek, J., & Holzbauer, H. R. (1994). Quantification of synergistic interaction between different surfactants using a generalized Frumkin-Damaskin adsorption isotherm. *Langmuir*, 10(10), 3738-3742.

18. Patil, S. R., Buchavzov, N., Carey, E., & Stubenrauch, C. (2008). Binary mixtures of β -dodecylmaltoside (β -C 12 G 2) with cationic and non-ionic surfactants: micelle and surface compositions. *Soft Matter*, 4(4), 840-848.
19. Andersson, G., Carey, E., & Stubenrauch, C. (2010). Disjoining pressure study of formamide foam films stabilized by surfactants. *Langmuir*, 26(11), 7752-7760.
20. Angarska, J., Stubenrauch, C., & Manev, E. (2007). Drainage of foam films stabilized with mixtures of non-ionic surfactants. *Colloids and Surfaces A: Physicochemical and Engineering Aspects*, 309(1), 189-197. Buchavzov, N., & Stubenrauch, C. (2007). A disjoining pressure study of foam films stabilized by mixtures of nonionic and ionic surfactants. *Langmuir*, 23(10), 5315-5323.
21. Carey, E., & Stubenrauch, C. (2013). Free drainage of aqueous foams stabilized by mixtures of a non-ionic (C 12 DMPO) and an ionic (C 12 TAB) surfactant. *Colloids and Surfaces A: Physicochemical and Engineering Aspects*, 419, 7-14.
22. Stubenrauch, C., Claesson, P. M., Rutland, M., Manev, E., Johansson, I., Pedersen, J. S., & Bain, C. D. (2010). Mixtures of n-dodecyl- β -D-maltoside and hexaoxyethylene dodecyl ether—Surface properties, bulk properties, foam films, and foams. *Advances in colloid and interface science*, 155(1), 5-18.
23. Stubenrauch, C., Shrestha, L. K., Varade, D., Johansson, I., Olanya, G., Aramaki, K., & Claesson, P. (2009). Aqueous foams stabilized by n-dodecyl- β -D-maltoside, hexaethyleneglycol monododecyl ether, and their 1: 1 mixture. *Soft Matter*, 5(16), 3070-3080.
24. Fainerman, V. B., Zholob, S. A., Leser, M., Michel, M., & Miller, R. (2004). Competitive adsorption from mixed nonionic surfactant/protein solutions. *Journal of colloid and interface science*, 274(2), 496-501.
25. Fainerman, V. B., Zholob, S. A., Leser, M. E., Michel, M., & Miller, R. (2004). Adsorption from mixed ionic surfactant/protein solutions: analysis of ion binding. *The Journal of Physical Chemistry B*, 108(43), 16780-16785.
26. Ward, A. F. H., & Tordai, L. (1946). Time-dependence of boundary tensions of solutions I. The role of diffusion in time-effects. *The Journal of Chemical Physics*, 14(7), 453-461.
27. Mysels, K. J. (1982). Diffusion-controlled adsorption kinetics. General solution and some applications. *The Journal of Physical Chemistry*, 86(23), 4648-4651.

28. Miller, R., Policova, Z., Sedev, R., & Neumann, A. W. (1993). Relaxation behaviour of human albumin adsorbed at the solution/air interface. *Colloids and Surfaces A: Physicochemical and Engineering Aspects*, 76, 179-185.
29. Miller, R., Aksenenko, E. V., Fainerman, V. B., & Pison, U. (2001). Kinetics of adsorption of globular proteins at liquid/fluid interfaces. *Colloids and Surfaces A: Physicochemical and Engineering Aspects*, 183, 381-390.
30. Baret, J. F. (1969). Theoretical model for an interface allowing a kinetic study of adsorption. *Journal of Colloid and Interface Science*, 30(1), 1-12.
31. Miller, R., & Kretzschmar, G. (1980). Numerische Lösung für ein gemischtes Modell der diffusions-kinetik-kontrollierten Adsorption. *Colloid and Polymer Science*, 258(1), 85-87.
32. Miller, R., Lunkenheimer, K., & Kretzschmar, G. (1979). Ein Modell für die diffusionskontrollierte Adsorption von Tensidgemischen an fluiden Phasengrenzen. *Colloid and Polymer Science*, 257(10), 1118-1120.
33. Miller, R., Makievski, A. V., Frese, C., Krägel, J., Aksenenko, E. V., & Fainerman, V. B. (2003). Adsorption kinetics of surfactant mixtures at the aqueous solution: Air interface. *Tenside, surfactants, detergents*, 40(5), 256-259.
34. Dieter-Kissling, K., Karbaschi, M., Marschall, H., Javadi, A., Miller, R., & Bothe, D. (2014). On the applicability of drop profile analysis tensiometry at high flow rates using an interface tracking method. *Colloids and Surfaces A: Physicochemical and Engineering Aspects*, 441, 837-845.
35. Frumkin, A., & Levich, V. G. (1947). On surfactants and interfacial motion. *Zh. Fiz. Khim*, 21, 1183-1204.
36. Levich, V. G., & Technica, S. (1962). *Physicochemical hydrodynamics* (Vol. 689). Englewood Cliffs, NJ: Prentice-hall.
37. Harper, J. F. (1974). On spherical bubbles rising steadily in dilute surfactant solutions. *The Quarterly Journal of Mechanics and Applied Mathematics*, 27(1), 87-100.
38. Cuenot, B., Magnaudet, J., & Spennato, B. (1997). The effects of slightly soluble surfactants on the flow around a spherical bubble. *Journal of Fluid Mechanics*, 339, 25-53.
39. Griffith, R. M. (1962). The effect of surfactants on the terminal velocity of drops and bubbles. *Chemical Engineering Science*, 17(12), 1057-1070.
40. Saville, D. A. (1973). The effects of interfacial tension gradients on the motion of drops and bubbles. *The Chemical Engineering Journal*, 5(3), 251-259.

41. Alves, S. S., Orvalho, S. P., & Vasconcelos, J. M. T. (2005). Effect of bubble contamination on rise velocity and mass transfer. *Chemical Engineering Science*, 60(1), 1-9.
42. Malysa, K., Krasowska, M., & Krzan, M. (2005). Influence of surface active substances on bubble motion and collision with various interfaces. *Advances in colloid and interface science*, 114, 205-225.
43. Zhang, Y., & Finch, J. A. (2001). A note on single bubble motion in surfactant solutions. *Journal of Fluid Mechanics*, 429, 63-66.
44. Chen, J., & Stebe, K. J. (1996). Marangoni retardation of the terminal velocity of a settling droplet: The role of surfactant physico-chemistry. *Journal of Colloid and interface science*, 178(1), 144-155.
45. Davis, R. E., & Acrivos, A. (1966). The influence of surfactants on the creeping motion of bubbles. *Chemical Engineering Science*, 21(8), 681-685.
46. Harper, J. F. (1982). Surface activity and bubble motion. *Applied Scientific Research*, 38(1), 343-352.
47. Harper, J. F. (1973). On bubbles with small immobile adsorbed films rising in liquids at low Reynolds numbers. *Journal of Fluid Mechanics*, 58(03), 539-545.
48. Leven, M. D., & Newman, J. (1976). The effect of surfactant on the terminal and interfacial velocities of a bubble or drop. *AIChE Journal*, 22(4), 695-701.
49. Liao, Y., & McLaughlin, J. B. (2000). Bubble motion in aqueous surfactant solutions. *Journal of colloid and interface science*, 224(2), 297-310.
50. Dukhin, S. S., Miller, R., & Loglio, G. (1998). Physico-chemical hydrodynamics of rising bubble. *Studies in Interface Science*, 6, 367-432.
51. Sadhal, S.S. and R.E. Johnson, Stokes flow past bubbles and drops partially coated with thin films. Part 1. Stagnant cap of surfactant film - exact solution, 1983, *Cambridge Journals Online*. p. 237-250.
52. He, Z., Maldarelli, C., & Dagan, Z. (1991). The size of stagnant caps of bulk soluble surfactant on the interfaces of translating fluid droplets. *Journal of colloid and interface science*, 146(2), 442-451.
53. Krzan, M., Lunkenheimer, K., & Malysa, K. (2004). On the influence of the surfactant's polar group on the local and terminal velocities of bubbles. *Colloids and Surfaces A: Physicochemical and Engineering Aspects*, 250(1), 431-441.

54. Krzan, M., & Malysa, K. (2002). Profiles of local velocities of bubbles in n-butanol, n-hexanol and n-nonanol solutions. *Colloids and Surfaces A: Physicochemical and Engineering Aspects*, 207(1), 279-291.
55. Krzan, M., Zawala, J., & Malysa, K. (2007). Development of steady state adsorption distribution over interface of a bubble rising in solutions of n-alkanols (C 5, C 8) and n-alkyltrimethylammonium bromides (C 8, C 12, C 16). *Colloids and Surfaces A: Physicochemical and Engineering Aspects*, 298(1), 42-51.
56. Ng, S., Warszynski, P., Zembala, M., & Malysa, K. (2000). Bitumen-air aggregates flow to froth layer: I. Method of analysis. *Minerals engineering*, 13(14), 1505-1517.
57. Stebe, K. J., & Maldarelli, C. (1994). Remobilizing surfactant retarded fluid particle interfaces: Ii. Controlling the surface mobility at interfaces of solutions containing surface active components. *Journal of colloid and interface science*, 163(1), 177-189.
58. Exerowa, D., & Kruglyakov, P. M. (1997). *Foam and foam films: theory, experiment, application* (Vol. 5). Elsevier. ISBN 9780080531809.
59. Bikerman, J. J. (1973). *Foams*. Springer-Verlag New York.
60. Derjaguin, B. V., & Landau, L. (1941). The theory of stability of highly charged lyophobic sols and coalescence of highly charged particles in electrolyte solutions. *Acta Physicochim. URSS*, 14, 633-52.
61. Verwey, E. J. W., Overbeek, J. T. G., & Overbeek, J. T. G. (1999). *Theory of the stability of lyophobic colloids*. Courier Corporation.
62. Sheludko, A. (1967). Thin liquid films. *Advances in Colloid and Interface Science*, 1(4), 391-464.
63. Scheludko, A., Platikanov, D., & Manev, E. (1965). Disjoining pressure in thin liquid films and the electro-magnetic retardation effect of the molecule dispersion interactions. *Discussions of the Faraday Society*, 40, 253-265.
64. Boinovich, L. (2010). DLVO forces in thin liquid films beyond the conventional DLVO theory. *Current Opinion in Colloid & Interface Science*, 15(5), 297-302.
65. Weaire, D., & Hutzler, S. *The physics of foams*. 1999.
66. Cascão Pereira, L. G., Johansson, C., Radke, C. J., & Blanch, H. W. (2003). Surface forces and drainage kinetics of protein-stabilized aqueous films. *Langmuir*, 19(18), 7503-7513.
67. Wilde, P. J., Rodríguez Niño, M. R., Clark, D. C., & Rodríguez Patino, J. M. (1997). Molecular diffusion and drainage of thin liquid films stabilized by bovine serum albumin-

- Tween 20 mixtures in aqueous solutions of ethanol and sucrose. *Langmuir*, 13(26), 7151-7157.
68. Kotsmar, C., Arabadzhieva, D., Khristov, K., Mileva, E., Grigoriev, D. O., Miller, R., & Exerowa, D. (2009). Adsorption layer and foam film properties of mixed solutions containing β -casein and C 12 DMPO. *Food hydrocolloids*, 23(4), 1169-1176.
 69. Verbist, G., Weaire, D., & Kraynik, A. M. (1996). The foam drainage equation. *Journal of Physics. Condensed Matter*, 8(21), 3715-3731.
 70. Gol'dfarb, I. I., Kann, K. B., & Shreiber, I. R. (1988). Liquid flow in foams. *Fluid Dynamics*, 23(2), 244-249.
 71. Koehler, S. A., Hilgenfeldt, S., Weeks, E. R., & Stone, H. A. (2002). Drainage of single Plateau borders: Direct observation of rigid and mobile interfaces. *Physical Review E*, 66(4), 040601.
 72. Prins, A. (1999). Stagnant surface behaviour and its effect on foam and film stability. *Colloids and Surfaces A: Physicochemical and Engineering Aspects*, 149(1), 467-473.
 73. Stevenson, P. (2005). Remarks on the shear viscosity of surfaces stabilised with soluble surfactants. *Journal of colloid and interface science*, 290(2), 603-606.
 74. Mysels, K. J. (1959). *Soap films: studies of their thinning and a bibliography*. Pergamon Press.
 75. Pitois, O., Fritz, C., & Vignes-Adler, M. (2005). Liquid drainage through aqueous foam: study of the flow on the bubble scale. *Journal of colloid and interface science*, 282(2), 458-465.
 76. Saint-Jalmes, A., Zhang, Y., & Langevin, D. (2004). Quantitative description of foam drainage: Transitions with surface mobility. *The European Physical Journal E*, 15(1), 53-60.
 77. Petkov, J. T., Danov, K. D., Denkov, N. D., Aust, R., & Durst, F. (1996). Precise method for measuring the shear surface viscosity of surfactant monolayers. *Langmuir*, 12(11), 2650-2653.
 78. Poskanzer, A. M., & Goodrich, F. C. (1975). Surface viscosity of sodium dodecyl sulfate solutions with and without added dodecanol. *The Journal of Physical Chemistry*, 79(20), 2122-2126.
 79. Patist, A., Axelberd, T., & Shah, D. O. (1998). Effect of long chain alcohols on micellar relaxation time and foaming properties of sodium dodecyl sulfate solutions. *Journal of colloid and interface science*, 208(1), 259-265.

80. Durand, M., & Langevin, D. (2002). Physicochemical approach to the theory of foam drainage. *The European Physical Journal E*, 7(1), 35-44.
81. Stevenson, P., & Stevanov, C. (2004). Effect of rheology and interfacial rigidity on liquid recovery from rising froth. *Industrial & engineering chemistry research*, 43(19), 6187-6194.
82. Elizalde, B. E., Giaccaglia, D., Pilosof, A. M. R., & Bartholomai, G. B. (1991). Kinetics of Liquid Drainage from Protein-Stabilized Foams. *Journal of food science*, 56(1), 24-26.
83. Disalvo, E. A. (1988). Permeability of water and polar solutes in lipid bilayers. *Advances in colloid and interface science*, 29(1), 141-170.
84. Murray, B. S., & Ettelaie, R. (2004). Foam stability: proteins and nanoparticles. *Current Opinion in Colloid & Interface Science*, 9(5), 314-320.
85. Wierenga, P. A., & Gruppen, H. (2010). New views on foams from protein solutions. *Current Opinion in Colloid & Interface Science*, 15(5), 365-373.
86. Harvey, P. A., Nguyen, A. V., Jameson, G. J., & Evans, G. M. (2005). Influence of sodium dodecyl sulphate and Dowfroth frothers on froth stability. *Minerals engineering*, 18(3), 311-315.
87. Brown, A. G., Thuman, W. C., & McBain, J. W. (1953). Transfer of air through adsorbed surface films as a factor in foam stability. *Journal of Colloid Science*, 8(5), 508-519.
88. Brown, A. G., Thuman, W. C., & McBain, J. W. (1953). The surface viscosity of detergent solutions as a factor in foam stability. *Journal of Colloid Science*, 8(5), 491-507.
89. Shah, D. O., Djabbarah, N. F., & Wasan, D. T. (1978). A correlation of foam stability with surface shear viscosity and area per molecule in mixed surfactant systems. *Colloid and Polymer Science*, 256(10), 1002-1008.
90. Wilde, P. J. (2000). Interfaces: their role in foam and emulsion behaviour. *Current Opinion in Colloid & Interface Science*, 5(3), 176-181.
91. Małysa, K., Miller, R., & Lunkenheimer, K. (1991). Relationship between foam stability and surface elasticity forces: fatty acid solutions. *Colloids and surfaces*, 53(1), 47-62.
92. Wantke, K., Małysa, K., & Lunkenheimer, K. (1994). A relation between dynamic foam stability and surface elasticity. *Colloids and Surfaces A: Physicochemical and Engineering Aspects*, 82(2), 183-191.
93. Fruhner, H., Wantke, K. D., & Lunkenheimer, K. (2000). Relationship between surface dilational properties and foam stability. *Colloids and Surfaces A: Physicochemical and Engineering Aspects*, 162(1), 193-202.

94. Acharya, D. P., Gutiérrez, J. M., Aramaki, K., Aratani, K. I., & Kunieda, H. (2005). Interfacial properties and foam stability effect of novel gemini-type surfactants in aqueous solutions. *Journal of colloid and interface science*, 291(1), 236-243.
95. Coke, M., Wilde, P. J., Russell, E. J., & Clark, D. C. (1990). The influence of surface composition and molecular diffusion on the stability of foams formed from protein/surfactant mixtures. *Journal of Colloid and Interface Science*, 138(2), 489-504.
96. Kim, S. H., & Kinsella, J. E. (1985). Surface activity of food proteins: relationships between surface pressure development, viscoelasticity of interfacial films and foam stability of bovine serum albumin. *Journal of Food Science*, 50(6), 1526-1530.
97. Martin, A. H., Grolle, K., Bos, M. A., Stuart, M. A. C., & van Vliet, T. (2002). Network forming properties of various proteins adsorbed at the air/water interface in relation to foam stability. *Journal of Colloid and Interface Science*, 254(1), 175-183.
98. Monteux, C., Fuller, G. G., & Bergeron, V. (2004). Shear and dilational surface rheology of oppositely charged polyelectrolyte/surfactant microgels adsorbed at the air-water interface. Influence on foam stability. *The Journal of Physical Chemistry B*, 108(42), 16473-16482.
99. Bhattacharyya, A., Monroy, F., Langevin, D., & Argillier, J. F. (2000). Surface rheology and foam stability of mixed surfactant-polyelectrolyte solutions. *Langmuir*, 16(23), 8727-8732.
100. Horiuchi, T., Fukushima, D., Sugimoto, H., & Hattori, T. (1978). Studies on enzyme-modified proteins as foaming agents: effect of structure on foam stability. *Food Chemistry*, 3(1), 35-42.
101. Kim, S. H., & Kinsella, J. E. (1987). Surface active properties of proteins: effects of progressive succinylation on film properties and foam stability of glycinin. *Journal of Food Science*, 52(5), 1341-1343.
102. Sarker, D. K., Wilde, P. J., & Clark, D. C. (1998). Enhancement of protein foam stability by formation of wheat arabinoxylan-protein crosslinks. *Cereal Chemistry*, 75(4), 493-499.
103. Ipsen, R., Otte, J., Sharma, R., Nielsen, A., Hansen, L. G., & Qvist, K. B. (2001). Effect of limited hydrolysis on the interfacial rheology and foaming properties of β -lactoglobulin A. *Colloids and Surfaces B: Biointerfaces*, 21(1), 173-178.

104. Husband, F. A., Wilde, P. J., Mackie, A. R., & Garrood, M. J. (1997). A comparison of the functional and interfacial properties of β -casein and dephosphorylated β -casein. *Journal of colloid and interface science*, 195(1), 77-85.
105. Le Floch-Fouéré, C., Pezenec, S., Lechevalier, V., Beaufils, S., Desbat, B., Pézolet, M., & Renault, A. (2009). Synergy between ovalbumin and lysozyme leads to non-additive interfacial and foaming properties of mixtures. *Food Hydrocolloids*, 23(2), 352-365.
106. Hawks, S. E., Phillips, L. G., Rasmussen, R. R., Barbano, D. M., & Kinsella, J. E. (1993). Effects of processing treatment and cheese-making parameters on foaming properties of whey protein isolates. *Journal of dairy science*, 76(9), 2468-2477.
107. Stevenson, P. (Ed.). (2012). *Foam engineering: fundamentals and applications*. John Wiley & Sons.
108. Nguyen, A., & Schulze, H. J. (2003). *Colloidal science of flotation* (Vol. 118). CRC Press.
109. Binks, B. P. (2002). Particles as surfactants—similarities and differences. *Current opinion in colloid & interface science*, 7(1), 21-41.

4. Material & Methods

4.1. Materials

4.1.1. Surfactants

Surfactants are amphiphilic substances which adsorb at either water/air or water/oil interface and decrease the interfacial tension. Proteins, polymers, polyelectrolytes and belong to the high molecular-weight group of substances characterized by some more specific properties. Generally, surfactants consist of two parts, which possess properties opposite to each other by their nature. One part of the molecule is the hydrophilic polar head group, for example, $-\text{NH}_2$, $-\text{OH}$, $-\text{COOH}$, $-\text{SO}_3\text{H}$, $-\text{OSO}_3\text{H}$, $-\text{N}(\text{CH}_3)_3\text{Cl}$, $-\text{CH}_2\text{CH}_2\text{O}$. The other part is formed by a rather long hydrocarbon or hydrofluorine, hydrophobic (oleophilic) chain. In contrast, high molecular-weight surfactants can contain hydrophilic and hydrophobic molecular groups distributed irregularly along the whole molecule chain.

Surfactants can be divided into two major categories – **ionic** and **non-ionic** based on whether the hydrophilic head group is charged or not. The non-ionic surfactants contain polar groups consisting of atoms of oxygen, nitrogen, phosphorus or sulphur (alcohols, amines, ethers, esters etc.). For example, Tween and Span are commonly used as food grade surfactants. These polar groups are unable to dissociate and possess a significant affinity to water and other polar substances. Contrary to this, ionic surfactants can be represented by anionic (-ve) and cationic (+ve) surfactants depending on the sign of the charge of the polar head group. Among the anionic surfactants, the most significant are salts of fatty acids (RCO_2Me), alkyl sulphates (sulphoether salts) ROSO_3Me , alkyl sulphonates RSO_3Me , alkyl aryl sulphonates $\text{RC}_6\text{H}_5\text{SO}_3\text{Me}$, alkyl phosphates $\text{ROPO}(\text{OMe})_2$, salts of sulphosuccinic acids. The typical surfactants which belong to this class are sodium dodecyl sulphate (SDS), sodium oleate and sodium dodecyl benzene sulphonate. Among the cationic surfactants, the most common are the salts of (primary, secondary and tertiary) amines, and quaternary salts of ammonium, for example, cetyl trimethyl ammonium bromide (C_{16}TAB) and octadecyl pyridinium chloride [1].

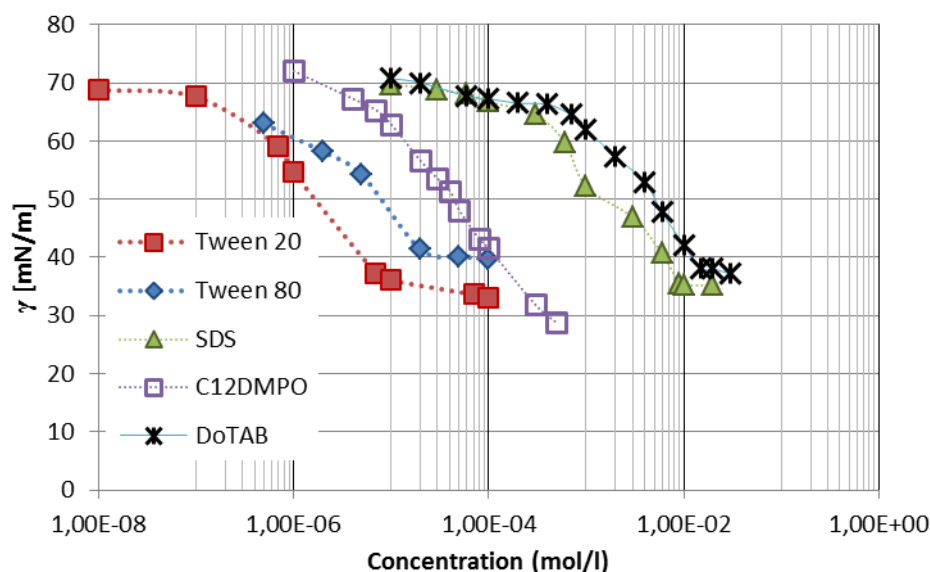


Figure 4.1 Adsorption isotherm of various surfactants at water/air interface, redrawn from [2-5].

The above figure gives us information on equilibrium surface tension values of different surfactants vs. concentration. These are the different surfactants used in this study. The Tween 20 (mol.wt. 1228 g/mol) and Tween 80 (mol.wt. 1312 g/mol) were chosen due to their food grade. We could notice from the above graph that at the same alkyl chain length the non-ionic surfactants are more surface active than the ionic surfactants.

4.1.2. Proteins

Proteins are macromolecules consisting of amino acids which are linked through peptide bonds. There are 20 different types of amino acids of which some are hydrophilic and some are hydrophobic. So the combination of these two kinds of amino acids gives rise to an amphiphilic character of proteins. In an aqueous solution the protein molecule is configured in such a way that the hydrophobic part is hidden in the interior core and the hydrophilic part remains in the outer part of the molecule though few non-polar residues could also remain in the exterior part. Due to this amphiphilic nature, the proteins are surface active though not as efficient in reducing the interfacial tension as surfactants.

The amino acids which form $\text{COO}^- \text{NH}^+$ bonds with each other would represent its primary structure and this polypeptide chain could configure in α -helix or in β sheets which defines the secondary structure of the protein stabilized by hydrogen bonds. The proteins can be either globular (β -lactoglobulin, BLG with mol.wt – 18,6kDa) or random-coiled (β -casein,

BCS mol.wt – 23,4kDa) based on their tertiary structure which are held together by disulphide bridges [6].

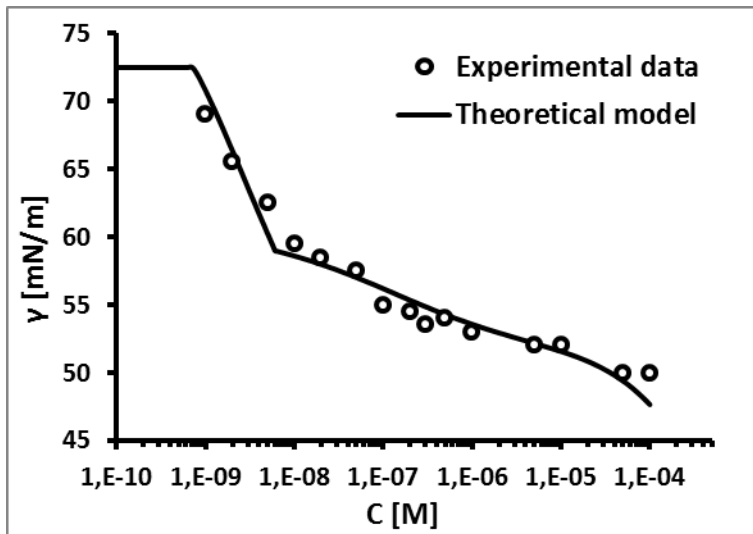


Figure 4.2 Adsorption isotherm of BLG solution prepared in 10mM citric phosphate buffer at pH 7 at water/air interface, redrawn from [7].

In this thesis the majority of the results presented are for BLG. By comparing the Fig. 4.1 and 4.2 we could see the difference in surface activity of BLG and low-molecular weight surfactants. Even a concentration as low as 1×10^{-8} M can reduce the surface tension until about 60 mN/m. Whereas for surfactants in Fig. 4.1 at this bulk solution concentration no surface tension change can be noticed yet.

4.2. Experimental Methods

4.2.1. Maximum bubble pressure tensiometer

This is a method based on the Laplace equation; while here it involves the measurement of the maximum pressure in a bubble growing at the tip of a capillary immersed into the liquid under study. When a bubble grows at the tip of a capillary, its radius of curvature decreases up to a hemisphere, and then increases again. Therefore, the pressure is maximum at the hemispherical shape of the bubble and at this point the radius of curvature is equal to that of radius of capillary [8] as shown in Fig.4.3.

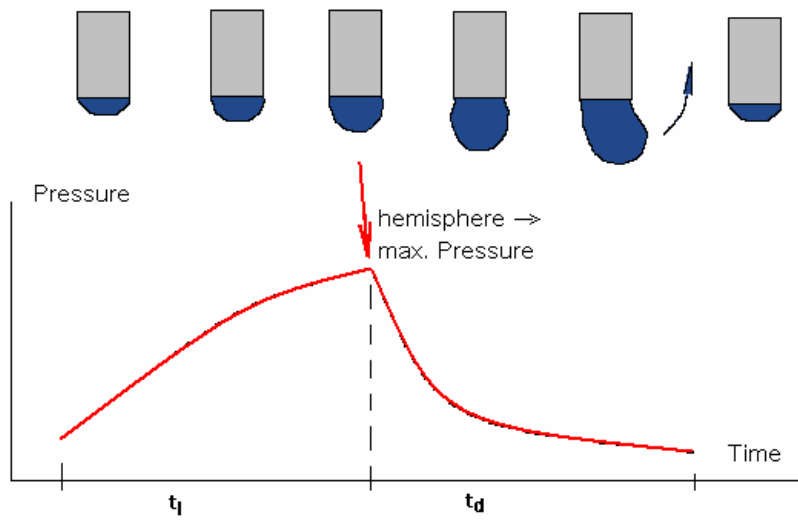


Figure 4.3. Schematic of the working principle for a maximum bubble pressure tensiometer.

The capillary pressure together with the hydrostatic pressure due to the immersion of the capillary tip into the liquid at a depth h gives the following form for the total pressure maximum.

$$P_{\max} = 2\gamma / R + \Delta\rho gh \quad (30)$$

$\Delta\rho$ is the density difference between the liquid and air, and g is the gravity constant. The time from the start of bubble growth to the maximum pressure at a hemispherical size is called lifetime t_l , and the interval from this hemisphere until bubble departure is called dead time, t_d . Both times together give the bubble time $t_b = t_l + t_d$. As the bubble surface grows during the experiment, the expansion has to be considered in the evaluation of the so-called effective surface age which is described in detail in [8].

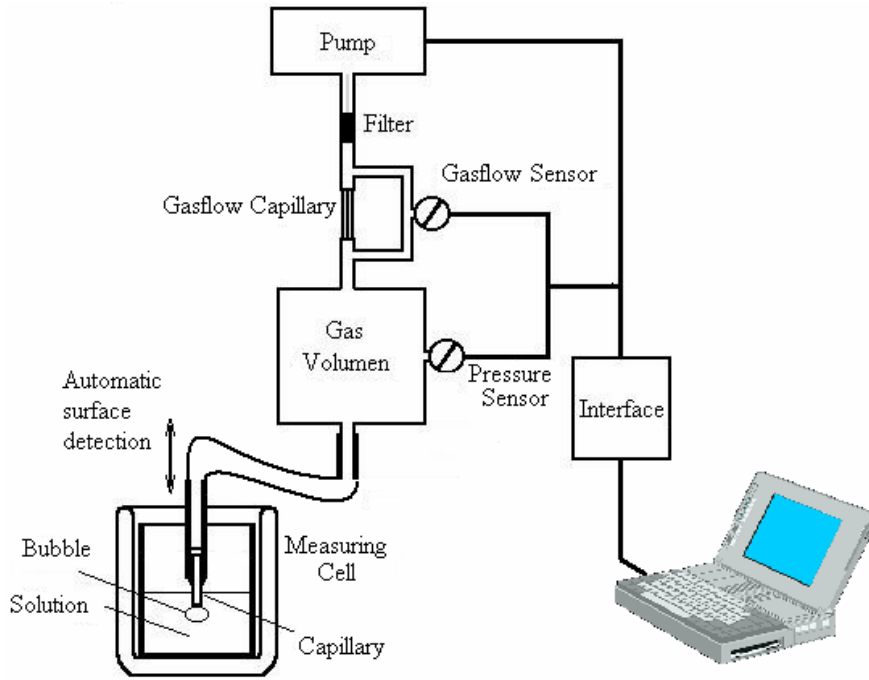


Figure 4.4. Schematic of a maximum bubble pressure tensiometer setup (BPA from SINTERFACE Technologies)

The Fig. 4.4 shows the schematic of the bubble pressure instrument BPA. A controlled smooth and continuous gas flow is produced by the pump connected to a gas flow sensor. The pressure sensor measures the pressure in the gas volume, which is proportional to the maximum pressure at the capillary tip. The pump and the two sensors are controlled by a computer via an electronic interface board. The measured data, i.e. the maximum pressure detected for each of several bubbles formed at a given gas flow rate is translated into surface tension vs. bubble life time (or the effective life time). This technique is complementary to the PAT in terms of time range [8]. It covers adsorption times of about 100 s down to few milliseconds. Special designed capillaries even allow to measure dynamic surface tension values for adsorption times less than 1 millisecond.

4.2.2. Bubble and drop profile analysis tensiometry

The surface tension γ of liquids can be also measured by the so-called profile analysis tensiometry (PAT). This method is based on the equation of capillarity, which was first formulated by Laplace in 1804 [9]

$$\gamma \left[\frac{1}{R_1} + \frac{1}{R_2} \right] = \Delta \rho g (z + z_0). \quad (31)$$

R_1 and R_2 are the two main radii of curvature of the axisymmetric drop, $\Delta\rho$ is the density difference between the two fluid media, g is the gravity constant and z is the height, while z_0 is a reference line, typically located in the apex of the drop.

After the formulation of the equation of capillarity by Laplace, a very important further step was done then by Rotenberg, Boruvka and Neumann in 1983 [10] who developed the so-called Axisymmetric Drop Shape Analysis (ADSA). This methodology fitted for the first time the Laplacian profiles to a completely measured drop profile for getting γ as the best fit parameter.

The scheme of a PAT instrument is shown in Fig. 4.5 with the key elements being a video camera with objective, a suitable light source, and an accurate dosing system. All of these elements are controlled by a computer.

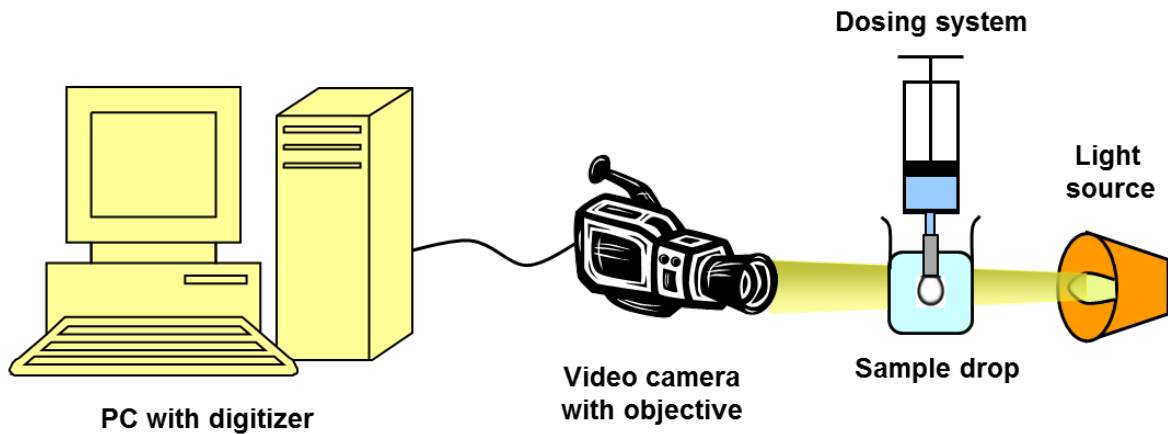


Fig. 4.5. Scheme of a PAT instrument with its main elements

The software of all PAT-type instruments provides different protocols for experiments to be performed. Such protocols can be composed of parts with a constant drop size, drop size oscillations at different frequencies, or ramp-type drop size changes. For all these drop size manipulations an accurate dosing system is required.

The Laplace equation, given by Eq. (31), can be rewritten into a set of first-order differential equations, as given by the set of equations (32) to (34):

$$\frac{dx}{ds} = \cos(\phi) \tag{32}$$

$$\frac{dz}{ds} = \sin(\phi) \tag{33}$$

$$\frac{d\phi}{ds} = \pm \frac{\beta z}{b^2} + \frac{2}{b} - \frac{\sin(\phi)}{x} \quad (34)$$

The sign in Eq. (34) is "plus" for sessile drops or captive bubbles and "minus" for pendant drops or emerging bubbles, b is the radius of curvature at the bubble apex (0,0) and β is the so-called shape factor

$$\beta = \frac{\Delta\rho g b^2}{\gamma} \quad (35)$$

The geometric parameters used in these equations are the arc length s , the normal angle ϕ , and x and z are the abscissa and ordinate of the profile point, as shown in Fig. 4.6.

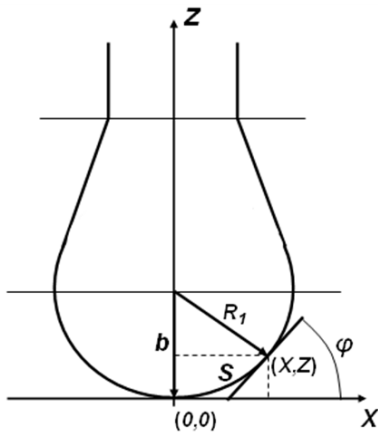


Figure 4.6. Axisymmetric liquid profile with the definition of all geometric parameters

The set of Eqs. (32) to (34) can be solved numerically by various methods out of which the fourth-order Runge-Kutta routine is the most frequently used one.

With an efficient code for solving the Laplace equation, in addition a strategy for fitting the calculated profile to the measured profile is required and a target function is needed to evaluate the quality of this fitting. The strategy proposed by Levenberg [11] and Marquardt [12] turned out to be the most efficient non-linear optimization method.

The typical application of PAT is the measurement of the dynamic interfacial tension at adsorption times of seconds to hours and longer. In addition the dilational surface visco-elasticity of aqueous solutions of surfactants and proteins can be obtained. As example, Fig. 4.7 shows the surface pressure $\Pi = \gamma_0 - \gamma(t)$ as a function of time t plotted on a logarithmic scale (γ_0 is the surface tension of water). Over the whole large time interval of this experiment, intermediate oscillations at a frequency of 0.1 Hz have been performed in order to determine the dilational visco-elasticity as a function of time.

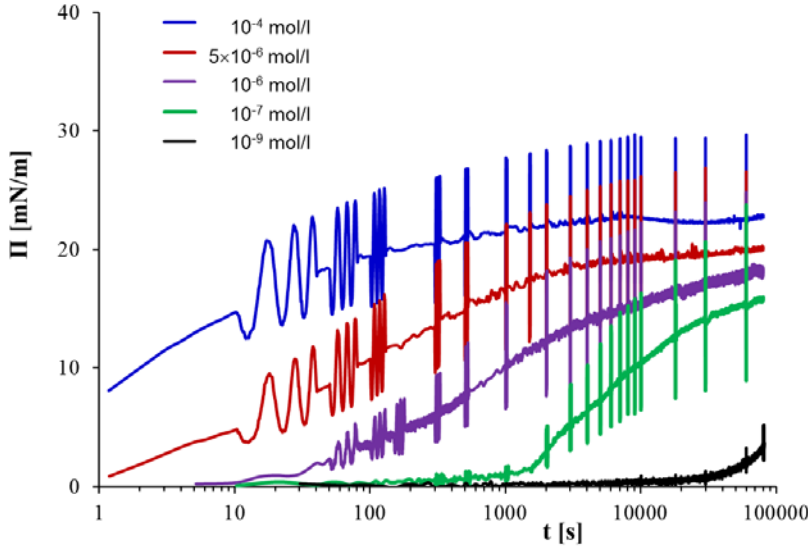


Figure 4.7. Surface pressure Π as a function of time for several BLG concentrations at pH 7, $C_{\text{buff}} = 10 \text{ mM}$; adapted from [7]

An important feature in the adsorption process of a protein is the so-called induction time. This is a time interval during which the protein molecules adsorb but do not lead to measurable changes in the surface tension. At the water/air interface this induction time is about 10 s for a BLG concentration of 10^{-6} mol/l .

The drop oscillations performed during the experiments as shown in Fig.4.7 allow to derive the dilational visco-elasticity of the adsorbed BLG layer. The amplitude of the oscillation is a measure for the dilational elasticity defined by

$$E = -\frac{d\gamma}{d \ln \Gamma} = \frac{d\gamma}{d \ln A} \quad (36)$$

while the phase shift is a measure for the dilational viscosity (A is the interfacial area). As discussed in [13], the visco-elasticity of an adsorption layer can be given by the complex function $E(i\omega)$

$$E(i\omega) = E' + iE'' = E_0 \frac{\sqrt{i\omega}}{\sqrt{i\omega} + \sqrt{2\omega_0}} \quad (37)$$

Here the parameters E' and E'' are the real and imaginary components of the complex visco-elasticity, E_0 is the elasticity modulus, ω is the circular frequency $\omega = 2\pi f$ (f is the frequency of the oscillation process). The characteristic frequency ω_0 is defined by the main characteristics of the studied surfactant

$$\omega_0 = \left[\frac{dc}{d\Gamma} \right]^2 (D/2) \quad (38)$$

Lucassen and van den Tempel [14] derived the corresponding equations for a diffusion controlled relaxation mechanism, which is the most frequently applied model to describe the frequency and concentration dependencies of E' and E'' :

$$E' = E_0 \frac{1 + \sqrt{\omega_0 / \omega}}{1 + 2\sqrt{\omega_0 / \omega} + 2\omega_0 / \omega} \quad (39)$$

$$E'' = E_0 \frac{\sqrt{\omega_0 / \omega}}{1 + 2\sqrt{\omega_0 / \omega} + 2\omega_0 / \omega} \quad (40)$$

The data shown in Fig. 4.8 are the results for E' measured at the end of the maximum adsorption time of 80.000 s (shown in Fig. 4.7) at frequencies between 0.01 Hz and 0.2 Hz. As one can see, there is a small dependence in this frequency range, as expected for adsorbed protein molecules in this concentration range.

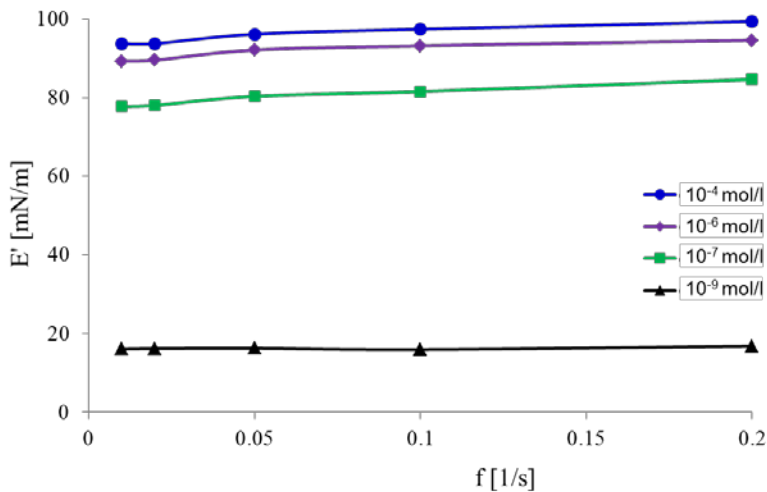


Figure. 4.8. Dilational elasticity E' as a function of the oscillation frequency at constant area deformation (oscillation amplitude) $\Delta A/A=0.05$, air bubble in BLG solution at pH 7, $C_{\text{buff}} = 10$ mmol/l; adapted from [7].

Even at bulk concentrations as low as 10^{-9} mol/l, a concentration range in which classical surfactants do not show any adsorption behaviour, the protein BLG adsorbs strongly and the corresponding adsorption layers exhibit a remarkable dilational surface elasticity.

4.2.3. Rising bubble setup

The setup consists of a glass column of a square cross section area of $40\text{ mm} \times 40\text{ mm}$ and a height of 50 cm , as shown in Fig. 4.9 below. A capillary of inner diameter 0.075 mm is fitted to the bottom of this glass column which is connected to a syringe pump for the air supply. The flow rate is set to level that the time interval between two bubbles is more than 10 seconds to be sure that the liquid in the column is quiescent. The digital camera is fitted to a calibrated scale which could be moved along the axis of glass column to capture the image of a bubble at any required distance. Finally, a stroboscope is used as light source and this would produce flashes of light at desired frequency, f_s .

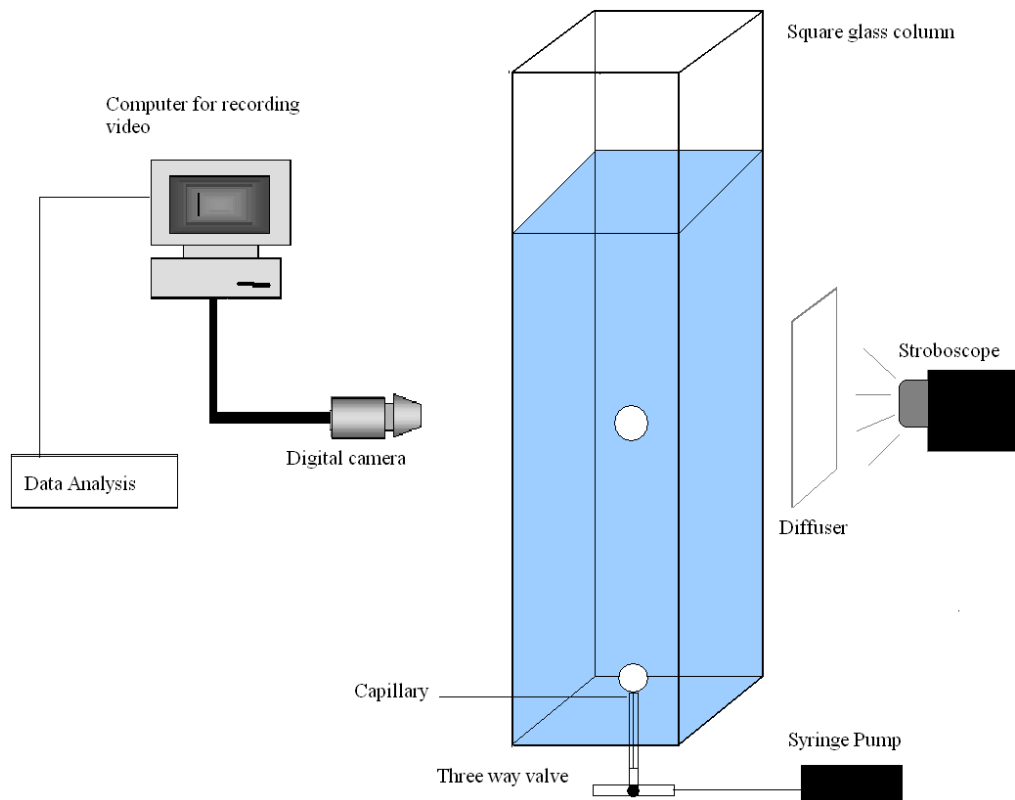


Figure 4.9. Schematic of the rising bubble instrument

Therefore, for obtaining velocity profiles the images were extracted from the video and analyzed as follows.

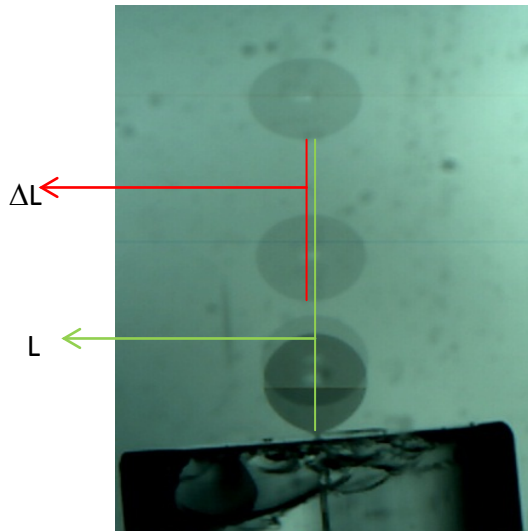


Figure 4.10. Image of a rising bubble taken with a stroboscopic light source

Here the distance L is the distance between the capillary tip and the bubble and its local velocity, U_L at this distance is $\Delta L/t$. The distance between the bottom poles of two subsequent bubble images is ΔL and t is the time between two subsequent flashes from the stroboscope i.e. $t=1/f$.

The detaching bubbles here have a time of adsorption which is 1.6 s and hence there would be a diffusion of surface active components toward the growing bubble surface. Depending on the bulk concentration there would be partial or complete coverage of the detaching bubble surface which would give different kind of velocity profiles of the subsequently rising bubble. In case of pure water there is an initial acceleration followed by a steady state velocity known as terminal velocity. This terminal velocity for a bubble size of 1.45 mm rising in clean water was measured to be 34.8 ± 0.2 cm/s [15]. Whereas when the bubble reaches a rigid surface the terminal velocity reaches around 16.5 cm/s.

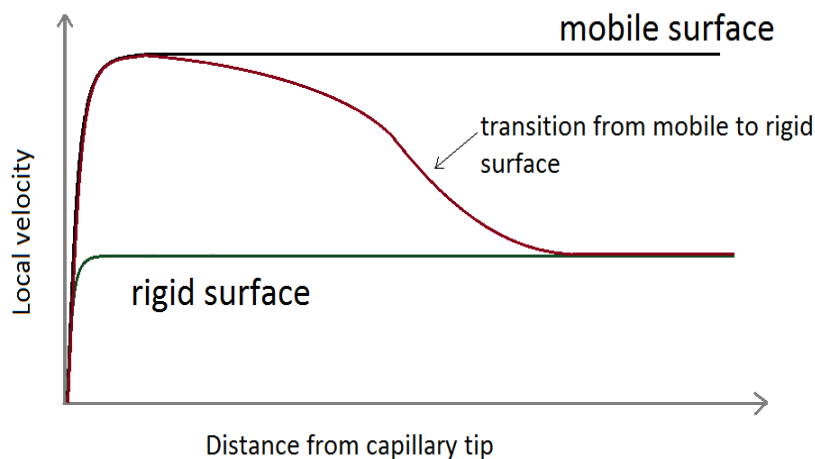


Figure 4.11. An example of local velocity profile plotted against distance travelled by the bubble from the tip of the capillary

Fig. 4.11 shows the typical graph with the local velocity of a bubble plotted against the distance from the capillary tip. For a bubble rising in clean water i.e. when the surface of the bubble is mobile there is an acceleration followed by a constant velocity which is the terminal velocity. The same is observed in case when the surfactant concentration is high enough that the bubble surface quickly attains a rigid surface. But the terminal velocity is lower than for a mobile surface as there is more drag force on a rigid surface.

At an intermediate concentration however the bubble surface undergoes a transition from a mobile surface to a rigid surface as seen in fig. 4.11. Therefore, the concentration at which the bubble behaves completely as a rigid sphere is the limit of this experimental technique as beyond this point any increase in concentration of surfactant would give the same velocity profile. Hence, the transitions from a mobile to rigid surface are studied at certain concentrations gives us information about the distance the bubble needs to travel during its rising to achieve a rigid surface. This information helps to understand empirically the adsorption coverage at dynamic conditions.

4.2.4. Foam stability setup

4.2.4.1. Square glass column foam setup

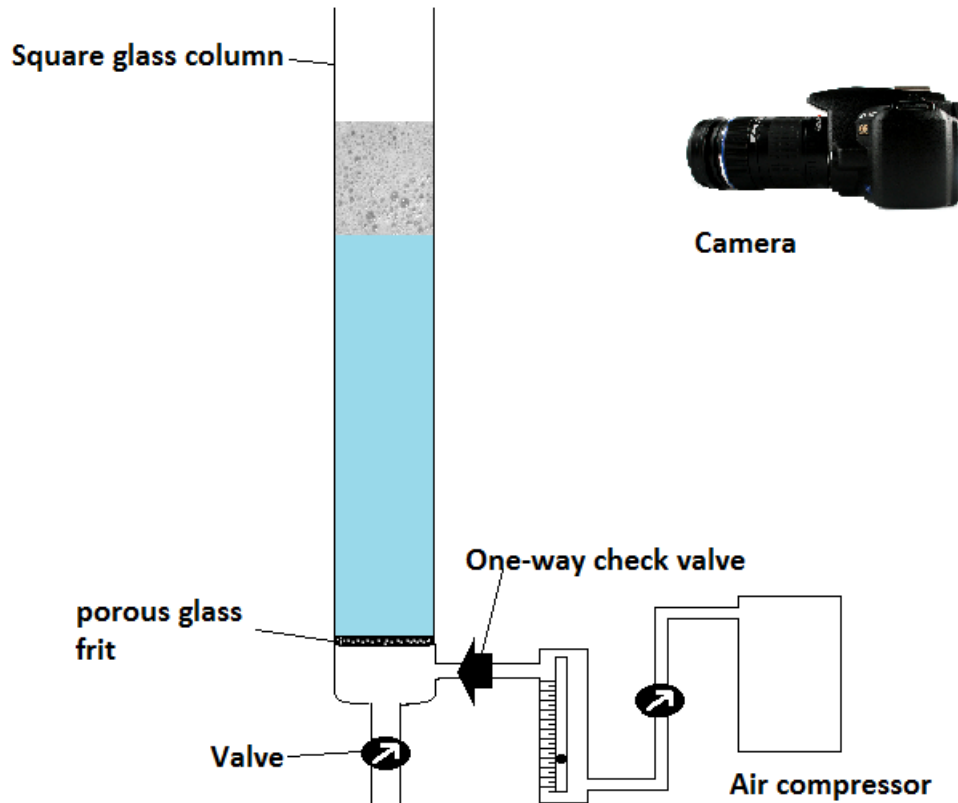


Figure 4.12. Foam formation and stability setup with square glass column.

The square glass column with a cross section area of $40 \text{ mm} \times 40 \text{ mm}$ and a height of 50 cm is fitted to a porous glass frit material. The air compressor is connected to an air flow meter as shown above. The air entering the flow meter is controlled by a valve and thereby the desired flow rate is achieved. At the bottom the frit material is connected to the glass column and there is an outlet with a valve. When the valve is open the liquid in the square glass column can drip through the frit and drain through the outlet below.

To fill the glass column with liquid, first the outlet valve below the frit is closed tightly. A little amount of air is let to pass through the one-way check valve. Therefore, there will a little pressure inside the chamber between the porous frit and the outlet valve. Then the liquid that needs to be foamed is poured along the walls into the square glass column. After filling in the liquid the air is pumped at a desired flow rate for a required period of time.

4.2.4.2. Dynamic foam analyzer (DFA 100, Krüss)

The dynamic foam analyzer setup DFA 100 consists of a glass column which is fitted in between a light sensor array and a LED light panel. The whole glass column is scanned at the same time and the intensity of the light detected by the sensors gives the height of the foam.

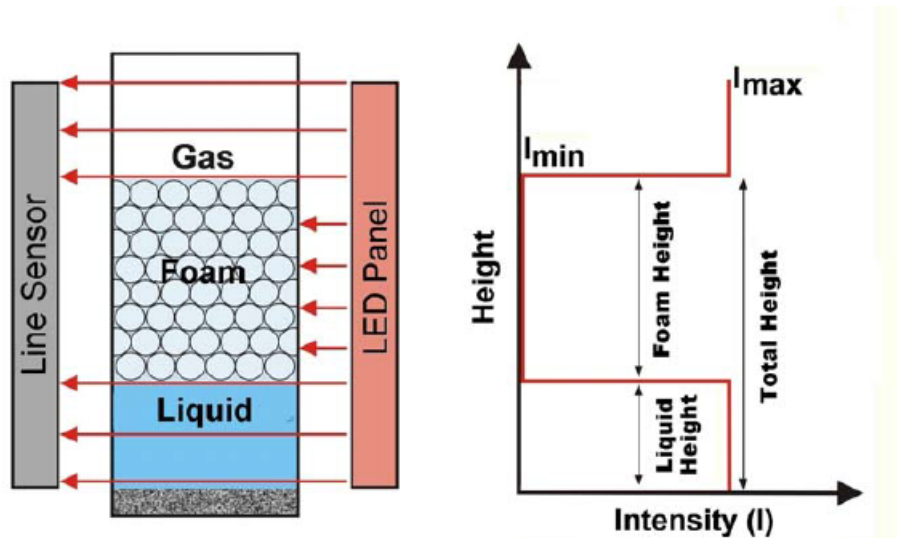


Figure 4.13. Schematic diagram for the working principle of the dynamic foam analyzer DFA 100 (Krüss).

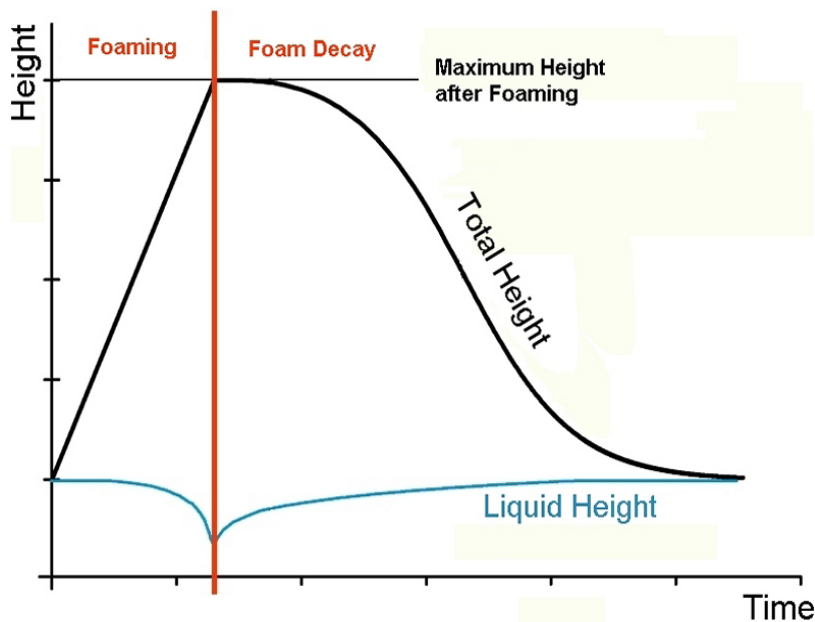


Figure 4.14. Example of a foaming experiment performed by the dynamic foam analyzer DFA 100 (Krüss).

The experiments were performed at constant foam height of 180mm. The instrument is programmed to sparge through the porous frit material at 0.15 l/min until the foam reaches a height of 180mm and the decay of the foam was scanned at regular intervals by the device as shown in Fig. 4.13. The volume of liquid which is used was 50 ml and it let allowed to flow gently into the glass cylinder. The liquid height was about 40 mm and, therefore, the total height of foam and liquid would be 220mm. The liquid height is subtracted in the data to derive the foam height. An illustration of the experimental result is given in the Fig. 4.13.

4.2.5. Foam fractionation setup

4.2.5.1. Foam fractionation setup at MPIKG, Golm

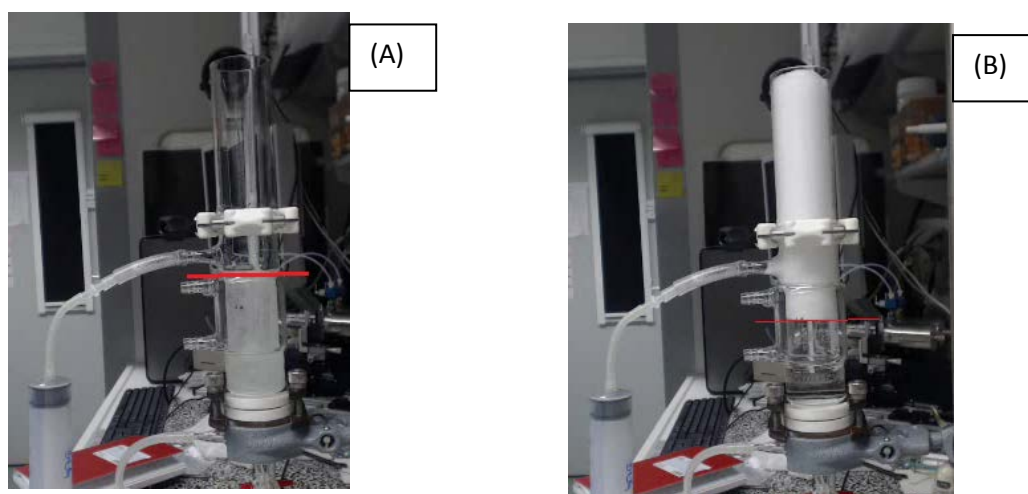


Figure 4.15. Photograph of foam column with an outlet to collect the foam with a syringe on the side. (A) The height of the liquid (shown in red) which is 8.9 cm measured from the frit. (B) The foam is collected when the liquid reaches a height of 6.6 cm.

The setup consists of a cylindrical column of height of ~ 25.5 cm. The foam is generated at an air flow rate of 0.2 l/min and the liquid volume was 100 ml. The foamate is collected from an outlet which is at a height of about 11 cm from the bottom and a disposable syringe is connected to it via a rubber tube.

The foam is generated to reach the top end of the cylindrical foam column. The interstitial liquid in the foam is allowed to reach until the level at 6.6 cm which is about two thirds of the initial liquid height of 8.9cm (for a liquid volume of 100 ml).

4.2.5.2. Foam fractionation setup at NRC, Lausanne

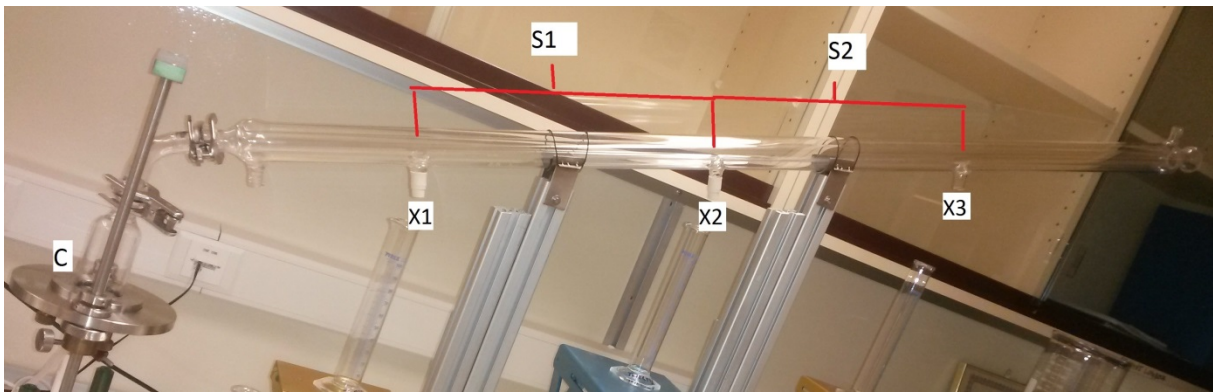


Figure 4.16. Foam fractionation column at NRC, Lausanne which is about 1.4 m long and has three exits X1, X2 and X3. The sections between the exits are termed S1 and S2.

The foam fractionation setup above has a container C in which a porous filter of G4 porosity is fitted. The volume capacity of this container is 100 ml and all the experiments were done with this solution volume. The porous filter is connected to a digital air flow meter controlled by a computer. The air flow rate of 100ml/min was kept constant for all experiments done with this setup. The foam was generated until it reaches the X3 exit of the foam column.

In the previous setup the foam was collected when the liquid height reached $\frac{2}{3}$ rd or 75% of the initial liquid height. In this case the volume of foam generated was greater and the dimensions of the column are different. As the drainage rate is observed to be much slower the foam was collected when the liquid height reached 60% of the original liquid height. The level of initial liquid level was marked on the container and 60% of its height was marked as well. After the foaming process when liquid drains to the desired level the foam is collected from the exits. A syringe (as shown in Fig. 4.16) was connected to the outlet for collecting the foamate.

4.2.6. References

1. Möbius, D., Miller, R., & Fainerman, V. B. (2001). *Surfactants: chemistry, interfacial properties, applications: chemistry, interfacial properties, applications* (Vol. 13). Elsevier. ISBN 9780080542133.
2. Krägel, J., O'Neill, M., Makievski, A. V., Michel, M., Leser, M. E., & Miller, R. (2003). Dynamics of mixed protein–surfactant layers adsorbed at the water/air and water/oil interface. *Colloids and Surfaces B: Biointerfaces*, 31(1), 107-114.
3. Miller, R., Fainerman, V. B., Leser, M. E., & Michel, M. (2004). Surface tension of mixed non-ionic surfactant/protein solutions: comparison of a simple theoretical model with experiments. *Colloids and Surfaces A: Physicochemical and Engineering Aspects*, 233(1), 39-42.
4. Grigoriev, D. O., Derkach, S., Krägel, J., & Miller, R. (2007). Relationship between structure and rheological properties of mixed BSA/Tween 80 adsorption layers at the air/water interface. *Food Hydrocolloids*, 21(5), 823-830.
5. Kotsmar, C., Kragel, J., Kovalchuk, V. I., Aksenenko, E. V., Fainerman, V. B., & Miller, R. (2008). Dilation and shear rheology of mixed β -casein/surfactant adsorption layers. *The Journal of Physical Chemistry B*, 113(1), 103-113.
6. Möbius, D., & Miller, R. (Eds.). (1998). *Proteins at liquid interfaces* (Vol. 7). Elsevier. ISBN 0080540007.
7. Gochev, G., Retzlaff, I., Aksenenko, E. V., Fainerman, V. B., & Miller, R. (2013). Adsorption isotherm and equation of state for β -Lactoglobulin layers at the air/water surface. *Colloids and Surfaces A: Physicochemical and Engineering Aspects*, 422, 33-38.
8. Fainerman, V.B., R. Miller, and P. Joos, The measurement of dynamic surface tension by the maximum bubble pressure method. *Colloid and Polymer Science*, 1994. 272(6): p. 731-739.
9. de Laplace P.S., *Mechanique celeste*, Paris: Gauthier-Villars. (1804). 1st Suppl. to Vol. 10, p. 10, 2nd Suppl. to Vol. 10, p. 35.
10. Rotenberg, Y., Boruvka, L., & Neumann, A. W. (1983). Determination of surface tension and contact angle from the shapes of axisymmetric fluid interfaces. *Journal of colloid and interface science*, 93(1), 169-183.
11. Levenberg, K. (1944). A method for the solution of certain non–linear problems in least squares.

12. Marquardt, D. W. (1963). An algorithm for least-squares estimation of nonlinear parameters. *Journal of the Society for Industrial & Applied Mathematics*, 11(2), 431-441.
13. Miller, R. and Liggieri, L. (Eds.), *Interfacial Rheology*, Vol. 1, *Progress in Colloid and Interface Science*, Brill Publ., Leiden, 2009, ISBN 978 90 04 17586 0.
14. Lucassen, J. and van den Tempel, M., *Chem. Eng. Sci.*, 27 (1972) 1283-1291; *J. Colloid Interface Sci.*, 41 (1972) 491-498.
15. Malysa, K., et al., *Bubbles Rising in Solutions; Local and Terminal Velocities, Shape Variations and Collisions with Free Surface*, in *Bubble and Drops Interfaces*, R. Miller and L. Liggieri, Editors. 2011. p. 243-292.

5. Results and discussion

The first two paragraphs of this chapter are brief summaries of two manuscripts published recently in peer reviewed journals. Copies of these publications are attached to this thesis as Appendices 8.1 and 8.2.

The following four paragraphs 5.3. to 5.6. then summarize further results and are presented in the style of a manuscript to be submitted later to journals for publication.

5.1. Evidence of negative surface pressure induced by β -lactoglobulin and β -casein at water/air interface

5.1.1. Summary

Protein adsorption is one of the most complex and intriguing phenomenon in interfacial science. This phenomenon has been addressed for the short time range of adsorption using maximum bubble pressure tensiometry. This study presents the issue of negative surface pressure of protein solutions which has been much of a speculation over a long period of time, as on a first glance it seems to be in conflict with the fundamentals of surface thermodynamics. Here β -lactoglobulin has been studied at different pH values and the experimental results agree with the theoretical model presented. This set of results was published in [1].

The materials studied in this paper comprise β -lactoglobulin (BLG) and β -casein (BCS) which both were purchased from Sigma Aldrich (90% pure). The stock solutions were prepared by dissolving the protein in respective buffer along with 4 times by weight of activated charcoal. The solution was stirred for 20 min and rested for 10 min and then centrifuged to remove the activated charcoal in the solution. For stock solutions of pH 7, an equimolar mixture of 10 mM Na_2HPO_4 and NaH_2PO_4 was used as buffer, whereas for solutions of BLG at pH 6.2, 10 mM NaH_2PO_4 solutions were adjusted with HCl. For solutions with pH values of 8 and 9 we used a 10 mM Na_2HPO_4 and adjusted the pH with NaOH such that we got the same ionic strength for all cases. The pH close to the isoelectric point (5.3) was not studied as precipitation was observed at higher concentrations. The maximum bubble pressure tensiometer BPA-1S (SINTERFACE Technologies, Berlin) was used for the experiments. The principle of this method was described in detail above in chapter 4.2.1

The main results of this publication [1] can be summarize in the following two Fig. 5.1 and 5.2.

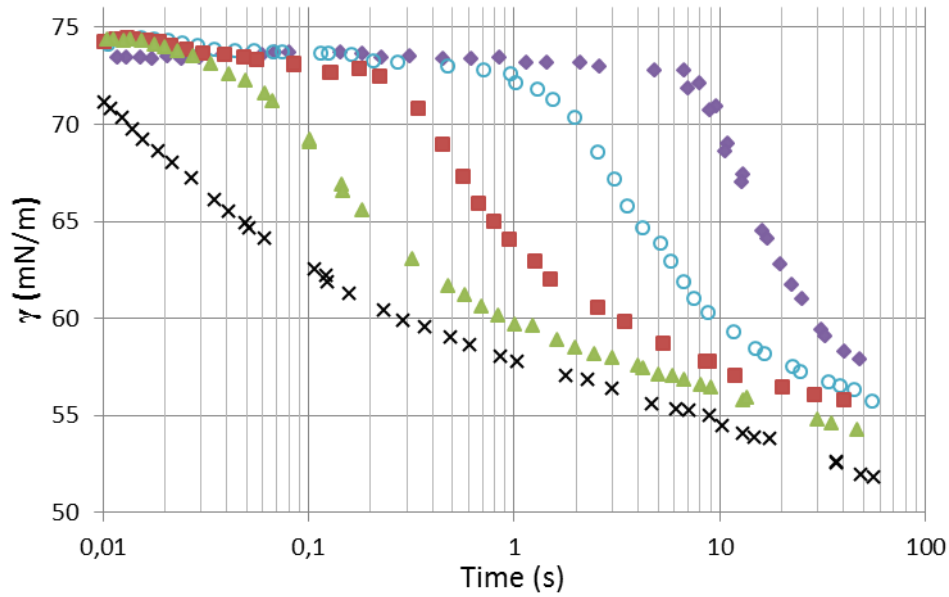


Figure 5.1 Dynamic surface tension of BCS solutions at pH 7 for different concentrations: (♦) 2×10^{-6} , (○) 5×10^{-6} , (■) 10^{-5} , (▲) 2×10^{-5} , (×) 5×10^{-5} mol/l

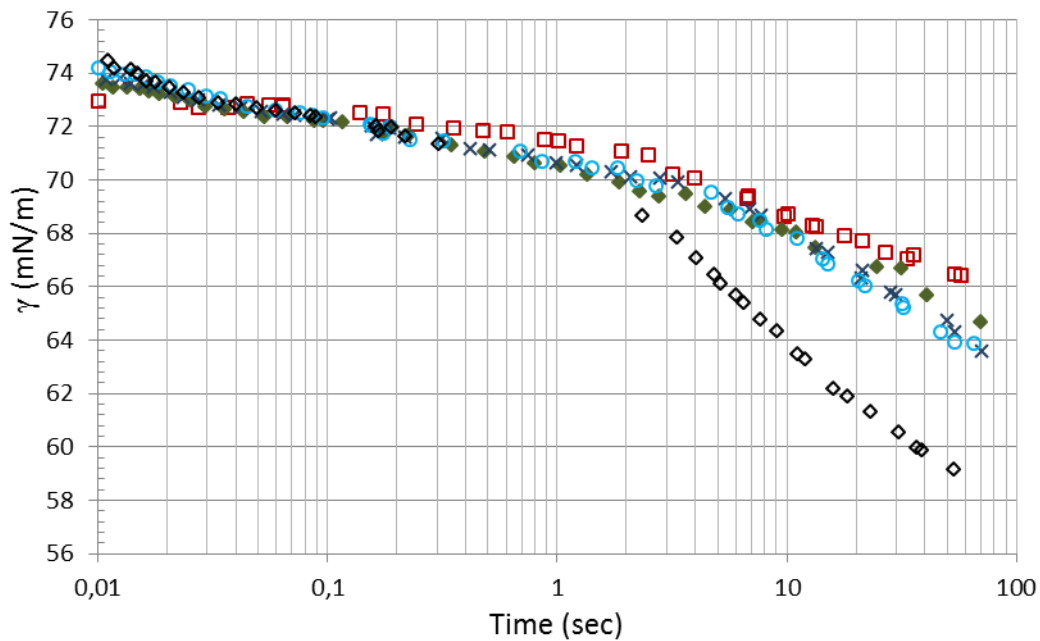


Figure 5.2 Dynamic surface tension of BLG solutions at a concentration of 5×10^{-5} mol/L and different pH values: (□) 6.2, (▲) 7, (×) 8, (○) 8.4 and (◇) 9.

The figures show the adsorption kinetics measured by maximum bubble pressure tensiometry. The concentrations of protein were chosen such that surface tension changes were detectable at the time range characteristic for this experimental methodology. It can be noted that for

BCS at $2 \times 10^{-6} \text{M}$ there is a lag time before the surface tension starts decreasing and this is termed as induction time. It varies with the type of protein and its bulk concentration [2].

The most interesting feature of this study is the increase in surface tension happening essentially during the induction times for both proteins (BCS and BLG). In case of BLG this increase in initial surface tension, or the appearance of negative surface pressure values, changes with pH for the same protein and concentration (see Fig. 5.2). We explained these results with the help of a theoretical model proposed by Fainerman et.al [2] (please refer to Eq.6 in section 3.1.2) which describes the equation of state for adsorption layer. A positive value of the non-ideality of enthalpy α_p indicates intermolecular attractions and also the non-ideality of entropy given by the second term on the right hand side of the mentioned equation would lead to a decrease in surface pressure π . In physical sense this means that the number of adsorbed kinetic species deplete due to aggregation of protein species. This effect is however transient and occurs only in non-equilibrium conditions for low surface concentrations. The prediction of such increase in surface tension at low surface pressure values for BCS is explained in detail in [1] which is attached as appendix 8.1.

5.1.2. References

1. Ulaganathan, V., Fainerman, V. B., Gochev, G., Aksenenko, E. V., Gunes, D. Z., Gehin-Delval, C., & Miller, R. (2014). Evidence of negative surface pressure induced by β -lactoglobulin and β -casein at water/air interface. *Food Hydrocolloids*, 34, 10-14.
2. Fainerman, V. B., Lucassen-Reynders, E. H., & Miller, R. (2003). Description of the adsorption behaviour of proteins at water/fluid interfaces in the framework of a two-dimensional solution model. *Advances in colloid and interface science*, 106(1), 237-259.

5.2. Influence of β -lactoglobulin and its surfactant mixtures on velocity of the rising bubbles

5.2.1. Summary

The rising velocity of air bubbles in surfactant solutions is a sensitive measure for the formation of a dynamic adsorption layer (DAL) at the bubble surface. Due to a certain surface coverage by adsorbed species the bubble surface starts to become immobilized and the rising velocity is retarded. There is a large difference in the retardation effect in presence of the protein β -lactoglobulin (BLG) alone and its mixed solutions with surfactants. In presence of added surfactants BLG forms complexes, which adsorb and retard the bubble rising velocity according to their respective surface activity and adsorption kinetics. While the nonionic surfactant C12DMPO does not show significant increase in retardation effects as compared to BLG alone, the ionic surfactants SDS and DoTAB form highly surface active complexes and change the rising velocity much stronger.

The surfactants used were dodecyl trimethyl ammonium bromide (DoTAB) and sodium dodecyl sulfate (SDS) both purchased from Fluka (Switzerland). The non-ionic surfactant dodecyl dimethyl phosphine oxide (C12DMPO) was synthesized in our lab following the protocol given in [23]. BLG was purchased from Sigma–Aldrich (90% pure). The stock solutions were prepared by dissolving the protein in Milli-Q water used for the preparation of the solutions had a surface tension of 72.4 mN/m at 22°C. All experiments were carried out at room temperature of 22°C.

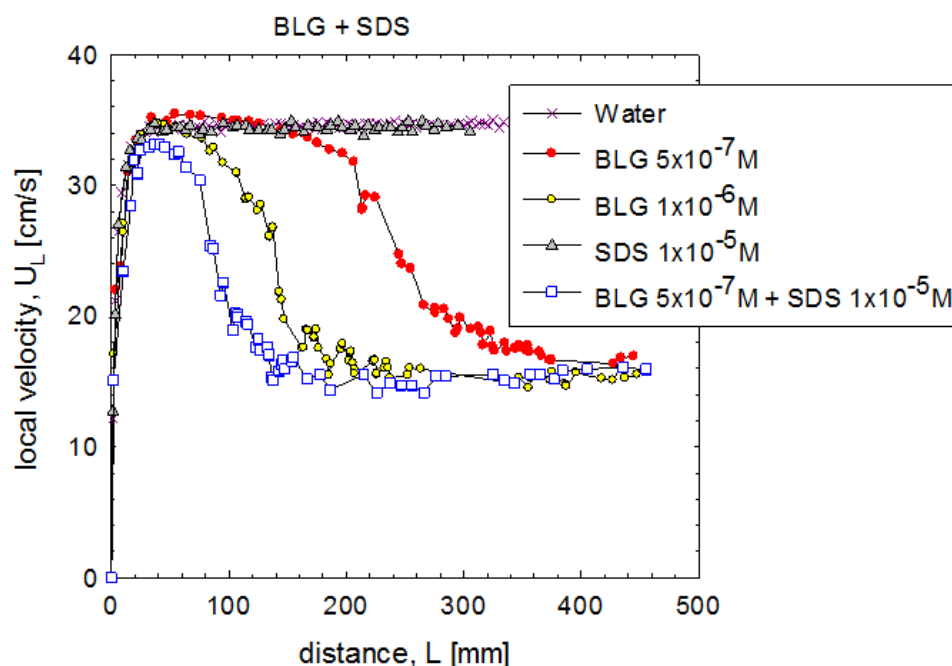


Figure 5.3 Local velocity profile of air bubble (diameter ~ 1.48 mm) rising in solutions of BLG, SDS and mixtures as a function of the distance from the capillary orifice.

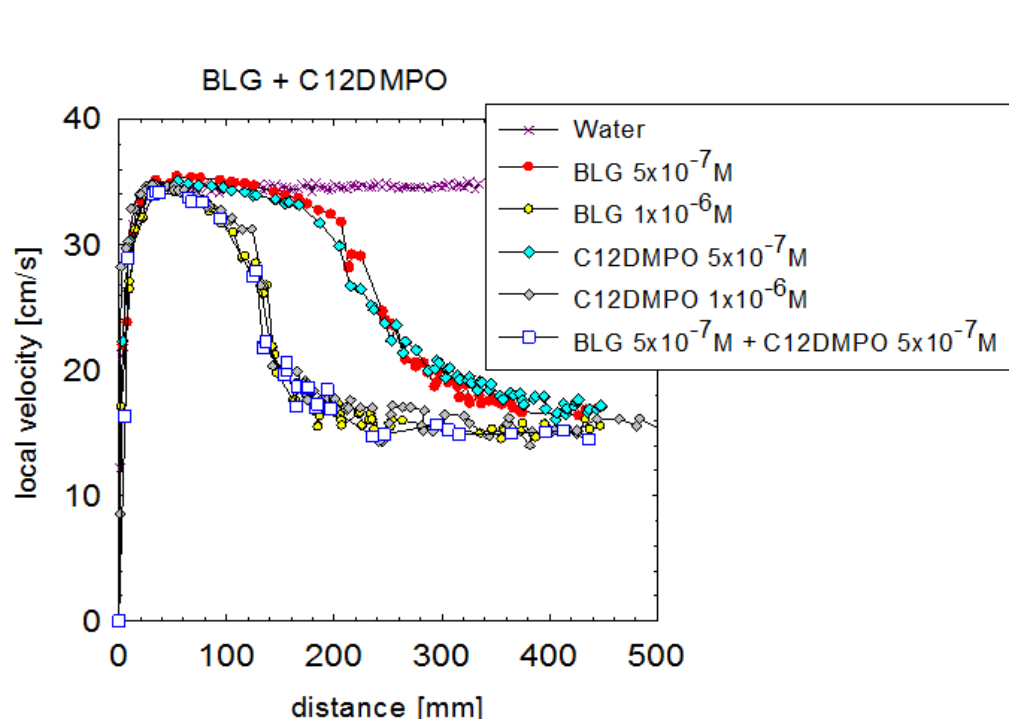


Figure 5.4 Local velocity profile of air bubble (diameter ~ 1.48 mm) rising in solutions of BLG, C₁₂DMPO and its mixtures, as a function of the distance from the capillary orifice.

From the Fig. 5.3 and 5.4, which represent the main results of this publication, we could see that the bubble rising in milli-Q water has initial acceleration followed by terminal velocity at 35.5 cm/s. But in presence of surfactant or protein there is a deceleration and the velocity

reaches about 16.5cm/s as distance from the capillary increases. These profiles of local velocity give us empirical understanding of adsorption layer formed at dynamic conditions. For BLG 5×10^{-7} M we could see that there is adsorption process taking place with the time regime of bubble rising which is less than 2 seconds. Whereas in static conditions the adsorption kinetics given in Fig. 5.13 shows us that there is no change in surface tension until 100 seconds. This shows us how different the adsorption process is under dynamic conditions. The striking feature observed with protein anionic surfactant mixtures is that for SDS at 1×10^{-5} M there is detectable deviation from pure water. But when mixed with BLG 5×10^{-7} M we notice a drastic decrease in velocity indicating the protein-surfactant complex formation which tends to be more surface active.

In case of non-ionic surfactant C_{12} DMPO we notice that the velocity profiles are identical to BLG for same concentrations. When BLG 5×10^{-7} M is mixed with C_{12} DMPO 5×10^{-7} M the velocity profile is identical to that of BLG 1×10^{-6} M or C_{12} DMPO 1×10^{-6} M. This indicates no interaction between these two molecules.

More details about these results and also mixtures with DoTAB are presented in the article [1] attached as appendix 8.2.

5.2.2. References

1. Ulaganathan, V., Krzan, M., Lotfi, M., Dukhin, S. S., Kovalchuk, V. I., Javadi, A., & Miller, R. (2014). Influence of β -lactoglobulin and its surfactant mixtures on velocity of the rising bubbles. *Colloids and Surfaces A: Physicochemical and Engineering Aspects*, 460, 361-368.

5.3 Effect of pH and ionic strength on static and velocity of rising bubbles in β -lactoglobulin solutions*

5.3.1. Introduction

Many food products are based on foamed or emulsified formulations. Foaming gives food products a well appreciated mouth feeling. However, to foam a certain product often requires more knowledge on the foaming process, i.e. how the bubbles are formed and stabilized against coalescence. These dynamic properties are not easily accessible. Therefore it is difficult to correlate the foam properties to surface tension measurements done in static conditions [1]. Growing and oscillating bubbles [2,3] are one of the options that provide dynamic surface properties under conditions rather close to process conditions. Another option is to study bubbles rising in solutions of respective formulations [4-9]. The local velocity of rising bubbles is strongly affected by the adsorption of surface-active species at the bubble surface. Measurements of the local velocity profiles (LVP) offer an insight into the adsorption layer formed under dynamic conditions (dynamic adsorption layer, DAL) which no other technique can provide [4-6]. Hence, rising bubble studies are very useful for understanding the mechanism and structure of interfacial layers, particularly when comprising proteins at various solvent conditions, such as pH and ionic strength [7].

In general, during the rising of an air bubble in water, it is assumed that the front part of the bubble surface is expanded and the rear part compressed. However, in a surfactant solution there is an adsorption flux towards the leading pole of the bubble surface which is swept to the rear and compressed there. Hence, there is a non-uniform distribution in the adsorption layer which gives rise to a Marangoni effect. This Marangoni force is directed against the tangential shear force which acts along the bubble surface. This in turn leads to immobilization of the surface which causes the bubble to behave as a rigid sphere. Therefore, the hydrodynamic drag force acting on an air bubble rising in a surfactant solution is greater than in pure water. A more detailed explanation is given by the recent theoretical model suggested by Dukhin et al. [8].

Recently it was shown that the addition of a surfactant to BLG solutions [9] or variation of the pH of bovine serum albumin solutions [7] cause dramatic effects on the LVP of a rising bubble. In the present work we report results on the influence of pH and ionic strength on the

* Ulaganathan, V., Gochev, G., Gehin-Delval, C., Leser, M. E., Miller, R. (2015). Effect of pH and electrolyte concentration on rising air bubbles in β -lactoglobulin solutions. Submitted to Colloids and Surfaces A: Physicochemical and Engineering Aspects.

velocity profiles of bubbles rising in buffered BLG solutions and hence on the DAL properties at the bubble surfaces.

5.3.2. Materials and methods

BLG sample that we used was obtained as described in [10] and provided by the group of Ulrich Kulozik (Technische Universität München, Germany). The solutions were prepared in Milli-Q water which had a surface tension of 72.2 mN/m at 22°C and conductivity of 0.05 μ S/cm. All experiments were done at room temperature \sim 22°C. The buffer used for controlling the pH was citric phosphate buffer. For the solutions prepared without buffer the pH was adjusted by adding 1 M HCl or NaOH.

For the experimental setup concerning the rising bubble experiments and profile analysis tensiometer please refer to chapter 4.2.2 & 4.2.3.

5.3.3. Results

Fig. 5.5 shows the LVP of bubbles rising in pure water and in BLG solutions with various protein concentrations; pH 7 and buffer concentration $C_{\text{buff}} = 10$ mM were kept constant. Basically two types of shapes of the LVP are recognized. In the first case, as these are the LVPs for pure water and for 5×10^{-6} M BLG, the LVP shows an acceleration period immediately followed by a period with the terminal velocity U_T ; for bubbles with a diameter of 1.5 mm rising in water we get $U_T = 35.5$ cm/s while for 5×10^{-6} M BLG $U_T = 16.5$ cm/s. This BLG concentration is the limit of the sensitivity of this technique. At any higher concentration the same velocity profile would have been obtained. This is due to the complete immobilization of the bubble surface caused by the adsorption process. Hence the protein concentrations at these particular condition (pH and ionic strength represented by the buffer concentration) were chosen such that the onset of a measurable bubble deceleration (at ca. 2×10^{-7} M) and the highest concentration limit (ca. 5×10^{-6} M), at which the bubble is fully retarded, could have been observed (see Fig. 5.1). In the second case, as these are the LVPs for the intermediate protein concentrations, the dynamic surface layer formed at the rising bubble surface leads to a monotonic decrease of the local velocity U_L after the moment at which the bubble reaches a maximum U_L -value and finally the terminal velocity U_T . With increasing the BLG concentration the distance at which the bubble starts to decelerate becomes shorter and the maximum rising velocity achieved by the bubble diminishes. It is

interesting to compare the time-scale of the adsorption process at a rising bubble and at a static bubble. From the data in Fig. 5.5 one can calculate the time until the maximum U_L in the LVP is reached and after which it starts to become decelerated by the drag force due to further adsorbed proteins. For example, at the concentration of 1×10^{-6} M, the maximum in the LVP is estimated to be at around 60 ms from the moment of bubble detachment whereas the induction time of the onset of measurable surface pressure of a static bubble fixed at a capillary immersed in a solution with the same composition is around 10 s [11], i.e. the adsorption process is about two orders of magnitude slower at the static bubble.

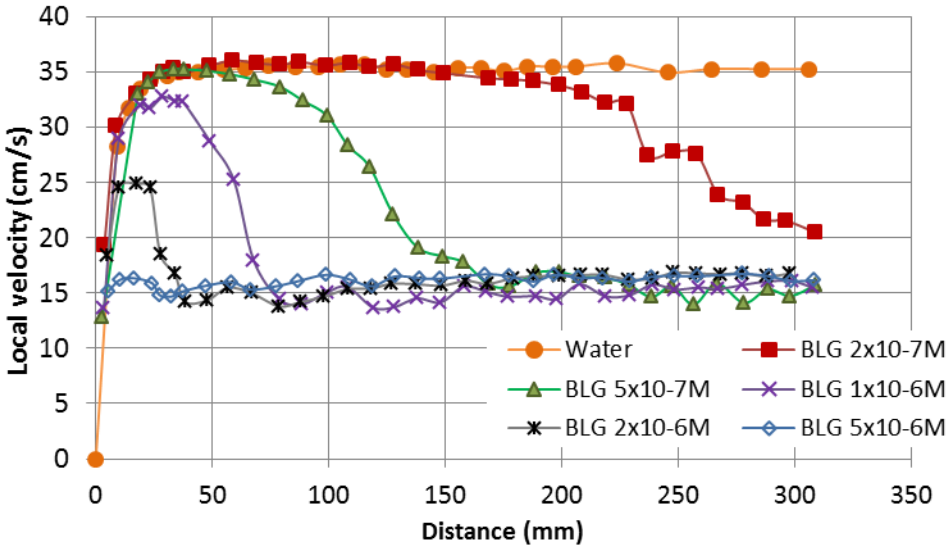


Figure 5.5 Local velocity vs distance from capillary tip for bubble rising in BLG solution prepared in 10mM citric phosphate buffer at pH 7.

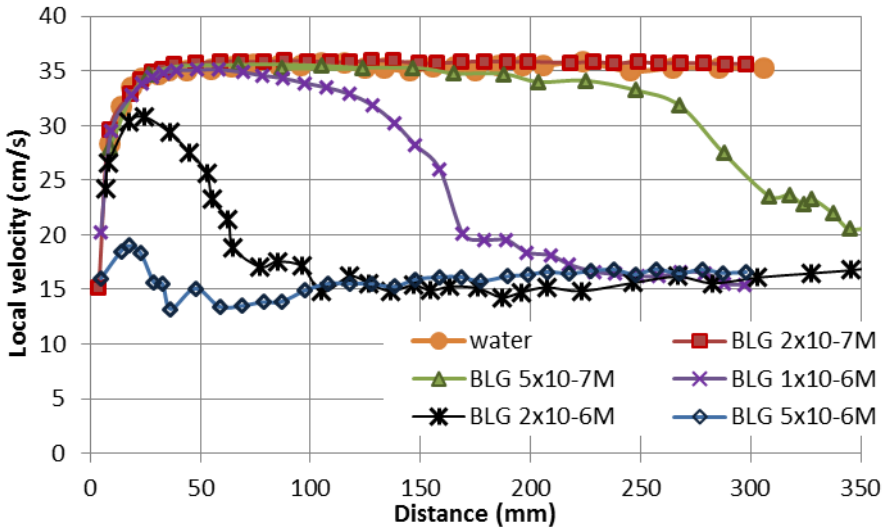


Figure 5.6 Local velocity vs distance from capillary tip for bubble rising in BLG solution prepared in 10mM citric phosphate buffer at pH 5.

In Fig. 5.6 the LVPs for the same BLG concentrations but at pH 5 (in the vicinity of the IEP) are shown. Here it can be already noted that the lowest BLG concentration of 2×10^{-7} M had no influence on the bubble motion. The results also infer that at pH 5 the immobilization of the bubble surface is less effective as compared to that at pH 7.

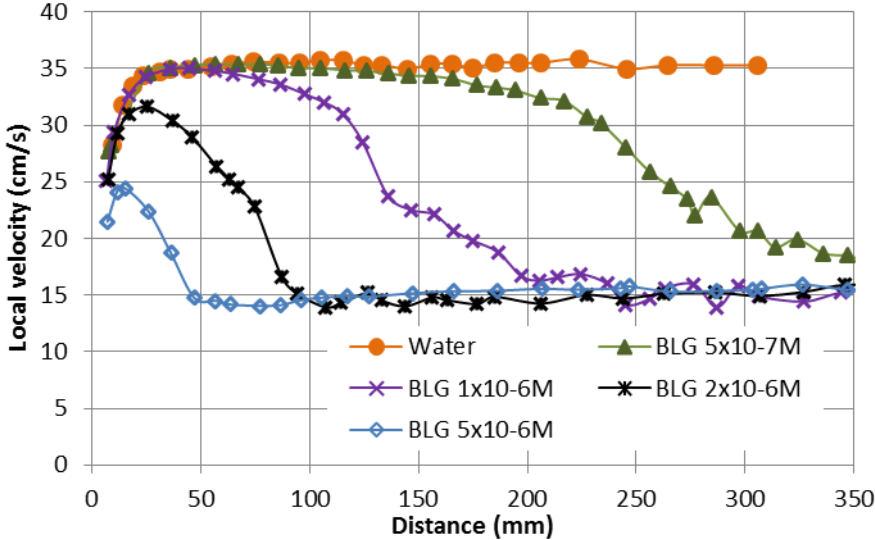


Figure 5.7 Local velocity vs distance from capillary tip for bubble rising in BLG solution prepared in 10mM citric phosphate buffer at pH 4.

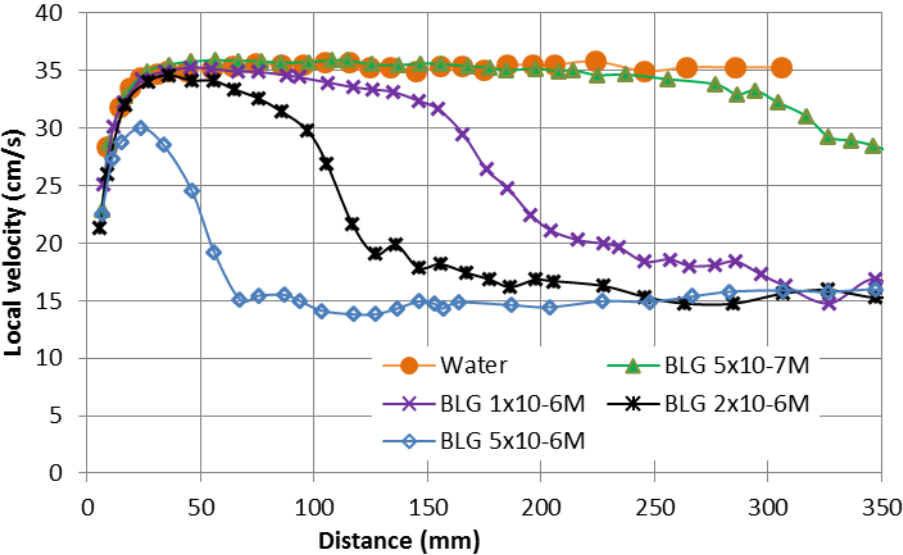


Figure 5.8 Local velocity vs. distance from capillary tip for bubble rising in BLG solution prepared in 10mM citric phosphate buffer at pH 3.

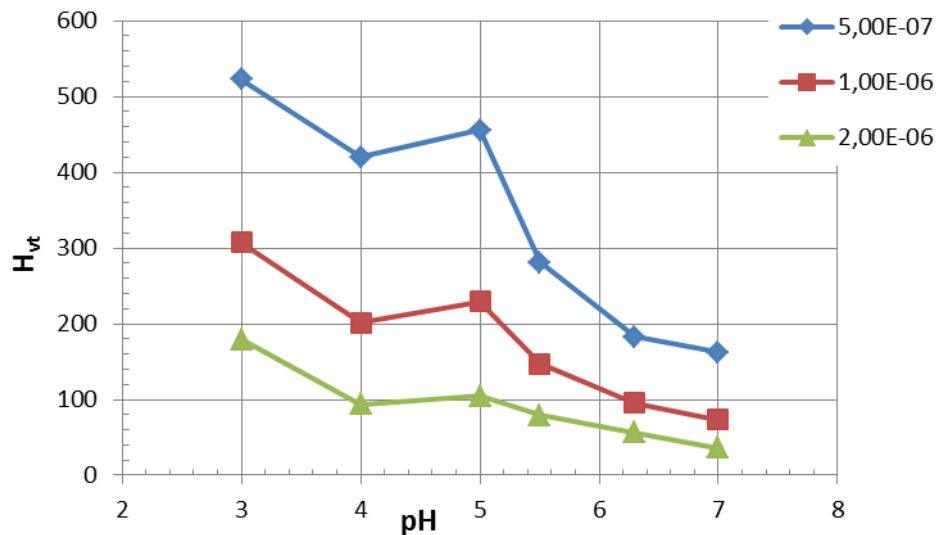


Figure 5.9 Distance at which the bubble reaches terminal velocity (H_{vt}) vs. pH of BLG solution prepared in 10mM citric phosphate buffer.

Additional experimental data measured at pH 4 and pH 3 are presented in Figs. 5.7 and 5.8, respectively. The data in Fig. 5.9 summarizes the measured distances (H_t) for different pH values at which a bubble of 1.5 mm in diameter reaches the limiting terminal velocity $U_T = 16.5\text{cm/s}$ at a completely rigid surface. These data were determined from the results presented in Figs. 1-4 and additional experiments performed at pH 5.5 and 6.3 (LVPs not shown). The longest distance for achieving U_T (immobilized surface) is observed at pH 3 whereas the shortest distance was observed for bubbles rising in solutions with pH 7. A general trend of gradual decrease in H_t with increasing pH can be recognized for all three protein concentrations in Fig. 5.9 with the exception of the data at pH 5 (in the vicinity of the IEP).

Along with the effect of pH (at constant $C_{\text{buff}} = 10\text{ mM}$) we also studied the influence of the ionic strength of the protein solutions (by varying the buffer concentration) on the LVPs for a given pH.

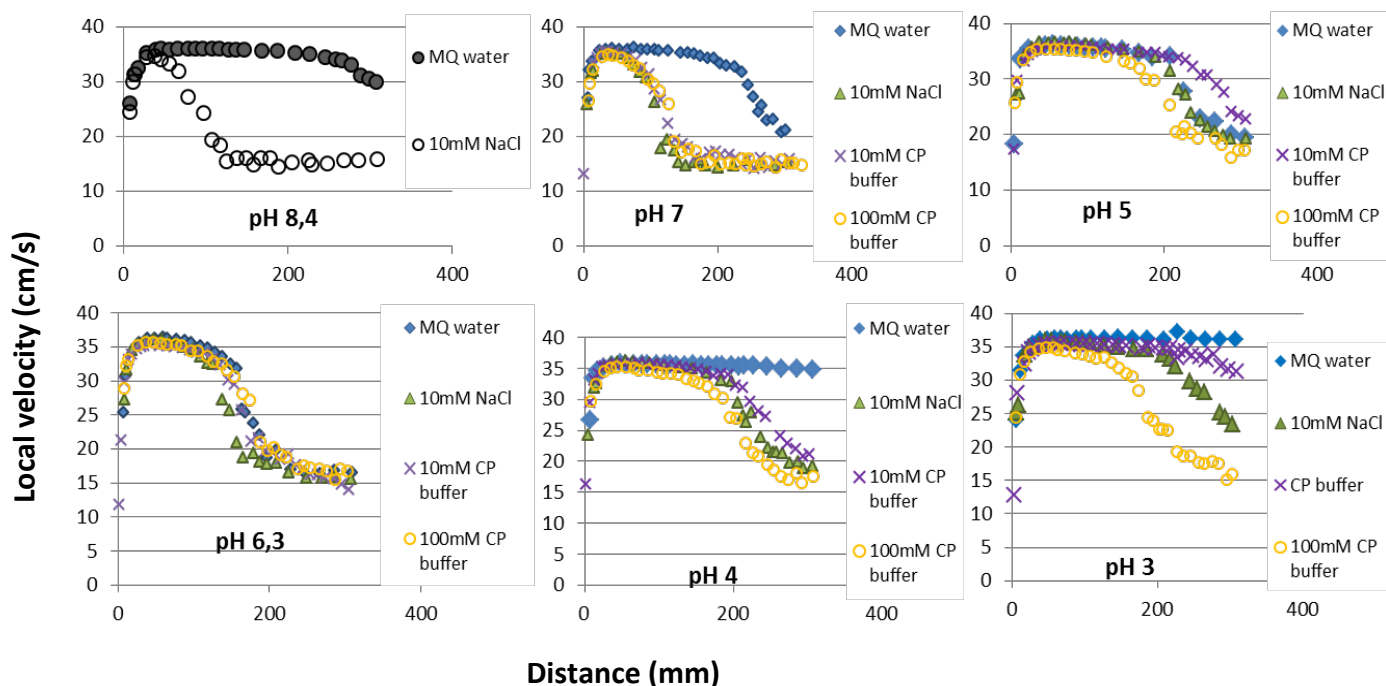


Figure 5.10 Local velocity vs. distance from the capillary tip for $5 \times 10^{-7} \text{M}$ BLG at different pHs and effect of salt concentration.

Fig. 5.10 shows the sensitivity of rising bubbles' velocity profiles to changes in C_{buff} for different pHs. The legend "MQ water" stands for buffer-free solutions adjusted to the desired pH by addition of small amounts of HCl or NaOH. Note, that a strict control of the ionic strength of the solutions requires taking into account the contribution of the concentration (more strictly the activity) of ions coming from HCl or NaOH; however since the highest concentration (HCl) required to adjust the extreme pH 3 is respectively in the order of 1 mM, we accept the effect of these pH regulators on the LVP as negligible when compared to the electrolyte concentrations of 10 and 100 mM used in the further studies and therefore the differences between the results either for pure water or for NaCl in the different examples in Fig. 5.10 are interpreted mainly on the basis of the pH effect. The pH 6.3 is the natural pH established after dissolving the BLG sample in pure water. For comparison purposes we also measured the LVPs for solutions containing 10 mM NaCl. The effect of the solution's ionic strength is noticeable in all cases except at the natural pH 6.3. It is interesting to note that the LVPs at pH 5 (negligible molecular net charge) are rather sensitive either to variation of the buffer concentration or to the presence of NaCl, while at pH 6.3 the LVPs are not sensitive to presence and variation of any electrolyte even though the BLG molecules carry a certain negative charge at these pH conditions.

5.3.4. Discussion

The BLG molecules in an aqueous solution exist in a dynamic equilibrium between monomers and dimers at $\text{pH} < 3.7$ and $\text{pH} > 5.1$ and within the pH range $3.7 < \text{pH} < 5.1$ larger oligomers can be formed [13-17]. Furthermore, the globular BLG molecule itself can adopt different conformations depending on the pH [17]. However, such a variety of structural characteristics of BLG was found in bulk environment. It was found that close to neutral pH conditions the BLG molecules retain a globular structure when adsorbed at the water/air surface [18,19] and the adsorption of the monomer is favored which implies dissociation of the dimer when affected by the interface [18].

The adsorption behavior of BLG at a static air/water surface was found to strongly depend on solvent conditions such as pH and ionic strength [12,20,21]. It was shown by ellipsometry measurements that a maximum BLG layer thickness is achieved at pH 5, while tensiometry and surface rheology show that the dependences of the surface pressure and the dilational elasticity as a function of pH exhibit a maximum at pHs close to the IEP, however, for BLG concentrations higher than those studied in the present work [12,21]. A maximum in the shear elastic constant of ovalbumin monolayers at the water/air surface was also found close to the IEP [22]. However, apparently the pH dependent ability of BLG to increase the surface pressure is affected by the protein concentration. Another set of results to be published in a forthcoming manuscript [21], revealed that at a certain protein concentration lower than ca. 10^{-8} M the induction time τ_{ind} (the adsorption time at which the onset of measurable Π -values arises) at the surface of a static bubble in BLG solutions is shortest for pH 7 as compared to pH 5 and pH 3. This correlates with the results in Fig. 5.9 where for pH 7 the shortest distance is obtained at which a terminal velocity is reached as compared to all other pH values. Similarity, these trends cannot be easily explained having in mind the differences in the protein concentrations and especially in the physical conditions (static and rising bubbles) but can give a hint about the generic surface properties of BLG in dependence of pH. The induction time measured [21] with drop/bubble profile analysis tensiometer PAT [23] is a suitable parameter to be compared with the rising time or with the distance from the capillary at which the maximum local velocity U_L in the LVP is achieved, thus to reveal similarities and differences in the adsorption on a rising and static bubble.

Let us compare the literature results reviewed above with those obtained in the present work, and let us try to reveal peculiarities of the dynamic adsorption layers formed at the moving surface of a rising bubble. Results on the adsorption dynamics of BLG for static bubbles

revealed that within the protein concentration range studied here the induction times are comparable for pH 7 and pH 5 while for pH 3 the induction times are much longer [21]. This finding correlates with the lowest adsorption activity of BLG at pH 3 as detected for rising bubbles .

On the other hand, with increasing the ionic strength of the BLG solutions at fixed pH the value of τ_{ind} diminishes and the rate of adsorption increases. In this respect, the data for pH 7 in Fig. 5.10 correlate very well with the adsorption kinetics data on a static bubble surface for different electrolyte concentrations [21].

The fact that the curves in Fig. 5 do not have a minimum at pH 5 shows that the formation of aggregates somehow does not favor the adsorption process at dynamic conditions with a flow field around the bubble surface. The mechanism of this process still remains quite unclear.

At pH 3, the BLG molecules predominantly have a monomeric configuration but the equilibrium shifts to a dimer with increasing ionic strength [15]. Below pH 3.5 and above pH 7.5, the BLG molecules favor the dissociation of dimers into monomers, depending on the ionic strength. The dissociation is favored by electrostatic repulsion between the molecules and the equilibrium shifts in favor of a dimer in presence of counter ions [16]. From Fig. 5.10 we could see that at pH values of 3, 4, 7 and 8.4 the dimer-monomer transition is more sensitive to the presence of salt. Therefore, the electrostatic repulsion between the molecules in a dynamic adsorption layer is an important factor which influences the velocity profiles of a rising bubble. When we compare the data for pH 3 and pH 7 in Fig. 5.10, at pH 7 and 10mM and 100mM salt concentrations there is no significant difference. This shows us that 10mM of salt concentration is sufficient to screen the charges at the bubble surface. At pH 3, however, we could notice that 10mM of salt concentration did not screen the charges sufficiently which is indicated by the higher velocity as compared to 100mM of salt concentration. Engelhardt et al. have shown differences in the properties of BLG derived from zeta potential measurements and sum frequency generation spectroscopy (SFG). Though the absolute zeta potential values of BLG at pH 3 and 7 are quite similar, the SFG signals measured for adsorbed layers of BLG for these two pH values vary. Hence, the SFG results show that the electric field generated by the adsorbed BLG molecules at pH 3, induces a higher polar ordering of the water molecules in the proximity of the interface, as compared to pH 7. The higher charge at pH 3 is attributed to the charge distribution at the surface due to the adsorbed protein molecules which is different to what is observed via the electrophoretic mobility [12]. The greater repulsion

between the adsorbed molecules at the interface could explain the differences in the LVPs which we noticed for pH 3 and 7, respectively.

From Fig. 5.10 we could see that at pH 5, which is close to the IEP, the presence of salt has a slight effect in decreasing the velocity profiles. This could be due to screening of the minor net charge present at this pH.

At pH 6.3, however, there is no significant influence of the salt concentration. This is the pH of a 5×10^{-7} M BLG solution acquires when dissolved in milli-Q water without any addition of HCl or NaOH. This condition is close to what is termed as isoionic point (IIP) of the protein, which is the pH of a protein solution in absence of any other ions except H^+ and OH^- [24]. The IIP is different from IEP because the latter corresponds to the immobility of protein molecules in an electric field. The IIP tends to deviate from the IEP and reaches pH 7 when the BLG bulk concentration tends to zero [24]. Therefore, at low concentrations such as 5×10^{-7} M, the pH of a BLG solution in deionized water is 6.3 ($pH < 7$). This is due to the protons dissociated from the amino groups of the BLG molecules which contribute to the acid-base balance in the solution. At this condition the retardation of the rising bubble velocity is highest as compared to other pH values in absence of any added salt. Therefore, due to the presence of few protons in the solution there could be a fluctuation in the charge distributions on each protein molecule which in turn could induce long range attractive forces due to existing dipole moments. Kirkwood et al. predicted such dipole moments which can arise leading to attractive forces between two protein molecules at the IIP though they carry a non-zero net charge [25]. In this case it would increase the interaction between the BLG molecules adsorbed at the interface and thereby retarding the bubble surface mobility. More studies are required to see if this effect is true for other proteins. However, at this point there is no other explanation that we could offer as to why at pH 6.3 with no added salt we have the most effective condition for retarding the bubble motion. With addition of salt at this pH we can explain the effective screening of the net charge as observed at pH 7.

5.3.5. Conclusion

The obtained results in terms of LVPs for air bubbles rising in BLG solutions demonstrate that this method is extremely sensitive to adsorption effects at the water/air interface. Already at very low bulk concentrations remarkable effects on the local rising velocity can be observed in time scales of a few seconds. As known from studies of the adsorption dynamics at stationary air bubbles as well as from the corresponding surface tension isotherms [12,21]

at sufficiently high bulk concentrations BLG is most surface active at the IEP. From the presented rising air bubble studies we learn, however, that the pH alone does not provide the necessary environmental conditions for a maximum surface retardation effect, when compared to other pH conditions. Also the total BLG bulk concentration and the ionic strength have to be sufficiently high to provide the bubble surface with a respective adsorption layer. Hence, with a small number of BLG molecules adsorbed in a rather short period of time (few seconds) and compressed at the rear parts of the rising bubble the resulting surface layer has obviously a structure quite different from that of a layer close to the adsorption equilibrium.

5.3.6. References

1. Malysa, K., & Lunkenheimer, K. (2008). Foams under dynamic conditions. *Current Opinion in Colloid & Interface Science*, 13(3), 150-162.
2. Ravera, F., Loglio, G., & Kovalchuk, V. I. (2010). Interfacial dilational rheology by oscillating bubble/drop methods. *Current Opinion in Colloid & Interface Science*, 15(4), 217-228.
3. Lotfi M., Karbaschi M., Javadi A., Mucic N., Krägel J., Kovalchuk V.I., Rubio R.G., Fainerman V.B., Miller R. (2014). Dynamics of liquid interfaces under various types of external perturbations. *Curr. Opin. Colloid Interface Sci.* 19(4), 309–319.
4. Krzan, M., & Malysa, K. (2002). Profiles of local velocities of bubbles in n-butanol, n-hexanol and n-nonanol solutions. *Colloids and Surfaces A: Physicochemical and Engineering Aspects*, 207(1), 279-291.
5. Krzan, M., Lunkenheimer, K., & Malysa, K. (2004). On the influence of the surfactant's polar group on the local and terminal velocities of bubbles. *Colloids and Surfaces A: Physicochemical and Engineering Aspects*, 250(1), 431-441.
6. Malysa, K., Krasowska, M., & Krzan, M. (2005). Influence of surface active substances on bubble motion and collision with various interfaces. *Advances in colloid and interface science*, 114, 205-225.
7. Zawala, J., Todorov, R., Olszewska, A., Exerowa, D., & Malysa, K. (2010). Influence of pH of the BSA solutions on velocity of the rising bubbles and stability of the thin liquid films and foams. *Adsorption*, 16(4-5), 423-435.
8. Dukhin, S. S., Kovalchuk, V. I., Gochev, G. G., Lotfi, M., Krzan, M., Malysa, K., & Miller, R. (2014). Dynamics of Rear Stagnant Cap formation at the surface of spherical

- bubbles rising in surfactant solutions at large Reynolds numbers under conditions of small Marangoni number and slow sorption kinetics. *Advances in colloid and interface science*.
9. Ulaganathan, V., Krzan, M., Lotfi, M., Dukhin, S. S., Kovalchuk, V. I., Javadi, A., ... & Miller, R. (2014). Influence of β -lactoglobulin and its surfactant mixtures on velocity of the rising bubbles. *Colloids and Surfaces A: Physicochemical and Engineering Aspects*, 460, 361-368.
 10. J. Toro-Sierra, A. Tolkach, U. Kulozik, (2013). Fractionation of α -Lactalbumin and β -Lactoglobulin from Whey Protein Isolate Using Selective Thermal Aggregation, an Optimized Membrane Separation Procedure and Resolubilization Techniques at Pilot Plant Scale. *Food Bioprocess Technol.* 6, 1032-1043.
 11. Gochev, G., Retzlaff, I., Aksenenko, E. V., Fainerman, V. B., & Miller, R. (2013). Adsorption isotherm and equation of state for β -Lactoglobulin layers at the air/water surface. *Colloids and Surfaces A: Physicochemical and Engineering Aspects*, 422, 33-38.
 12. Engelhardt, K., Lexis, M., Gochev, G., Konnerth, C., Miller, R., Willenbacher, N., ... & Braunschweig, B. (2013). pH effects on the molecular structure of β -lactoglobulin modified air–water interfaces and its impact on foam rheology. *Langmuir*, 29(37), 11646-11655.
 13. Gottschalk M., Nilsson H., Roos H., Halle B., (2003). Protein self-association in solution: The bovine β -lactoglobulin dimer and octamer. *Protein Science*, 12, 2404-2411.
 14. Mercadante D., Melton L.D., Norris G.E., Loo T.S., Williams M.A.K., Dobson R.C.J., Jameson G.B., (2012). Bovine β -Lactoglobulin Is Dimeric Under Imitative Physiological Conditions: Dissociation Equilibrium and Rate Constants over the pH Range of 2.5–7.5. *Biophysical Journal*, 103, 303-312.
 15. Sakurai, K., Oobatake, M., & Goto, Y. (2001). Salt-dependent monomer–dimer equilibrium of bovine β -lactoglobulin at pH 3. *Protein Science*, 10(11), 2325-2335.
 16. Verheul M., Pedersen J.S., Roefs S.P.F.M., de Kruif K.G. (1999). Association Behavior of Native β -Lactoglobulin. *Biopolymers*, 49, 11-20.
 17. Taulier N., Chalikian T.V. Characterization of pH-induced Transitions of β -Lactoglobulin: Ultrasonic, Densimetric, and Spectroscopic Studies.

18. A. W. Perriman, M. J. Henderson, S. A. Holt, J. W. White, (2007). Effect of the Air-Water Interface on the Stability of β -Lactoglobulin. *J. Phys. Chem. B*, 111, 13527-13537.
19. B. A. Noskov, (2014). Protein conformational transitions at the liquid-gas interface as studied by dilational surface rheology. *Adv. Colloid Interface Science*, 206, 222-238.
20. F.L. Jara, C.C. Sánchez, J.M.R. Patino, A.M.R. Pilosof. Competitive adsorption behavior of b-lactoglobulin, a-lactalbumin, bovin serum albumin in presence of hydroxypropylmethylcellulose. Influence of pH. *Food Hydrocolloids* 35 (2014) 189-197.
21. V. Ulaganathan, I. Retzlaf, J.Y. Won, G. Gochev, C. Gehin-Delval, M. Leser, B.A. Noskov, R. Miller (2016). β -Lactoglobulin Adsorption Layers at the Water/Air Surface: 1. Kinetics of Adsorption, Effect of pH and Ionic Strength. *Colloids Surface A*, *to be submitted*.
22. S. Pezenneca, F. Gauthierb, C. Alonsob, F. Granerb, T. Croguennecc, G. Brule' c, A. Renault, (2000). The protein net electric charge determines the surface rheological properties of ovalbumin adsorbed at the air-water interface. *Food Hydrocolloids* 14, 463-472.
23. A. Javadi, N. Mucic, M. Karbaschi, J.Y. Won, M. Lotfi, A. Dan, V. Ulaganathan, G. Gochev, A.V. Makievski, V.I. Kovalchuk, N.M. Kovalchuk, J. Krägel, R. Miller, (2013). Characterization methods for liquid interfacial layers, *Eur. Phys. J. Spec. Top.* 222, 7-29.
24. Bryan W.P. (1978). The isoionic point of amino acids and proteins. *Biochemical Education*, 6(1), 14-15.
25. Kirkwood, J. G., & Shumaker, J. B. (1952). Forces between protein molecules in solution arising from fluctuations in proton charge and configuration. *Proceedings of the National Academy of Sciences of the United States of America*, 38(10), 863.

5.4. Adsorption kinetics of β -Lactoglobulin at the surface of static bubble for varying pH and salt concentration[†]

5.4.1. Introduction

The adsorption of proteins at liquid/fluid interfaces depends on several factors in respect to the solution composition. At fixed solvent conditions, the increase of the protein bulk concentration causes 1) the increase of the rate of surface pressure change; 2) the increase of the equilibrium values of surface pressure Π ; and 3) the decrease of the induction time τ_{ind} [1-8], i.e., the time of adsorption prior to the onset of measurable Π -values. On the other hand, at a fixed protein concentration the adsorption kinetics and the adsorbed amount depend on pH and the ionic strength of the solution [8-22]. Generally, the increase of the ionic strength enhances the adsorption and leads to increasing Π -values [8,10,12,20]. Thickening of the adsorption layer with increasing electrolyte concentration was observed for lysozyme [18] and β -lactoglobulin (BLG) [21] layers. The influence of pH on the surface layer characteristics seems to be more complex. Extensive systematic studies, encompassing a large pH range below, close to and above the isoelectric point of different proteins, are needed to elucidate this effect and some attempts have been already made in the recent years to better understand these effects [9,14,17].

Protein molecules are zwitterions which contain free amino and carboxyl groups, and therefore the molecular net charge depends on the solution pH. For every protein there is a specific pH-value, referred to as the isoelectric point IEP, at which the molecular net charge inclines to zero while at $\text{pH} \neq \text{IEP}$ the net charge is either positive ($\text{pH} < \text{IEP}$) or negative ($\text{pH} > \text{IEP}$). Peak values of the surface pressure were found at pH close to IEP for catalase [13], lysozyme [13], bovine serum albumin (BSA) [14] and BLG [17]. The surface pressure isotherm for β -casein shows higher Π -values at pH 5 (close to IEP), as compared to pH 7 and 9, only at sufficiently high protein concentrations, while for relatively low concentration, the Π -values are lower at pH 5 [16]. To the best of our knowledge, the effect of pH on the surface pressure isotherm for globular proteins, including the case of pH close to IEP, has not been

[†] Ulaganathan, V., Retzlaff I., Won J.Y, Gochev G., Gehin-Delval, C., Leser, M.E., Noskov B.A., Miller R. (2016). β -Lactoglobulin Adsorption Layers at the Water/Air Surface: 1. Kinetics of Adsorption, Effect of pH and Ionic Strength. submitted to Colloids Surface A,.

yet reported in the literature. Jara et al. [19] recently reported the surface pressure isotherm for BLG measured at pH 3 and 6, which are respectively below and above IEP ≈ 5.1 [17].

Engelhardt et al. investigated the effect of pH on the surface pressure, the dilational rheology and the structure of BLG adsorption layers at the water/air interface using tensiometry, ellipsometry and sum frequency generation (SFG) spectroscopy [17]. In that combined study, a single protein concentration was studied, while in this paper we communicate a richer set of experimental data, including measurements of the dynamic surface pressure as a function of the BLG concentration, pH and ionic strength of the solutions. The surface pressure isotherm was obtained at pH 3, 5 and 7 on the basis of the $\Pi(t)$ data after a long time of adsorption (~ 22.2 hours). This chapter presents the part of a large set of experimental results on the effect of pH and the properties of BLG adsorption layers at the water/air interface. The dilational rheology data is not included in the thesis but will be published later.

5.4.2. Materials and Methods

BLG sample that we used was obtained as described in [23] and provided by the group of Ulrich Kulozik (Technische Universität München, Germany). BLG solutions with various protein concentrations C_{BLG} and pH were prepared in Na_2HPO_4 /Citric Acid/Milli-Q water buffer with concentrations of $C_{\text{buff}} = 1, 10$ and 100 mM. To eliminate low-molecular mass surface active contaminations, the initial stock solutions were purified with activated charcoal (BLG/charcoal mass ratio 1/3, stirred for 20 min) [24]. After this treatment, the solutions were filtered through a $0.45 \mu\text{m}$ pore size filter. The stock solutions at pH 3 and 7 were stored in a fridge for a maximum of 3 days and the desired dilutions were freshly prepared before each measurement. In the case of pH 5, all working solutions were freshly prepared from a stock solution with pH 7 by diluting with buffer with an appropriate pH to reach a final value of pH 5. Solutions at pH 5 with a concentration higher than 2×10^{-5} M were not studied since they precipitate.

Adsorption kinetics experiments were performed using the drop/bubble Profile Analysis Tensiometer PAT-1 (SINTERFACE Technologies, Germany) (see section 4.2.2). The dynamic surface pressure, $\Pi(t) = \gamma_0 - \gamma(t)$ with $\gamma_0 = 72.3 \pm 0.3$ mN/m for pure buffer/air interface and γ_t – the measured surface tension of a solution after time t , was determined with a $10 \mu\text{l}$ ($A \approx 21.2 \text{ mm}^2$) buoyant bubble in solutions for time of 80 000 s (around 22.2 h).

In order to gain information about the surface dilational rheology of the studied BLG layers, we used an experimental protocol allowing for application of harmonic area

oscillations and measuring the surface pressure response [25,26]. The timeline of the experimental protocol is illustrated in Fig. 5.11. It contains periods with three cycles of area oscillations at a fixed frequency of 0.1 Hz and area deformation $\Delta A/A = 7\%$ in the course of adsorption. For each three oscillations, a single Π -value was calculated equal to the average of all Π -values which correspond to the undisturbed constant bubble area (blue circles in Fig. 5.11). These Π -values are plotted in blue squares in Fig. 1 as a function of the time moment in the middle of a triplet (blue circles in Fig. 5.11). The $\Pi(t)$ data in Figs. 5.14-5.18 are presented in the same manner. We chose such kind of expression of the dynamic surface pressure data in order to adequately plot the obtained dilational rheology data as a function of the surface pressure. These results will be presented and discussed in a forthcoming paper.

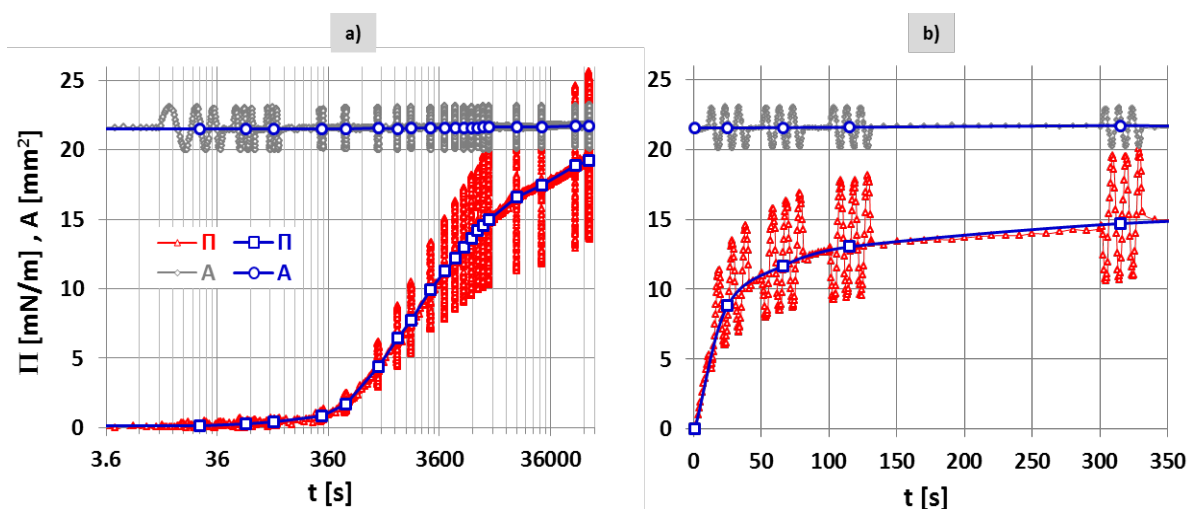


Figure 5.11. Timeline of the experimental protocol, Π – surface pressure and A – bubble area.

Examples: a) $C_{BLG} = 10^{-5}$ M, pH 3, $C_{buff} = 10$ mM; b) $C_{BLG} = 10^{-4}$ M, pH 3, $C_{buff} = 10$ mM
(short-times plot is presented for the sake of better illustration).

5.4.3. Results and discussion

We measured the time evolution of the surface pressure $\Pi(t)$ of a bubble aging in a protein solutions at various protein concentrations in the range $10^{-9} - 10^{-4}$ M in presence of 10 mM buffer or in pure water. The final Π -values in the $\Pi(t)$ curves after 80 000 s (~ 22.2 hours) were used to construct the surface pressure isotherm $\Pi(C_{BLG})$. The isotherm at pH 7, obtained in the same manner, was previously reported [7]. In this study we present experimental $\Pi(C_{BLG})$ data measured at pH 3 and pH 5 (in 10 mM buffer), and at pH 6.3 (in pure water); all these results are shown together in Fig. 5.12 (top).

Any thermodynamic analysis of interfacial adsorption layers inevitably involves the dependence of the equilibrium surface pressure on the solution bulk concentration of the adsorbing surfactant or protein (C_P) in particular, i.e., the $\Pi(C_P)$ isotherm. We performed a thermodynamic analysis of the $\Pi(C_{BLG})$ data in Fig. 5.12 and the quantitative results obtained will be discussed only in a forthcoming paper. In the present work we use the $\Pi(C_{BLG})$ data to qualitatively describe the behavior of BLG adsorption layers close to equilibrium for different pH-values in order to support the interpretation of the dynamic surface pressure data.

The $\Pi(C_{BLG})$ curves in Fig. 5.12 are rather different, which implies a variation of the surface activity of BLG molecules as a function of pH [12,17,19]. The onset of measurable surface pressure (within the experimental time-scale) for pH 3 is shifted to higher protein concentrations by around one order of magnitude in comparison to the case of pH 7, which indicates lower surface activity of the protein molecules at pH 3. Similar results were reported recently by Jara et al. [19] for $\Pi(C_{BLG})$ data measured at pH 3 and 6. The shapes of the $\Pi(C_{BLG})$ curves for pH 3 and 7 in Fig. 5.12 are similar whereas the data at pH 5 show a steeper slope. Such steeper slope of the $\Pi(C_P)$ curves at pH close to IEP, as compared to the data at $pH \neq IEP$, was reported for β -casein adsorption layers as well [16]. The reasons for such a behavior can be attributed to stronger intermolecular interactions in the surface layer at pH values close to the isoelectric point. At pH 3 and 7 the interactions between adsorbed BLG or β -casein molecules are mainly electrostatic and thereby long-ranged and relatively weak. However, the $\Pi(C_{BLG})$ data for pH 5 and pH 7 in Fig. 5.12 are very close to each other within the BLG concentration region between ca. 5×10^{-8} and 5×10^{-7} M.

The data for salt-free BLG solutions (denoted ‘water’ in Figs. 5.12, 5.18 and 5.19) shows a striking difference in the course of the surface pressure isotherm. In comparison to the other three pH values in Fig. 5.12, the ‘water’ curve exhibits a noticeable kink at a protein concentration of around 10^{-7} M followed by a well distinguished plateau within a large concentration region up to $C_{BLG} = 10^{-4}$ M. The natural pH of BLG in water is around 6.3 – 6.5 and the protein molecules carry a negative net charge. H^+ -titration experiments of BLG solutions have shown that the absolute values $|Z|$ of the net charge at these pH-values are only slightly different from those for pH 7 ($|Z|_{pH 7}$) [27,28,29]. Assuming a negligible effect of the variation of pH between pH 6.3 and 7, our results obtained in ‘water’ and in buffered solutions at pH 7 show that, apparently, the presence of electrolyte strongly affects the adsorption of BLG and the surface pressure isotherm in particular. On the other hand, Fig. 5.12 (bottom) shows virtually no differences among the data for the induction times in the

cases of ‘water’, pH 7 and pH 5 at $C_{BLG} > 2 \times 10^{-7}$ M. Based only on these data, we cannot propose presently a satisfactory explanation of these findings.

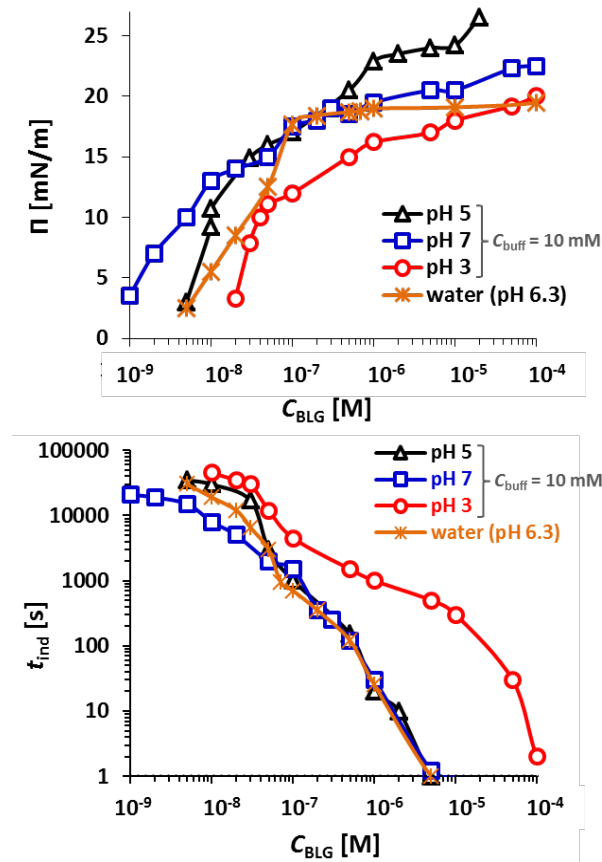


Figure 5.12. Top: Surface pressure isotherm $\Pi(C_{BLG})$. Bottom: Induction time τ_{ind} vs. C_{BLG} .
(Lines are guides to the eye)

The lower surface activity of BLG at pH 3, as compared to pH 5 [12, 17] and pH 7 [17, 30], is confirmed by the significantly longer induction times for the whole studied BLG concentration range at pH 3 (Fig. 5.12). For pH 7 and 5, the $\tau_{ind}(C_{BLG})$ curves virtually overlap for concentrations higher than 5×10^{-8} M, whereas for lower concentrations the induction times for pH 5 are longer. For example, at $C_{BLG} = 5 \times 10^{-9}$ M, τ_{ind} at pH 5 is around 10 hours, while for pH 7 it is around 4 hours; and at $C_{BLG} = 10^{-8}$ M, τ_{ind} is around 8.3 hours for pH 5, while it is around 2.2 hours for pH 7. The corresponding dynamic surface pressure data are shown in Fig. 5.13. For both protein concentrations, the Π -values after 80 000 s of adsorption are lower for pH 5 (see also Fig 2). These data are in contradiction with results for several proteins reported in literature, namely for 1.16×10^{-7} M catalase and 8×10^{-6} M lysozyme [13], for 3×10^{-8} M BSA [14], and for 10^{-5} and 5×10^{-5} M BLG [17], which show surface pressure

peaks at pH close to IEP. In this respect, the dynamic surface pressure data at the BLG concentrations of 5×10^{-9} and 10^{-8} M in Fig. 5.13 show ‘anomalous’ behavior. One can assume that after certain time of adsorption, for which the surface pressure increase is only very small, the protein adsorption layer can be considered to be in a steady regime, i.e., in a ‘quasi-equilibrium’ state. Hence, such a state is assumed to possess certain degree of the approach to equilibrium which degree diminishes with decrease of the protein concentration. Therefore, the ‘anomalous’ behavior of the surface pressure data in Fig. 5.13 can be related to the assumption that the interfacial layer is in a ‘quasi-equilibrium’ state which is far from equilibrium at these relatively low protein concentrations. At relatively high protein concentrations, the behavior of the BLG layer at pH 5 and 7 follows a different scenario and we discuss this below.

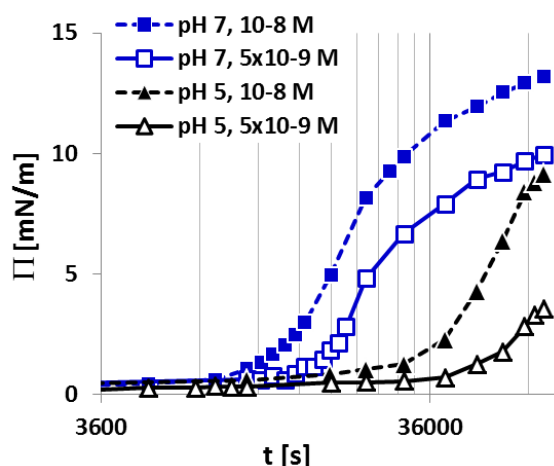


Figure 5.13. Evolution of the surface pressure $\Pi(t)$ for ‘low’ protein concentrations at $C_{\text{buff}} = 10$ mM. (Lines are guides to the eye)

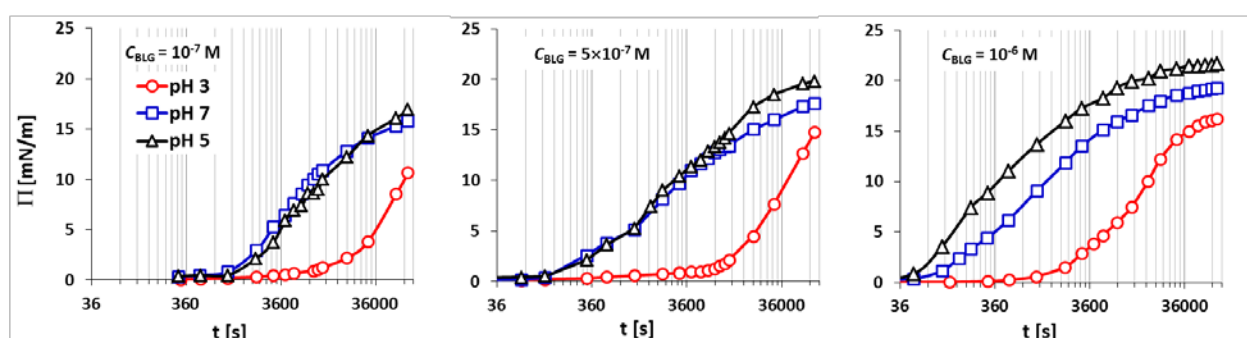


Figure 5.14. Evolution of the surface pressure $\Pi(t)$ for different protein concentrations at $C_{\text{buff}} = 10$ mM. (Lines are guides to the eye)

We observed that generally, at any protein concentration in the studied range, the adsorption kinetics at pH 3 is always the slowest and results in the lowest final Π -values. The lowest concentration for pH 3 at which we detected experimentally an increase of the surface pressure is 2×10^{-8} M; after an induction time of around 35 000 s, Π started to increase slowly and after totally 80 000 s of adsorption it reached a value of 3.5 mN/m, whereas at the same concentration, but at pH 5 or 7, the surface pressure reached values of around 13-14 mN/m (see Fig. 5.12). Fig. 5.14 shows the evolution of the surface pressure with time for three BLG concentrations in the range $10^{-7} - 10^{-6}$ M. The $\Pi(t)$ data for pH 5 and 7 at 10^{-7} M and 5×10^{-7} M do not differ significantly. For the concentration $C_{\text{BLG}} = 10^{-6}$ M, the highest Π -values at any time of adsorption, after the induction period, were measured at pH 5. This trend remains valid for all other higher protein concentrations studied in this work (see Figs. 5.15 and 5.16) and is in agreement with the literature [12, 17].

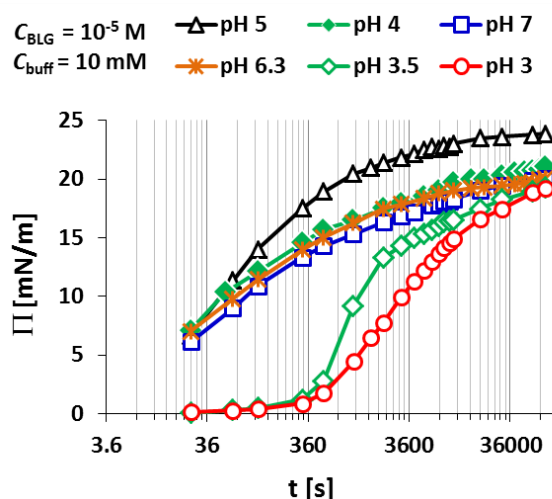


Figure 5.15. Evolution of the surface pressure $\Pi(t)$ at constant $C_{\text{BLG}} = 10^{-5}$ M and various pHs; $C_{\text{buff}} = 10$ mM. (Lines are guides to the eye)

To illustrate the effect of pH on the surface pressure for a larger set of pH values, we choose a protein concentration of $C_{\text{BLG}} = 10^{-5}$ M (Fig. 5.15). The trend among the $\Pi(t)$ curves for pH 3, 5 and 7 is similar to that at $C_{\text{BLG}} = 10^{-6}$ M (Fig. 5.14), but in this case, the induction times for pH 5 and 7 become already very short (below 1 second). For pH 3, an induction time of few minutes was detected. For pH 3.5, a similar τ_{ind} was observed, but the subsequent Π -increase is faster than that for pH 3 and finally a slightly higher value is reached. The data for pH 4, 6.3 and 7 are very similar. At pH 4, BLG molecules in solution carry a net charge of about $Z = +12$ [31] and $|Z|_{\text{pH4}}$ is comparable to $|Z|_{\text{pH6.3}}$ and $|Z|_{\text{pH7}}$. However, at any

time of adsorption longer than ca. 2 min, the highest Π -values were measured at pH 5, as it is the case for $C_{\text{BLG}} = 10^{-6}$ M in Fig. 5.14.

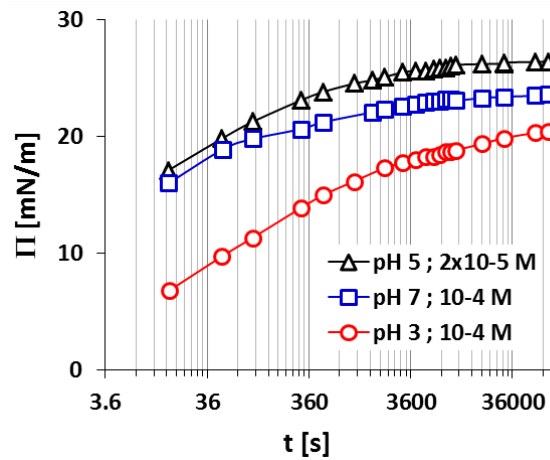


Figure 5.16. Evolution of the surface pressure Π for the highest protein concentrations measured in this study at pH 3, 5 and 7; $C_{\text{buff}} = 10$ mM. (Lines are guides to the eye)

Fig. 5.16 presents the $\Pi(t)$ data for the highest BLG concentrations measured in this study. The adsorption kinetics is the fastest at pH 5 even at a 5-fold lower protein concentration, in comparison to pH 7 and 3, and determines the maximum surface pressure values in the $\Pi(C_{\text{BLG}})$ isotherm (Fig. 5.12).

The results shown so far reveal that beyond a certain protein concentration (ca. $C_{\text{BLG}} \geq 10^{-6}$ M) the adsorption kinetics is the strongest at pH 5 [12, 17]. At protein concentrations $C_{\text{BLG}} \leq 10^{-8}$ M, the data for pH 5 shows “anomalous” behavior, i.e., longer induction times and lower Π -values in comparison to the data for pH 7. This finding opens the question why and how the adsorption process is influenced so dramatically by the protein concentration. In the next two paragraphs we discuss the main factors that could be used to explain the effect of pH on the adsorption properties of BLG at the water/air interface.

As far as a significant effect of pH on the diffusion coefficient of BLG is not expected [2,32], the well pronounced effect of pH on the adsorption behavior of BLG should be attributed to other factors, such as changes in the surface activity of the protein with variation of the molecular net charge [10]. BLG and proteins in general carry a certain net charge with an absolute value $|Z|$; ideally $Z = 0$ at the isoelectric point IEP, in other cases Z is negative ($-Z$) at $\text{pH} > \text{IEP}$ and positive ($+Z$) at $\text{pH} < \text{IEP}$. H^+ -titration experiments of BLG solutions revealed that $|Z|_{\text{pH}7}$ is about 2-2.5 times lower than $|Z|_{\text{pH}3.5}$ and about 2.5-3 times lower than $|Z|_{\text{pH}3}$ [27,28,29]. Assuming no effect of the sign of the net charge, we relate the lower

surface activity of BLG at pH 3 and 3.5, in comparison with pH 7, to the larger $|Z|$ -value of the net charge. Such argumentation is confirmed by the $\Pi(t)$ data for pH 3.5 in Fig. 5.15 showing faster adsorption kinetics than that for pH 3; nevertheless, the induction time seems unaffected.

The physical background behind the effect of the protein net charge on the surface pressure and on the adsorption kinetics in general, can be related to changes in the surface activity of the protein molecules and to the existence of an electrostatic barrier of adsorption [10,33]. Protein's surface activity intrinsically depends on the ability of the molecules to expose hydrophobic segments (naturally buried in aqueous bulk environment) when they get into contact with an interface, thus ensuring cohesion with the air phase. It is expected that the higher the net charge (molecular hydrophilicity) the lower this possibility appears. Therefore, basically, reduction of $|Z|$ leads to increase of the affinity of the protein to the interface, thus promoting adsorption [10].

Let us now consider the effect of the solution ionic strength on the adsorption kinetics. Generally, the increase of the electrolyte concentration enhances the BLG adsorption [10,12,20,21]. This fact can be attributed to screening of the protein net charge by counterions, hence increasing the protein surface activity. At negligible molecular net charge, one could expect that changes of the ionic strength of the solution should not significantly affect the surface activity of the protein molecules and accordingly the surface pressure [12]. Indeed, the $\Pi(t)$ data for pH 5 at three different buffer concentrations of 1, 10 and 100 mM are rather similar (Fig. 5.17). Small differences are observed in the initial parts of the $\Pi(t)$ curves. Surprisingly, for these initial parts, the dynamic surface pressure is slightly reduced with increasing C_{buff} . A possible explanation of this observation could be related to small deviations of the IEP -value due to variations of the ionic strength as reported in Refs. [27,29]. However, after around 10-20 min of adsorption, the data for the different buffer concentrations virtually overlap.

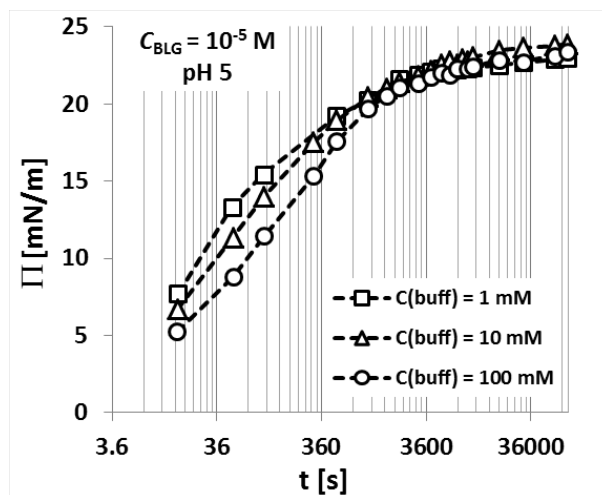


Figure 5.17. Evolution of the surface pressure $\Pi(t)$ for solutions with $C_{\text{BLG}} = 10^{-5}$ M and pH 5 \rightarrow IEP at different buffer concentrations. (Lines are guide to the eye)

The influence of electrolytes on the adsorption of BLG is significantly pronounced in solutions at $\text{pH} \neq \text{IEP}$ [10,12,20,21]. Fig. 5.18 shows the dynamic surface pressure for solutions with $C_{\text{BLG}} = 10^{-5}$ M for pH 3, 3.5, 6.3 and 7 at different buffer concentrations. Induction times of few seconds (pH 6.3 and 7) or few minutes (pH 3 and 3.5) were measured for the lowest buffer concentration $C_{\text{buff}} = 1$ mM and for the buffer-free solution (water, pH 6.3).

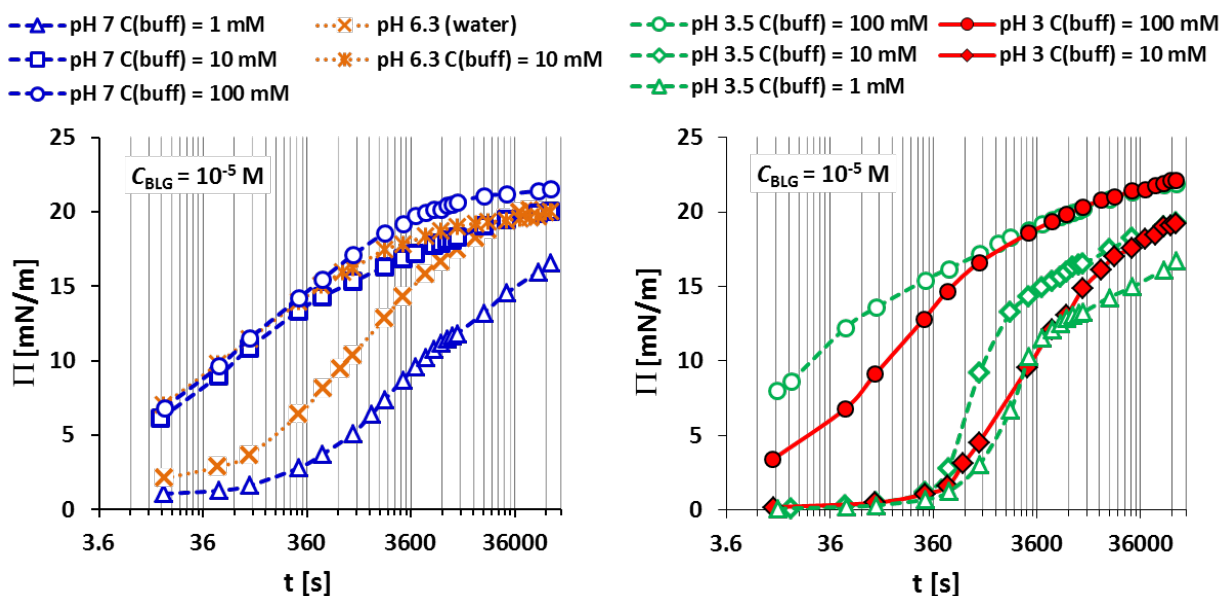


Figure 5.18. Evolution of the surface pressure $\Pi(t)$ for solutions of $C_{\text{BLG}} = 10^{-5}$ M; $\text{pH} > \text{IEP}$ (left) and $\text{pH} < \text{IEP}$ (right) at different buffer concentrations. (Lines are guide to the eye)

For pH 7 and 6.3, the induction time τ_{ind} disappears at $C_{\text{buff}} = 10$ mM, i.e., it is below the experimentally accessible minimum adsorption time, and leads to a considerable enhancement of the adsorption. For pH 6.3, the adsorption in absence of buffer is faster than the adsorption for pH 7 at $C_{\text{buff}} = 1$ mM, whereas virtually no difference is observed between the $\Pi(t)$ data for these two pH values at $C_{\text{buff}} = 10$ mM (same data as in Fig. 5). These results reveal that the effects of pH and ionic strength are coupled – the difference in the protein net charge $|Z|$ for pH 6.3 and 7 is operative at relatively low ionic strength and it is ‘screened’ at sufficiently high buffer concentration (10 mM). At pH 7, a further increase from 10 to 100 mM buffer causes only a slight shift of the $\Pi(t)$ data towards higher Π -values (note, that during the first few minutes both data-sets virtually overlap).

For pH 3.5, the increase of C_{buff} from 1 to 10 mM does not appreciably reduce the induction time, but enhances the adsorption during the following stage of Π -increase. A noticeable difference between the data for pH 3 and 3.5 at $C_{\text{buff}} = 10$ mM appears only after the induction period, where the $\Pi(t)$ curve for pH 3.5 is shifted to higher Π -values; however, both data-sets achieve similar final surface pressure after 80 000 s of adsorption. The data for pH 3 and 3.5 at $C_{\text{buff}} = 100$ mM, follow a comparable scenario, but in this case the induction time becomes negligible and maximum surface pressure values are achieved.

As discussed above, the molecular net charge $|Z|$ of BLG at pH 3 and 3.5 is larger than that at pH 6.3 or 7 [27,28,29]. The results in Fig. 5.18 reveal that the higher the net charge is the higher is the ionic strength required to enhance adsorption.

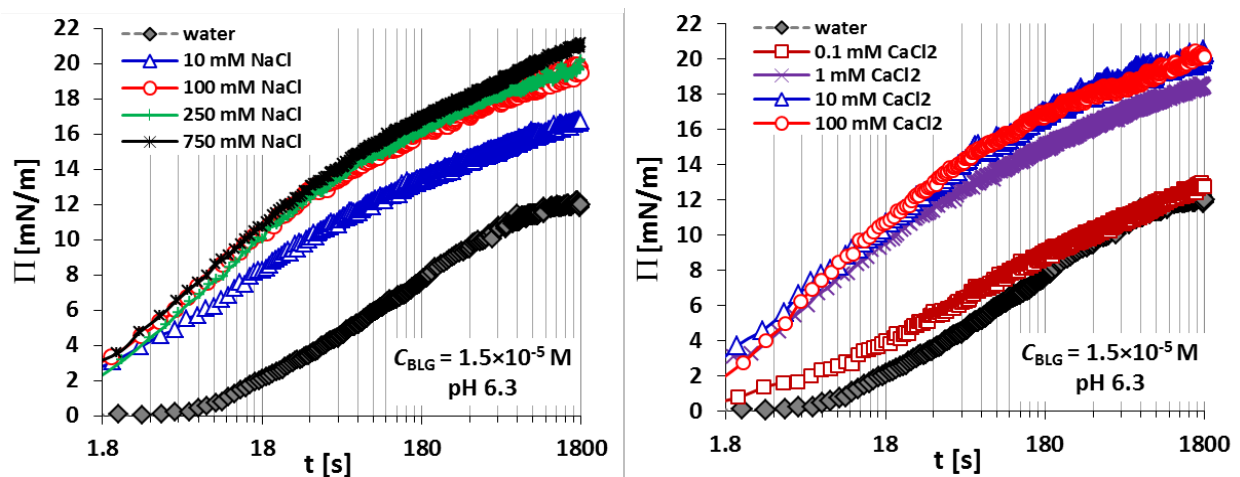


Figure 5.19. Evolution of the surface pressure $\Pi(t)$ for solutions with $C_{\text{BLG}} = 1.5 \times 10^{-5}$ M; pH 6.3 at different NaCl (left) and CaCl_2 (right) concentrations. (Lines are guide to the eye)

In order to follow the role of different salts in the adsorption kinetics of BLG, we measured the dynamic surface pressure of buffer-free solutions with $C_{\text{BLG}} = 1.5 \times 10^{-5}$ M, containing different electrolyte concentrations of either NaCl or CaCl₂ for adsorption time of half hour (Fig. 5.19). The general trend of surface pressure increase with increasing electrolyte concentration C_{el} is valid for these two salts as well [10,12]. The presence of 10 mM NaCl in aqueous BLG solutions leads to a considerable enhancement of the adsorption kinetics as compared to the salt-free system. Note, that no significant difference in the layer thickness, as measured by ellipsometry (about 3.5 nm), was observed within this NaCl concentration range [21]. Increase of C_{el} from 10 to 100 mM NaCl further enhances the adsorption, which is accompanied by an increase in the layer thickness with about 1 nm [21]. Virtually no change in the adsorption kinetics was detected in the data for the higher concentration $C_{\text{el}} = 250$ mM and only a slight increase of the surface pressure was observed at 750 mM NaCl (Fig. 5.19). However, in the same time, the layer thickness progressively increases for NaCl concentrations higher than 100 mM. This fact can be attributed to the formation of a secondary layer which does not affect significantly the surface pressure of the primary monolayer.

The influence of CaCl₂ on the adsorption kinetics is much stronger pronounced. In comparison to the salt-free system, the presence of 0.1 mM CaCl₂ reduces the induction time to values unmeasurable by the technique used in this study. 1 mM CaCl₂ remarkably accelerates the adsorption kinetics and leads to Π -values even higher than those achieved in presence of 10 mM NaCl. The adsorption enhancement by increasing C_{el} somehow levels off at 10 mM CaCl₂ and no appreciable effect is observed at CaCl₂ concentration of 100 mM.

Apparently, the adsorption of BLG is enhanced much stronger by CaCl₂ than by NaCl. According to electrical double-layer arguments, this should be related to the stronger screening effect of the divalent Ca²⁺ ions, in comparison to the monovalent Na⁺ ions, on the protein's negative net charge, $-Z$, (pH 6.3 > IEP in buffer-free solutions). On the other hand, binding of Ca²⁺ to negative charges of BLG (at pH \geq 6) [34], as discussed above, can reduce the absolute net charge $|Z|$ thus enhancing the adsorption. It is reasonable to assume that these two factors act cooperatively. Binding studies revealed that no more than one Ca²⁺ ion binds to a single BLG molecule in solutions of $C_{\text{BLG}} \approx 10^{-3}$ M and $C_{\text{el}} = 1 - 10$ mM CaCl₂ [34]. Hence, this leads to elimination of one negative charge and the excess Ca²⁺ ions pursue strong screening effects on the reduced $|Z|$. Apart from the net charge effects, Ca²⁺-induced cross-linking of BLG molecules could play a certain role in the adsorption process.

5.4.4. Conclusions

In this paper we studied major factors that influence the adsorption kinetics of β -lactoglobulin (BLG) at the water/air surface, namely protein concentration, pH and electrolyte content. The effect of pH on the adsorption kinetics, as measured in terms of dynamic surface pressure $\Pi(t)$ and on the corresponding surface pressure isotherm $\Pi(C_{BLG})$ is due to variation of the net charge $|Z|$ of the protein molecules. Negligible net charge $|Z|$ IEP in the vicinity of the isoelectric point (IEP ≈ 5.1) results in surface pressure peak values for pH 5 as it was also found for β -casein [16]. For the studied pH-range 3 – 7 and at constant buffer concentration, the higher the net charge $|Z|$ pH \neq IEP the weaker the adsorption. The comparison of the data for pH 3, 5 and 7 revealed that this principle is valid for the case of pH 3 throughout the whole BLG concentration region studied in this work ($10^{-9} - 10^{-4}$ M), but surprisingly, for pH 5 and 7, it is valid only for sufficiently high BLG concentrations, ca. $C_{BLG} \geq 10^{-6}$ M, as reported also in the literature [12,17]. At low concentrations, ca. $C_{BLG} < 10^{-8}$ M, an ‘anomalous’ decrease of the surface activity of BLG was observed at pH 5. Such peculiar behavior is demonstrated by the adsorption kinetics data (Fig. 5.13) and is reflected in the $\Pi(C_{BLG})$ isotherm by crossing of the two data sets for pH 5 and 7 (Fig. 5.12). The same scenario was observed for β -casein as well [16]. The reasons behind these intriguing findings remain yet unclear. Further valuable information can be gained by a theoretical description of the experimental data using an appropriate model. The concept that the protein interfacial layer is in a ‘quasi-equilibrium’ state with certain degree of the approach to equilibrium can be used to explain this finding by assuming that the system is far from equilibrium at relatively low protein concentrations and at the times of adsorption in experiments presented in this study. It is quite probable that at longer times the ‘anomalous’ behavior at low concentrations would disappear.

At constant pH (constant $|Z|$), the surface activity of BLG can be modified by the ionic strength of the solution due to the screening effect of the electrolytes. This effect is negligible for pH-values in the vicinity of the isoelectric point IEP and is well pronounced at pH \neq IEP. In buffer-free solutions, $CaCl_2$ significantly enhances the adsorption kinetics at much lower concentrations than it is observed for NaCl. The mechanism of this effect can be attributed simultaneously to stronger screening of $|Z|$ by the divalent Ca^{2+} ion and to partial reduction of $|Z|$ due to Ca^{2+} binding.

The mechanism by which the net charge controls the protein surface activity, as discussed in the literature, is consistent with an electrostatic barrier of adsorption [10,33]. On another hand, ionization/deionization of different functional groups, as dictated by the pH value of the solution, inevitably results in conformational changes in the tertiary structure of the BLG globules, which should have an additional impact on the molecular surface activity of BLG. The contribution of the latter factors to the adsorption behavior of BLG is not clear and, therefore, discrimination between electrostatic and structural effects is still a challenge.

5.4.5. References

1. Tripp, B. C., Magda, J. J., & Andrade, J. D. (1995). Adsorption of globular proteins at the air/water interface as measured via dynamic surface tension: concentration dependence, mass-transfer considerations, and adsorption kinetics. *Journal of colloid and interface science*, 173(1), 16-27.
2. Wüstneck, R., Krägel, J., Miller, R., Fainerman, V. B., Wilde, P. J., Sarker, D. K., & Clark, D. C. (1996). Dynamic surface tension and adsorption properties of β -casein and β -lactoglobulin. *Food Hydrocolloids*, 10(4), 395-405.
3. Miller, R., Fainerman, V. B., Wüstneck, R., Krägel, J., & Trukhin, D. V. (1998). Characterisation of the initial period of protein adsorption by dynamic surface tension measurements using different drop techniques. *Colloids and Surfaces A: Physicochemical and Engineering Aspects*, 131(1), 225-230.
4. Erickson, J. S., Sundaram, S., & Stebe, K. J. (2000). Evidence that the induction time in the surface pressure evolution of lysozyme solutions is caused by a surface phase transition. *Langmuir*, 16(11), 5072-5078.
5. Miller, R., Aksenenko, E. V., Fainerman, V. B., & Pison, U. (2001). Kinetics of adsorption of globular proteins at liquid/fluid interfaces. *Colloids and Surfaces A: Physicochemical and Engineering Aspects*, 183, 381-390.
6. Álvarez Gómez, J. M., & Rodríguez Patino, J. M. (2006). Formulation engineering of food model foams containing diglycerol esters and β -lactoglobulin. *Industrial & engineering chemistry research*, 45(22), 7510-7519.
7. Gochev, G., Retzlaff, I., Aksenenko, E. V., Fainerman, V. B., & Miller, R. (2013). Adsorption isotherm and equation of state for β -Lactoglobulin layers at the air/water surface. *Colloids and Surfaces A: Physicochemical and Engineering Aspects*, 422, 33-38.
8. Pal, P., Kamilya, T., Mahato, M., & Talapatra, G. B. (2011). Protein Monolayer Formation At Air–Electrolyte Interface: A Langmuir–Blodgett Study. *Surface Review and Letters*, 18(06), 267-279.
9. Pezennec, S., Gauthier, F., Alonso, C., Graner, F., Croguennec, T., Brule, G., & Renault, A. (2000). The protein net electric charge determines the surface rheological properties of ovalbumin adsorbed at the air–water interface. *Food Hydrocolloids*, 14(5), 463-472.

10. Song, K. B., & Damodaran, S. (1991). Influence of electrostatic forces on the adsorption of succinylated. beta.-lactoglobulin at the air-water interface. *Langmuir*, 7(11), 2737-2742.
11. Atkinson, P. J., Dickinson, E., Horne, D. S., Leermakers, F. A. M., & Richardson, R. M. (1996). Theoretical and experimental investigations of adsorbed protein structure at a fluid interface. *Berichte der Bunsengesellschaft für physikalische Chemie*, 100(6), 994-998.
12. Davis, J. P., Foegeding, E. A., & Hansen, F. K. (2004). Electrostatic effects on the yield stress of whey protein isolate foams. *Colloids and Surfaces B: Biointerfaces*, 34(1), 13-23.
13. Roberts, S. A., Kellaway, I. W., Taylor, K. M., Warburton, B., & Peters, K. (2005). Combined surface pressure-interfacial shear rheology study of the effect of pH on the adsorption of proteins at the air-water interface. *Langmuir*, 21(16), 7342-7348.
14. Noskov, B. A., Mikhailovskaya, A. A., Lin, S. Y., Loglio, G., & Miller, R. (2010). Bovine serum albumin unfolding at the air/water interface as studied by dilational surface rheology. *Langmuir*, 26(22), 17225-17231.
15. Miquelim, J. N., Lannes, S. C., & Mezzenga, R. (2010). pH Influence on the stability of foams with protein-polysaccharide complexes at their interfaces. *Food Hydrocolloids*, 24(4), 398-405.
16. Wüstneck, R., Fainerman, V. B., Aksenenko, E. V., Kotsmar, C., Pradines, V., Krägel, J., & Miller, R. (2012). Surface dilatational behavior of β -casein at the solution/air interface at different pH values. *Colloids and Surfaces A: Physicochemical and Engineering Aspects*, 404, 17-24.
17. Engelhardt, K., Lexis, M., Gochev, G., Konnerth, C., Miller, R., Willenbacher, N., ... & Braunschweig, B. (2013). pH effects on the molecular structure of β -lactoglobulin modified air-water interfaces and its impact on foam rheology. *Langmuir*, 29(37), 11646-11655.
18. Yano, Y. F., & Uruga, T. (2013). Effect of salt ions on protein layers at the air-water interface under a crystallization condition. *Chemical Physics*, 419, 153-155.
19. Jara, F. L., Sánchez, C. C., Patino, J. M. R., & Pilosof, A. M. (2014). Competitive adsorption behavior of β -lactoglobulin, α -lactalbumin, bovin serum albumin in presence of hydroxypropylmethylcellulose. Influence of pH. *Food Hydrocolloids*, 35, 189-197.

20. Delahaije, R. J., Gruppen, H., Giuseppin, M. L., & Wierenga, P. A. (2014). Quantitative description of the parameters affecting the adsorption behaviour of globular proteins. *Colloids and Surfaces B: Biointerfaces*, 123, 199-206.
21. Beierlein, F. R., Clark, T., Braunschweig, B., Engelhardt, K., Glas, L., & Peukert, W. (2015). Carboxylate Ion Pairing with Alkali-Metal Ions for β -Lactoglobulin and Its Role on Aggregation and Interfacial Adsorption. *The Journal of Physical Chemistry B*, 119(17), 5505-5517.
22. Tucker, I. M., Petkov, J. T., Penfold, J., Thomas, R. K., Cox, A. R., & Hedges, N. (2015). Adsorption of Hydrophobin-Protein Mixtures at the Air-Water Interface: The Impact of pH and Electrolyte. *Langmuir*, 31(36), 10008-10016.
23. Toro-Sierra, J., Tolkach, A., & Kulozik, U. (2013). Fractionation of α -lactalbumin and β -lactoglobulin from whey protein isolate using selective thermal aggregation, an optimized membrane separation procedure and resolubilization techniques at pilot plant scale. *Food and Bioprocess Technology*, 6(4), 1032-1043.
24. Clark, D. C., Husband, F., Wilde, P. J., Cornec, M., Miller, R., Krägel, J., & Wüstneck, R. (1995). Evidence of extraneous surfactant adsorption altering adsorbed layer properties of β -lactoglobulin. *Journal of the Chemical Society, Faraday Transactions*, 91(13), 1991-1996.
25. Loglio, G., Pandolfini, P., Miller, R., Makievski, A. V., Ravera, F., Ferrari, M., & Liggieri, L. (2001). Drop and bubble shape analysis as a tool for dilational rheological studies of interfacial layers. *Studies in interface science*, 11, 439-483.
26. Javadi, A., Mucic, N., Karbaschi, M., Won, J. Y., Lotfi, M., Dan, A., ... & Kovalchuk, N. M. (2013). Characterization methods for liquid interfacial layers. *The European Physical Journal Special Topics*, 222(1), 7-29.
27. Nozaki, Y., Bunville, L. G., & Tanford, C. (1959). Hydrogen Ion Titration Curves of β -Lactoglobulin¹. *Journal of the American Chemical Society*, 81(21), 5523-5529.
28. Basch, J. J., & Timasheff, S. N. (1967). Hydrogen ion equilibria of the genetic variants of bovine β -lactoglobulin. *Archives of Biochemistry and Biophysics*, 118(1), 37-47.
29. Ghosh, S. K., Chaudhuri, S., Roy, J., Sinha, N. K., & Sen, A. (1971). Physicochemical investigations on buffalo β -lactoglobulin. Studies on sedimentation, diffusion, and hydrogen ion titration. *Archives of biochemistry and biophysics*, 144(1), 6-15.

30. Shimizu, M., Saito, M., & Yamauchi, K. (1985). Emulsifying and structural properties of β -lactoglobulin at different pHs. *Agricultural and biological chemistry*, 49(1), 189-194.
31. Yan, Y., Seeman, D., Zheng, B., Kizilay, E., Xu, Y., & Dubin, P. L. (2013). pH-Dependent aggregation and disaggregation of native β -lactoglobulin in low salt. *Langmuir*, 29(14), 4584-4593.
32. Jung, D. M., & Ebeler, S. E. (2003). Investigation of binding behavior of α - and β -ionones to β -lactoglobulin at different pH values using a diffusion-based NOE pumping technique. *Journal of agricultural and food chemistry*, 51(7), 1988-1993.
33. MacRitchie, F., & Alexander, A. E. (1963). Kinetics of adsorption of proteins at interfaces. Part III. The role of electrical barriers in adsorption. *Journal of Colloid Science*, 18(5), 464-469.
34. Jeyarajah, S., & Allen, J. C. (1994). Calcium binding and salt-induced structural changes of native and preheated. β -lactoglobulin. *Journal of Agricultural and Food Chemistry*, 42(1), 80-85.

5.5. Foam Stability of β -Lactoglobulin solutions

5.5.1. Introduction

Foams are a colloidal system comprising of air dispersed in liquid. Generating foam requires introducing of air bubbles in a surfactant solution. One way of doing this is sparging, which is air being pumped through a porous material in a surfactant solution. Due to the large density difference between air and water the bubbles gather up quickly at the top of the liquid being aerated and the surfactant molecules stabilize the bubbles against the coalescence process. Similarly, protein solutions can also be sparged to generate foam as the proteins adsorbed at the bubble surfaces and stabilize them. However, the stabilization involves various mechanisms owing to the solution conditions and the concentration of protein molecules and the sparging conditions.

This chapter presents the results for the foam stability experiments done by varying the volume of the BLG solution and solution conditions like BLG concentration, pH and salt concentration.

5.5.2. Materials & methods

The BLG sample was obtained as described in [10] and provided by the group of Ulrich Kulozik (Technische Universität München, Germany). The solutions were prepared in Milli-Q water which had a surface tension of 72.2 mN/m at 22°C and a conductivity of 0.05 μ S/cm. All experiments were done at room temperature of $\sim 22^\circ\text{C}$. The buffer used for controlling the pH was citric phosphate buffer.

For the experimental setup regarding the foam stability please refer to chapter 2.3.4.

5.5.3. Results

The following experiments were performed with a square glass column ($\sim 50\text{cm}$) fitted to a glass frit of porosity (10-16 μm). Please refer to the experimental section above for more details on this method.

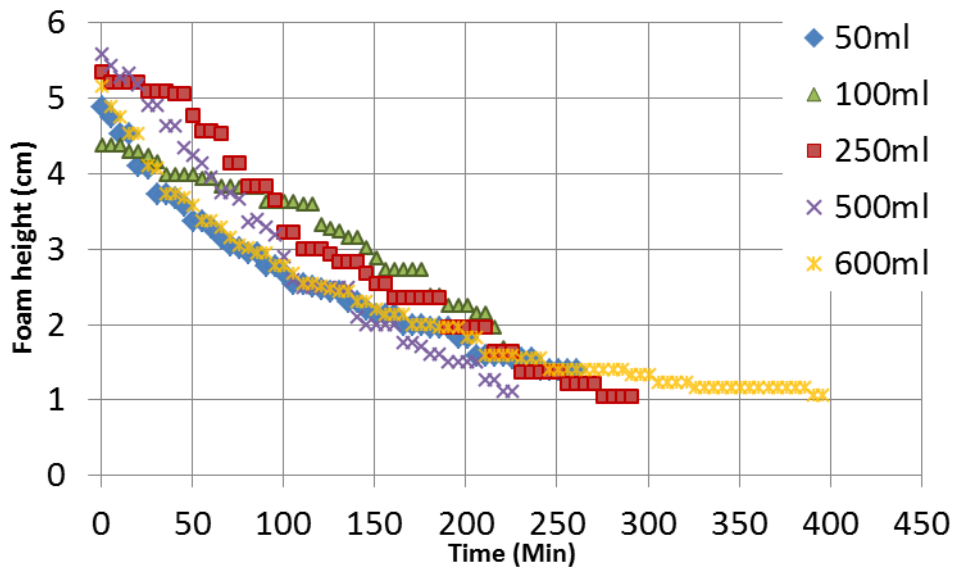


Figure 5.16 Foam height vs. time for 5×10^{-6} M BLG solution prepared in 10mM citric phosphate buffer at pH 7. The solution is sparged at 0.2 l/min flow rate for 30 seconds and the foam stability is compared for different solution volumes.

The Fig. 5.16 demonstrates the effect of liquid volume on the foam stability. Here the volume of the liquid varies from 50ml to 600ml keeping the concentration of BLG constant (5×10^{-6} M). By changing the volume of liquid we change eventually the liquid height. So at a higher liquid height the bubbles rising have more time to accumulate the molecules at the surface and thereby could contribute to a better foam stability. But in this case no significant difference in the foam stability was observed.

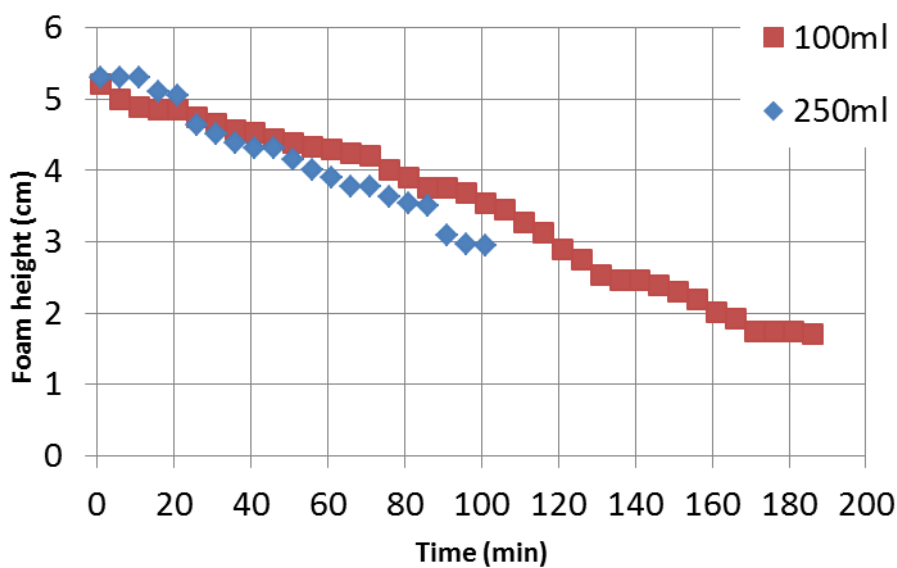


Figure 5.17 Foam height (cm) vs. time (min) for $1 \times 10^{-5} \text{M}$ BLG solution prepared in 10mM citric phosphate buffer at pH 7. The solution is sparged at 0.2 l/min flow rate for 30 seconds and the foam stability is compared for different solution volumes.

Also Fig. 5.17 indicates that there is no substantially difference when the liquid volume is changed for a BLG concentration of $1 \times 10^{-5} \text{M}$.

The following results were obtained from foam scan instrument and the flow rate was 0.15 l/min in all cases. The solution was sparged until the foam had reached 180mm height in all cases.

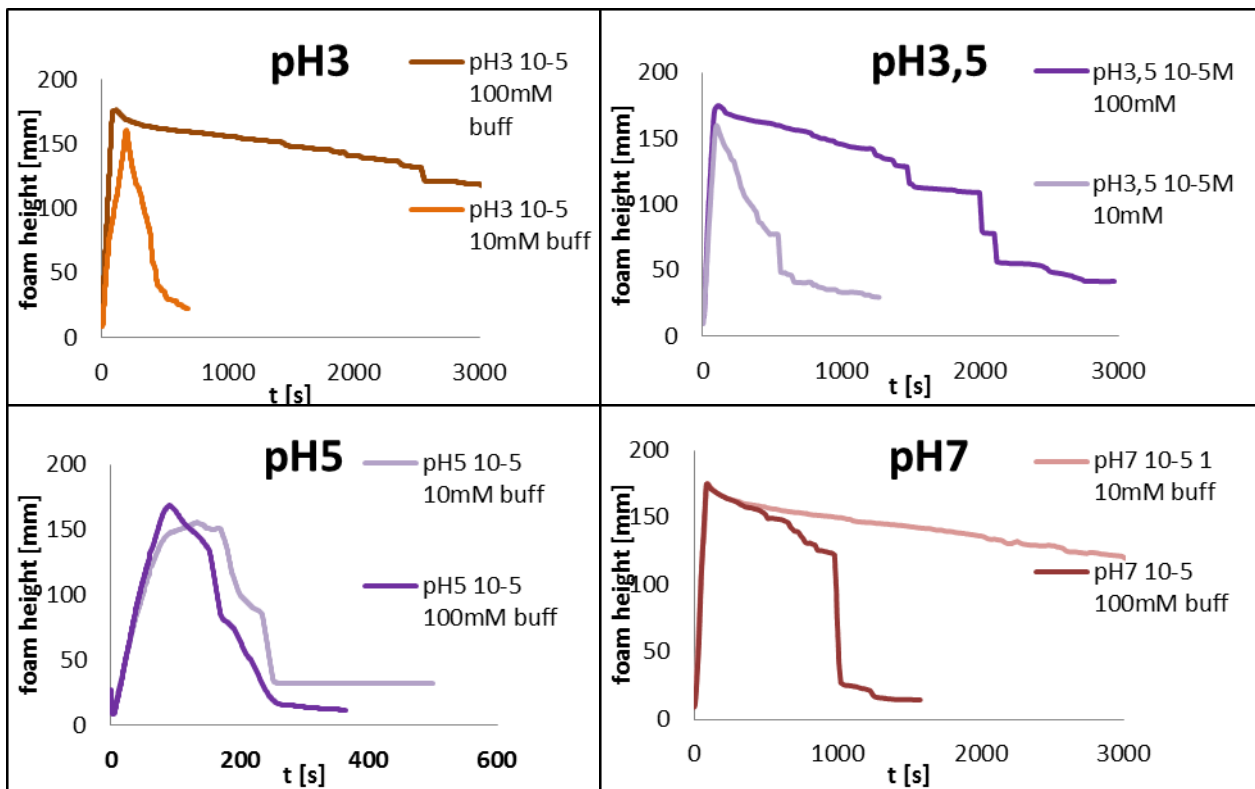


Figure 5.18 Foam stability of $1 \times 10^{-5} \text{M}$ BLG solution at different pH and ionic strength.

The Fig. 5.18 shows the foam stability curves vs time for BLG solutions at varying pH and buffer concentration. The foam scan instrument was set to sparge until the foam reached 180mm. Later on the foam height decrease over time was monitored. The above figure is an example of experiments performed and to visualize the foam stability the half life time of the foam is presented below.

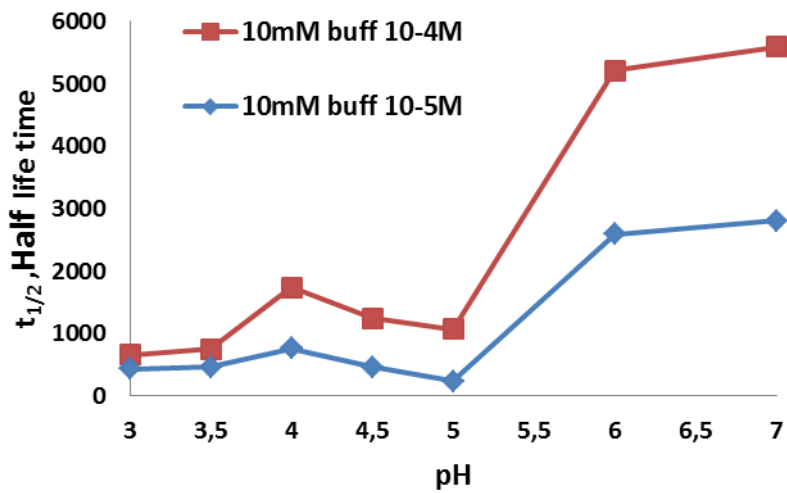


Figure 5.19 Half-life of foam generated with BLG solution at 10mM citric phosphate buffer at different pHs

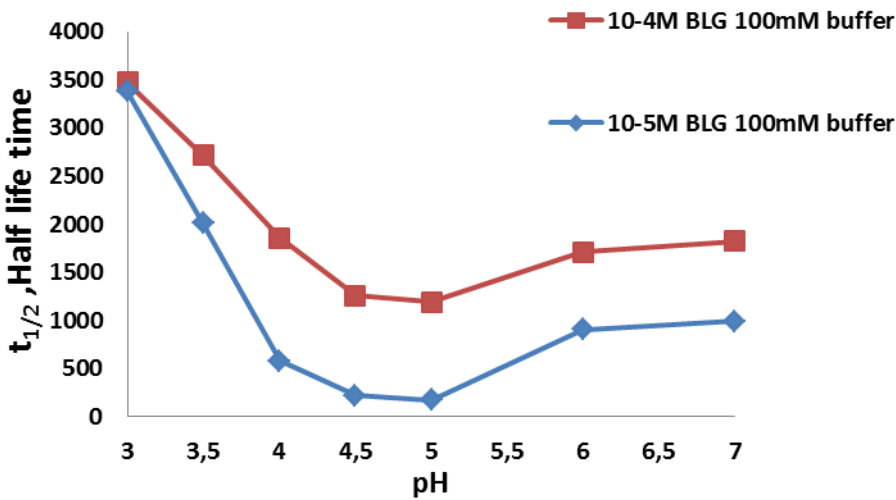


Figure 5.20 Half-life of foam generated with BLG solution at 100mM citric phosphate buffer at different pH values.

Fig. 5.19 and 5.20 present the half-life times of the BLG solution for the concentrations $1 \times 10^{-5} \text{M}$ and $1 \times 10^{-4} \text{M}$. The buffer concentrations used were 10mM and 100mM. The half-life time over varying pH were presented here. For 10mM buffer concentration in Fig. 5.19, the solutions at pH 3 have the least foam stability whereas the solutions at pH 7 have the highest. In Fig. 5.20 we can notice that at pH 3 we have the best condition for stable foam for solutions with 100mM buffer concentration.

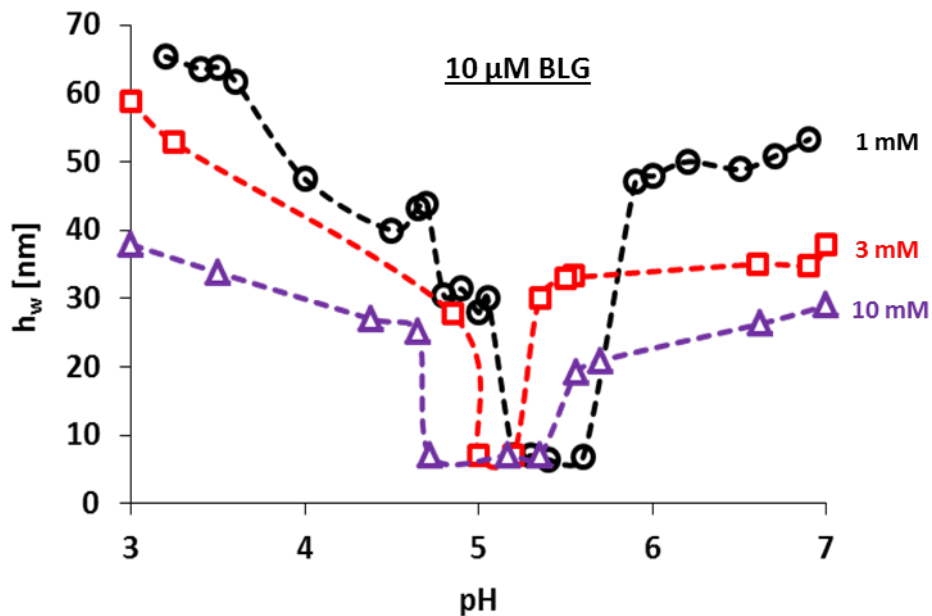


Figure 5.21 Thin liquid film thickness of 1×10^{-5} M BLG at different pH and ionic strengths (redrawn from [1]).

Fig. 5.21 shows us the thickness of thin liquid films for 1×10^{-5} M BLG for varying pH and buffer concentrations. The thickness of the film has a minimum at pH 5 as it gets closer to the isoelectric point (IEP). At pH 3 however we could notice that the thickness is much larger than that at pH 7 for 1mM and 3mM buffer concentrations. At 10mM buffer concentration, however, it gets closer to the results for pH 7. This could be one of the reasons for the low stability of foams at pH 3 for lower buffer concentrations. The larger thickness would mean faster drainage.

5.5.4. Discussion

The IEP of protein is generally considered to be the most ideal condition of optimum foam stability compared to other pH values. This is due to the fact that the net charge of the protein is neutralized which would allow more intermolecular interactions. If the proteins adsorbed at the air water interface would interact, then this would create a film which would counteract against the coalescence. The structural-mechanical barrier of the adsorbed protein layer which plays a key role in foam and emulsion stability was developed by Rehinder [2]. Due to this reasoning the shear and dilational rheology of adsorbed protein layers are important to understand the foam or emulsion stability [3-10].

In the case of BLG which is a globular molecule the solution conditions such as pH and ionic strength alter its molecular configuration. At pH values in the range <3.5 and >7.5 , it exists predominantly as monomer which again depends on the ionic strength and BLG bulk concentration. The presence of counter ions would naturally favor the self-association of these monomers to dimers or even oligomers. At pH close to IEP the conditions are most favorable for self-association and hence even octomers are formed [11-15]. IEP is the pH where the net charge of the protein is zero and also the solubility is the least as the hydrophobic patches of the proteins are exposed toward the solution [16]. This also favors the aggregation as there is negligible electrostatic repulsion and there are enhanced hydrophobic interactions. The IEP is also the pH at which proteins are known to show the highest surface activity. This has been attributed to the surface hydrophobicity of the protein which in turn should enhance the foaming properties [17-19].

Lexis et al. have studied the effect of pH and valency of added salt on BLG foam rheological properties. They have also compared to the shear rheological properties and found that at pH 3 the adsorbed layers had the least shear elasticity of all pH values while pH 5 (close to IEP) had the highest. Also their foam results complement these finding, i.e. the solutions at pH 5 gave the best foam stability [16]. From Figs. 5.19 and 5.20, however, we could see that it is not the case. The concentration of BLG that they have used was 1wt% and in our case this would be 0.18 wt% for $1 \times 10^{-4}M$ and 0.018 wt% for $1 \times 10^{-5}M$. Therefore, the bulk concentration of BLG is important at the isoelectric point as the formation of aggregates and their size could be the reason for these discrepancies.

Partially hydrophobic particles are known to be excellent stabilizers of foam. Dickinson et al, have demonstrated that silica nano-particles can help produce highly stable foams [20,21]. At the IEP which is the best pH conditions for protein aggregation, these aggregates can act as particles. These particles can therefore interact strongly creating a network which would explain a high foaming capacity and surface rheological properties as shown in [16]. A detailed review by Murray et al. [22], explains why one should not discredit such possibility. While to explain the Figs. 5.19 and 5.20, at pH 5 the concentration of BLG molecules might not be just enough to cover the bubble surfaces. Even though the molecules aggregate and these aggregates act as particles, it is possible that their concentration as such could be less. Lech et al. presented recently an article about the concentration dependence of foamability

and foam stability for BLG at different pH values [23]. They have identified a critical concentration where the foamability is no longer dependent on the BLG bulk concentration. They also observed that solutions at pH 5 have less foam stability than at pH 7 for the concentration range presented in Figs. 5.19 and 5.20.

At pH 3 the BLG is known to be primarily in a monomer configuration and the equilibrium shifts to dimers in presence of salt [24]. In the previous chapters we saw that the rising bubble velocity for BLG at pH 3 was also sensitive to the salt concentration. Engelhardt et al. have shown that though the pH 3 and pH 7 have similar net charge observed by electrophoretic mobility, the sum frequency generation (SFG) technique points out something different. A higher surface charge for BLG molecules adsorbed at air water interface was observed by SFG at pH 3 compared to pH 7 [25]. This could explain the higher foam stability that we observe for solutions at pH 3 and 100mM buffer concentration.

5.5.5. References

1. Gochev, G., Retzlaff, I., Exerowa, D. & Miller, R. (2014). Electrostatic stabilization of foam films from β -lactoglobulin solutions. *Colloids and Surfaces A: Physicochemical and Engineering Aspects*, 460, 272-279.
2. Izmailova, V. N., Yampolskaya, G. P., & Tulovskaya, Z. D. (1999). Development of the Reh binder's concept on structure-mechanical barrier in stability of dispersions stabilized with proteins. *Colloids and Surfaces A: Physicochemical and Engineering Aspects*, 160(2), 89-10.
3. Petkov, J. T., Gurkov, T. D., Campbell, B. E., & Borwankar, R. P. (2000). Dilatational and shear elasticity of gel-like protein layers on air/water interface. *Langmuir*, 16(8), 3703-3711.
4. Roth, S., Murray, B. S., & Dickinson, E. (2000). Interfacial shear rheology of aged and heat-treated β -lactoglobulin films: Displacement by nonionic surfactant. *Journal of Agricultural and Food Chemistry*, 48(5), 1491-1497.
5. Bos, M. A., & van Vliet, T. (2001). Interfacial rheological properties of adsorbed protein layers and surfactants: a review. *Advances in Colloid and Interface Science*, 91(3), 437-471.
6. Lucassen-Reynders, E. H., Benjamins, J., & Fainerman, V. B. (2010). Dilational rheology of protein films adsorbed at fluid interfaces. *Current Opinion in Colloid & Interface Science*, 15(4), 264-270.
7. Benjamins, J., & Lucassen-Reynders, E. H. (1998). Surface dilational rheology of proteins adsorbed at air/water and oil/water interfaces. *Proteins at liquid interfaces*, 341-384.
8. Dickinson, E. (2001). Milk protein interfacial layers and the relationship to emulsion stability and rheology. *Colloids and Surfaces B: Biointerfaces*, 20(3), 197-210.
9. Monteux, C., Fuller, G. G., & Bergeron, V. (2004). Shear and dilational surface rheology of oppositely charged polyelectrolyte/surfactant microgels adsorbed at the air-water interface. Influence on foam stability. *The Journal of Physical Chemistry B*, 108(42), 16473-16482.
10. Miller, R., Wüstneck, R., Krägel, J., & Kretzschmar, G. (1996). Dilational and shear rheology of adsorption layers at liquid interfaces. *Colloids and Surfaces A: Physicochemical and Engineering Aspects*, 111(1), 75-118.

11. Gottschalk M., Nilsson H., Roos H., Halle B., (2003). Protein self-association in solution: The bovine β -lactoglobulin dimer and octamer. *Protein Science*, 12, 2404-2411.
12. Mercadante D., Melton L.D., Norris G.E., Loo T.S., Williams M.A.K., Dobson R.C.J., Jameson G.B., (2012). Bovine β -Lactoglobulin Is Dimeric Under Imitative Physiological Conditions: Dissociation Equilibrium and Rate Constants over the pH Range of 2.5–7.5. *Biophysical Journal*, 103, 303-312.
13. Sakurai, K., Oobatake, M., & Goto, Y. (2001). Salt-dependent monomer–dimer equilibrium of bovine β -lactoglobulin at pH 3. *Protein Science*, 10(11), 2325-2335.
14. Verheul M., Pedersen J.S., Roefs S.P.F.M., de Kruif K.G. (1999). Association Behavior of Native β -Lactoglobulin. *Biopolymers*, 49, 11-20.
15. Taulier N., Chalikian T.V. Characterization of pH-induced Transitions of β -Lactoglobulin: Ultrasonic, Densimetric, and Spectroscopic Studies.
16. Lexis, M., & Willenbacher, N. (2014). Relating foam and interfacial rheological properties of β -lactoglobulin solutions. *Soft matter*, 10(48), 9626-9636.
17. Kato, A., & Nakai, S. (1980). Hydrophobicity determined by a fluorescence probe method and its correlation with surface properties of proteins. *Biochimica et Biophysica Acta (BBA)-Protein Structure*, 624(1), 13-20.
18. Moro, A., Gatti, C., & Delorenzi, N. (2001). Hydrophobicity of whey protein concentrates measured by fluorescence quenching and its relation with surface functional properties. *Journal of Agricultural and Food Chemistry*, 49(10), 4784-4789.
19. Townsend, A. A., & Nakai, S. (1983). Relationships between hydrophobicity and foaming characteristics of food proteins. *Journal of Food Science*, 48(2), 588-594.
20. Du, Z., Bilbao-Montoya, M. P., Binks, B. P., Dickinson, E., Ettelaie, R., & Murray, B. S. (2003). Outstanding stability of particle-stabilized bubbles. *Langmuir*, 19(8), 3106-3108.
21. Dickinson, E., Ettelaie, R., Kostakis, T., & Murray, B. S. (2004). Factors controlling the formation and stability of air bubbles stabilized by partially hydrophobic silica nanoparticles. *Langmuir*, 20(20), 8517-8525.
22. Murray, B. S., & Ettelaie, R. (2004). Foam stability: proteins and nanoparticles. *Current Opinion in Colloid & Interface Science*, 9(5), 314-320.

23. Lech F.J., Delahaije, R.J.B.M., Meinders, M.B.J. Gruppen, H. & Wierenga, P.A. Identification of critical concentrations determining foamability and stability of β -lactoglobulin. Food hydrocolloids, in press.
24. Sakurai, K., Oobatake, M., & Goto, Y. (2001). Salt-dependent monomer–dimer equilibrium of bovine β -lactoglobulin at pH 3. *Protein Science*, 10(11), 2325-2335.
25. Engelhardt, K., Lexis, M., Gochev, G., Konnerth, C., Miller, R., Willenbacher, N., ... & Braunschweig, B. (2013). pH effects on the molecular structure of β -lactoglobulin modified air–water interfaces and its impact on foam rheology. *Langmuir*, 29(37), 11646-11655.

5.6. Foam Fractionation of proteins and surfactants

5.6.1. Introduction

Foam fractionation is a technique which is used to separate the dissolved species of surface active molecules in aqueous phase. It can be achieved by sparging air into the liquid containing surface active materials. An example of such process can be seen in cleaning of aquariums where protein-like substances are removed by sparging and discarding the foam obtained [1]. Lemlich was probably the first to describe and develop the process of foam fractionation with different methods such as batch, semi-batch and continuous foam fractionation [2].

In all the methods of foam fractionation employed, the underlying principle is to produce air bubbles in a solution to be foamed. It is required that the foam produced has to be relatively stable in order to be able to harvest it. The foam has to be allowed to drain to remove the interstitial fluid in between the bubbles. This is crucial because the dryer the foam the better is the enrichment in the foam fractionation process [3].

5.6.2. Materials & methods

Non-ionic surfactants Tween 80 and Tween 20 and anionic surfactant, sodium dodecyl sulphate (SDS) that were used in this study were purchased from Sigma-Aldrich®.

The BLG used in this study is of technical grade with about 85% purity provided by Nestle Research Center, Lausanne, Switzerland.

The soluble instant coffee powder obtained from Nestle Research Center to study a practical food system.

Foam fractionation

A cylindrical glass column of height 25.5 cm is used for sparging air into the liquid. The liquid volume used was 100 ml in all cases. This corresponds to the liquid height of 8.9 cm and the foam is generated until it reaches the top end of the column. The flow rate of sparging air is set to 0.2 l/min and the liquid is allowed to drain until the height of the liquid is 6.6cm (approx. 2/3 of the initial liquid height). The details of the foam fractionation setup are given above in chapter 4.2.6.

Velocity profiles of rising bubbles to estimate the bulk concentration.

The previous chapters provided the details about the measurements of the velocity profiles of a rising bubble in dilute protein and surfactant solutions. Due to the accuracy and sensitivity

of this technique we employ it to estimate the bulk concentration of the harvested foamates. The results show the velocity profiles of known concentrations of the material which is studied and of the foamates collected by foam fractionation which is diluted further to the range of concentrations applicable to the rising bubble technique. This is the way we estimate the enrichment in material that we observe in the foam.

5.6.3. Results

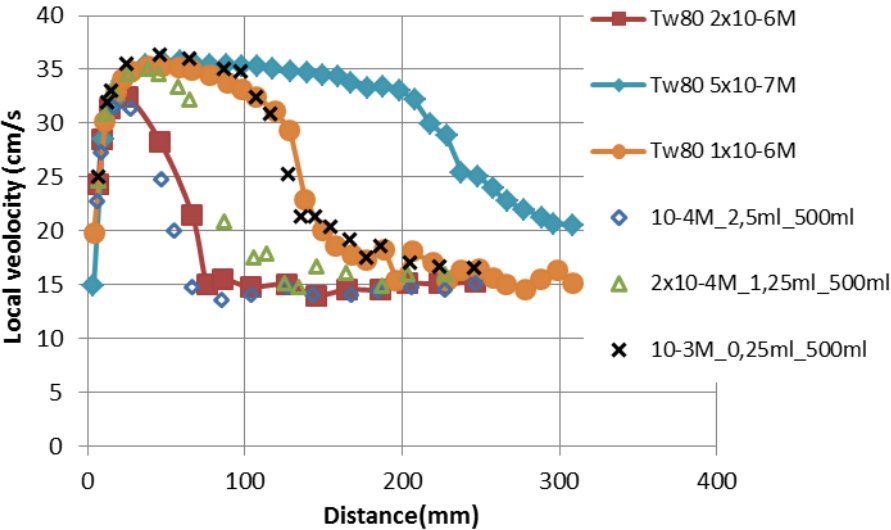


Figure 5.22 Local velocity vs distance from the capillary tip of a bubble (diameter ~ 1.45mm) rising in Twen 80 in milli Q water and the foamates collected are compared.

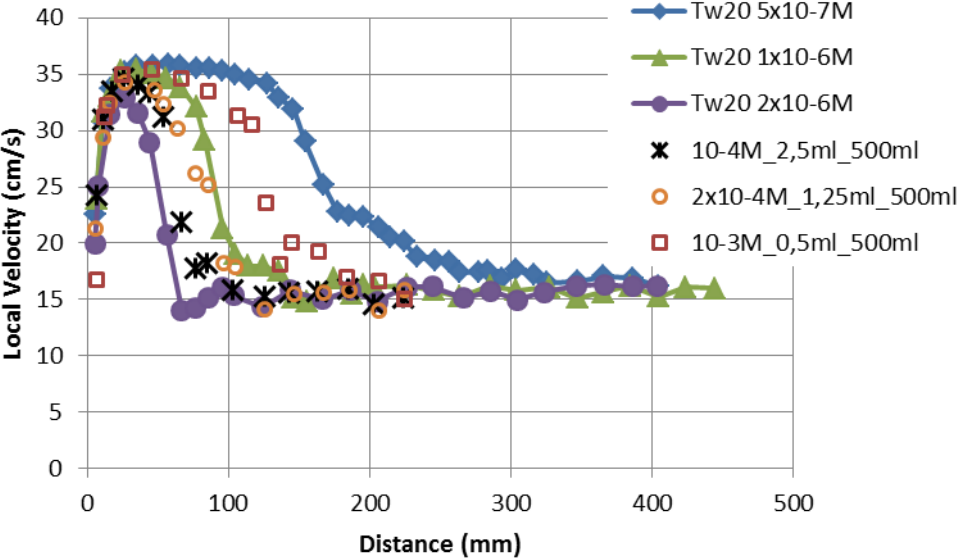


Figure 5.23 Local velocity vs distance from the capillary tip of bubble (diameter ~ 1.45mm) rising in Twen 80 in milli Q water and the foamates collected are compared.

In the Figs. 5.22 & 5.23, the velocity profiles of Tween 80 and Tween 20 for concentrations are shown. Here the legend “10-4M_2.5ml_500ml” refers to foam collected when 100 ml of $1 \times 10^{-4} \text{M}$ of solution (in both cases) was sparged at 0.2 l/min and 2.5 ml of foamate was diluted to 500 ml. So if the concentration of the foamate was $1 \times 10^{-4} \text{M}$ (i.e. there is no enrichment in foam) then the velocity profile should match the profile of $5 \times 10^{-7} \text{M}$.

For the plot in open triangles in Fig. 5.22, a $2 \times 10^{-4} \text{M}$ solution of Tween 80 was used for foaming and 1.25ml of foamate was diluted to 500 ml in milli-Q water. In case of plot with open squares in Fig.5.23, $1 \times 10^{-3} \text{M}$ of solution was used for foaming and 0.25 ml of foamate was diluted to 500 ml. All the dilutions were made in such a way that if there is no enrichment the concentration should reach $5 \times 10^{-7} \text{M}$. Any deviation from this curve would mean that there is a difference in concentration between the solution used for foaming and that which is obtained from the foamate.

The surfactants Tween 80 and Tween 20 were chosen for their differences in surface activities and closer chemical composition. In the above figures it can be noted that at the same concentrations the enrichment was higher for Tween 80. Also it is evident from the figures that by increasing the concentration of the solution which is foamed, the enrichment in the foamate is decreased.

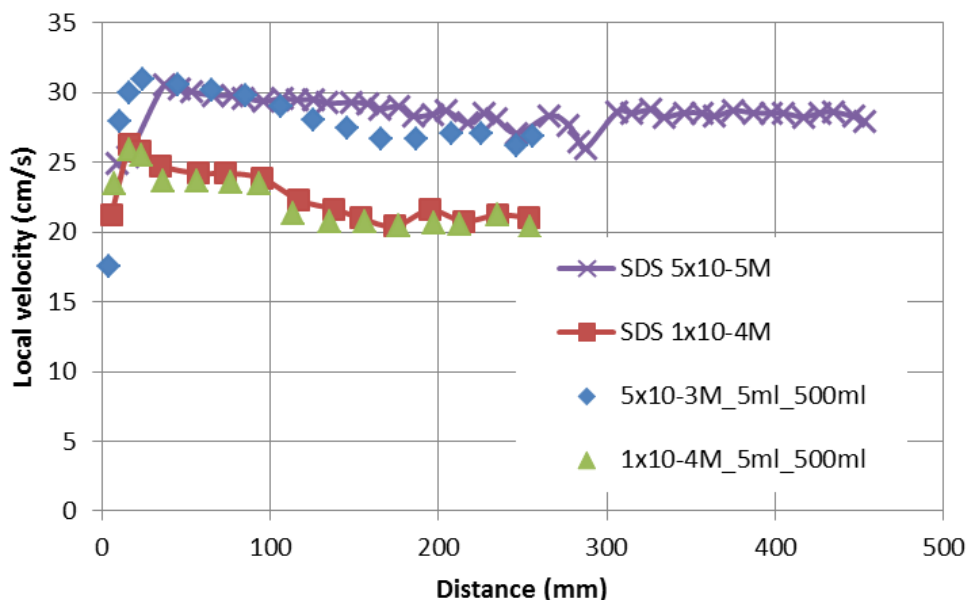


Figure 5.24 Local velocity vs distance from the capillary tip of bubble (diameter $\sim 1,45 \text{mm}$) rising in SDS solutions prepared in Milli-Q water and the foamates collected are compared.

Further foam fractionation were done with SDS, an ionic surfactant of much less surface activity, as we can see from Fig. 5.25. In Fig. 5.24 the results for SDS are summarized. (◆)

denotes foamate collected for SDS solution of concentration $5 \times 10^{-3} \text{M}$ which is used for foaming, while (\blacktriangle) denotes foamate collected from a solution of $1 \times 10^{-2} \text{M}$ of SDS used for foaming. 5 ml of foamate collected was diluted to 500 ml and used to study the rising bubble velocity in both cases. No significant enrichment in the foamate was noticed.

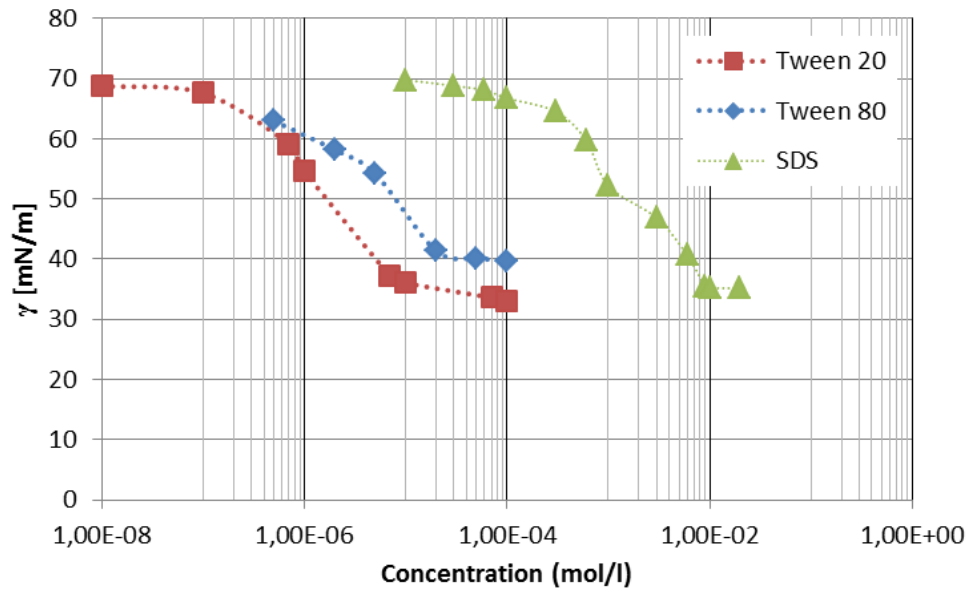


Figure 5.25 Adsorption isotherms of Tween 20, Tween 80 and SDS solutions at water/air interface. Redrawn from [4-6].

Fig.5.25 shows the adsorption isotherm of three different surfactants used for foam fractionation as presented in the previous graphs. The surface activity is significantly low for SDS compared to Tween systems and hence requires higher concentrations to stabilize the foam. This causes the foam to be less enriched.

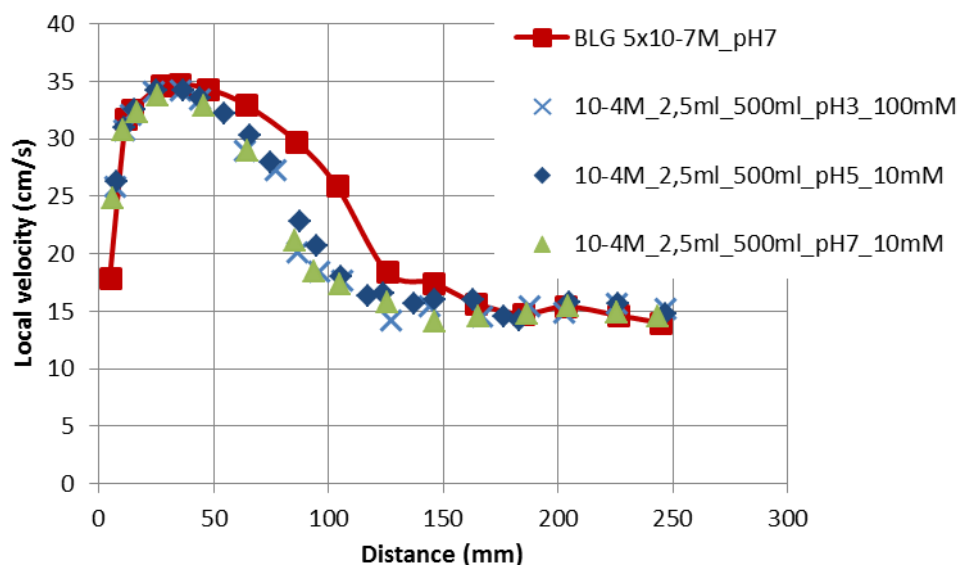


Figure 5.26 Local velocity vs distance from the capillary tip of bubble (diameter $\sim 1.45\text{mm}$) rising in BLG in 10mM citric phosphate buffer at pH 7 and the foamates collected are compared.

In Fig. 5.26, all the foamates are collected for $1 \times 10^{-4}\text{M}$ of BLG solution and 2.5 ml of foamate is diluted further to 500ml in 10mM citric phosphate buffer at pH 7 and compared with velocity profile of $5 \times 10^{-7}\text{M}$ of BLG. (\blacktriangle)denotes the foamate which is produced by foaming $1 \times 10^{-4}\text{M}$ of BLG solution in 10mM citric phosphate buffer at pH 7. (\blacklozenge)denotes the foamate which is produced by foaming $1 \times 10^{-4}\text{M}$ of BLG solution in 10mM citric phosphate buffer at pH 5. (\times)denotes the foamate which is produced by foaming $1 \times 10^{-4}\text{M}$ of BLG solution in 100mM citric phosphate buffer at pH 3. As we can see the enrichment didn't vary by changing the pH and also the ionic strength.

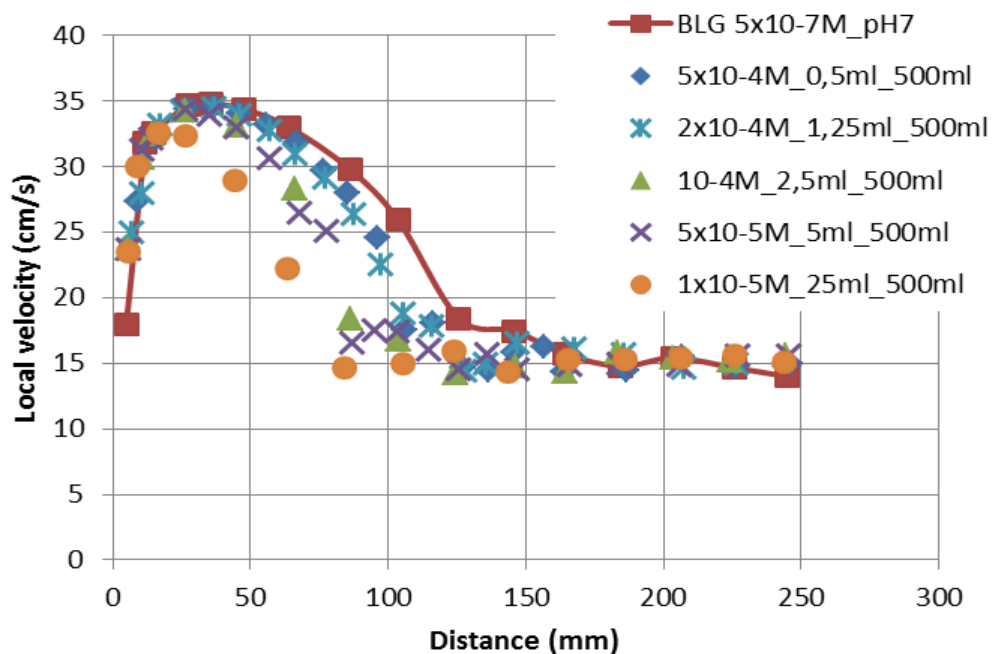


Figure 5.27. Local velocity vs distance from the capillary tip of bubble (diameter ~ 1.45 mm) rising in BLG solutions prepared in 10mM citric phosphate buffer at pH 7 and the foamates collected are compared.

The Fig. 5.27 shows different concentrations of BLG solution at pH 7 used for producing foam. The volume of foamates diluted to 500ml is given in the graph above. For example the legend " $1 \times 10^{-5} \text{M}_5 \text{ ml}_500 \text{ ml}$ " indicates foamate collected by foaming a solution of $1 \times 10^{-5} \text{M}$ and then 25ml of this foamate was diluted to 500 ml. Here we could notice that the increase in BLG concentration of foaming solution decreases its enrichment in the foam as seen in case of tween systems.

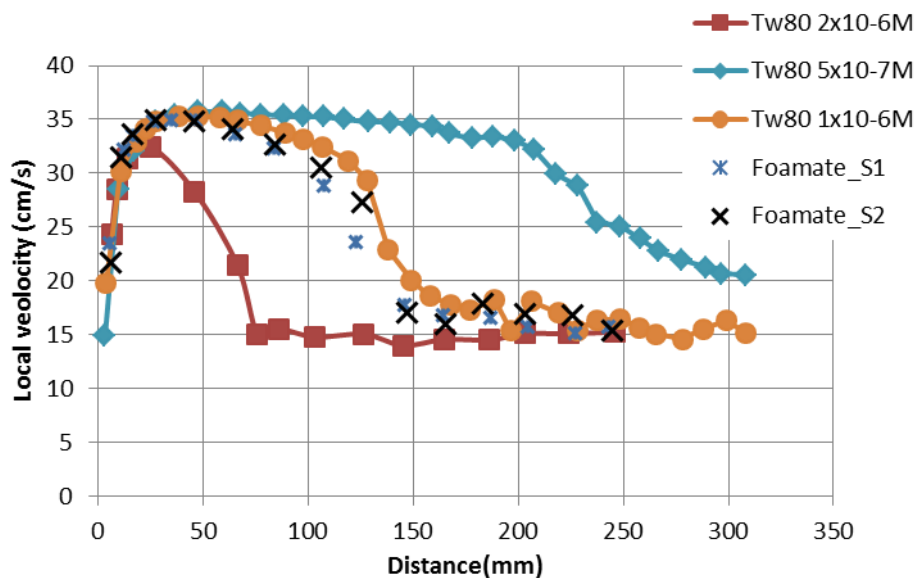


Figure 5.28. Local velocity vs distance from the capillary tip of bubble (diameter ~ 1.45 mm) rising in Twen 80 in milli Q water and the foamates collected are compared.

The above Fig. 5.28 presents the results obtained from the foam fractionation setup in NRC, Lausanne, Switzerland. The description of this setup is given in section 4.2.5.2 and the foamates are collected from the two exits X1 and X2 which belong to the sections S1 and S2. The flow rate of air was 100 ml/min in this case and the foamates were collected when the liquid height reached 60% of its original height. The time required for the liquid to drain until this level was approximately 30 min. Whereas for the other results done with setup in MPIKG the drainage time for liquid to reach 75% was 5-6 minutes.

The concentration of the Tween 80 solution used was 1×10^{-4} M and 2.5 ml of the foamate was diluted to 500 ml. When we compare Fig. 5.22 and 5.28, for the foamates collected for concentrations 1×10^{-4} M the differences in enrichments are large. For the setup at MPIKG the enrichment was 4 times higher than original concentration whereas for setup at NRC the enrichment was 2 times. This is due to the physical dimensions of the setup. The setup which allows faster drainage would be ideal to allow higher enrichments. For the setup at NRC, it was not possible to wait until the liquid reaches 75% of its original height because the volume of foam produced is larger and waiting for longer time was leading to decay of the foam produced.

5.6.4. Discussion

From the Figs. 5.22, 5.23 and 5.25, when we compare the enrichments for Tween 80, Tween 20 and SDS, the Tween surfactants show far higher enrichments than SDS. The surface activity between the adsorbed molecules can explain the differences in the enrichment between SDS and Tween systems. This can be noted in the Fig. 5.24 where we can see that the Tween surfactants have CMC values which are three orders of magnitude less than SDS. This high surface activity explains their high foam stability at lower concentrations. Scamehorn et al. have presented that cetylpyridinium chloride has a much better (about 90% recovery) by a continuous foam fractionation when compared to that of sodium dodecyl sulphate solutions [7,8].

But to explain the differences between the Tween 80 and Tween 20, one should also consider the composition of these two surfactants [9]. Tween surfactants are mixtures of isosorbide polyethoxylates, and sorbitan polyethoxylates and the adsorption rates of these components could be different in the short time range. Therefore, even though the adsorption isotherms show that Tween 20 is more surface active, the surfaces of the foam bubbles formed at short time range can have a different composition.

Brown et al. have studied the foam fractionation of bovine serum albumin (BSA) and found that the lower feed concentrations produced a better enrichment of the foam [9]. We can notice this in our experimental results for both surfactants and the BLG presented above. The minimal bulk concentration at which the surfaces of foam bubbles are covered by adsorbed molecules which would be the most ideal condition for enrichment. In case of BLG, the desorption rate is infinitesimally small and therefore once adsorbed they would not essentially desorb. Yet we do not see the enrichment as high as for the Tween systems. This could be attributed to the differences in adsorption layers of proteins and surfactants. The proteins when adsorb to the surface undergo changes in their configurations and they would occupy much larger space due to the huge differences in molecular weights between proteins and surfactants [10]. Though the surface of the bubble is covered by the protein molecules the total number would be less when compared to surfactants. Moreover, the foams produced from protein solutions contain much more liquid as the foam films are typically much thicker than surfactant foam films. This could be the reasons for differences in enrichments that we notice between BLG and Tween systems.

Moreover, the difference in pH also did not influence the enrichment of foam. Close to the IEP, i.e. at pH 5, we notice that the difference is not significant when compared to pH 7.

There is very little charge repulsion between the adsorbed molecules and the surface pressure measurements show a maximum in adsorption. Nevertheless, these measurements are done at a static interface and in dynamic condition and this could be most important difference between the two situations. The foam stability results shown in the previous chapter show that in this concentration range at pH 5 we observed poor foam stability. This is concentration dependent and when we increase the concentration we would risk lowering the enrichment.

5.6.5. Conclusions

For the sake of having a common technique to detect the concentration of adsorbing molecules in the bulk, the rising bubble technique was chosen. From these studies we can see that the enrichment of surfactant molecules depends mainly on the surface activity and the bulk concentration that was used in the foaming process. The ideal condition for a maximum enrichment is to have a minimum concentration which would provide optimum foam stability to allow us to drain the interstitial liquid. Therefore there is interplay of several factors here which come into account for foam fractionation of surfactants alone.

When it comes to protein solutions it gets more complex due to the physico-chemical properties of proteins itself and the way they influence the foam properties. So for a maximum enrichment of protein solutions one would need the best solution conditions such as bulk concentration, solution pH, ionic strength and other factors which influence the protein's surface activity and foam stability. For foam which is stable at lowest possible concentration of protein a better enrichment can be expected.

By comparing the foam fractionation setups from MPIKG and NRC we can see that the construction of the column has major influence and for a better enrichment a column which allows quicker drainage would be the best condition.

5.6.6. References

1. Stevenson, P., & Li, X. (2014). *Foam Fractionation: Principles and Process Design*. CRC Press.
2. Lemlich, R. (1968). Adsorptive bubble separation methods—foam fractionation and allied techniques. *Industrial & Engineering Chemistry*, 60(10), 16-29.
3. Leonard, R. A., & Lemlich, R. (1965). A study of interstitial liquid flow in foam. Part I. Theoretical model and application to foam fractionation. *AIChE journal*, 11(1), 18-25.

4. Krägel, J., O'Neill, M., Makievski, A. V., Michel, M., Leser, M. E., & Miller, R. (2003). Dynamics of mixed protein–surfactant layers adsorbed at the water/air and water/oil interface. *Colloids and Surfaces B: Biointerfaces*, 31(1), 107-114.
5. Miller, R., Fainerman, V. B., Leser, M. E., & Michel, M. (2004). Surface tension of mixed non-ionic surfactant/protein solutions: comparison of a simple theoretical model with experiments. *Colloids and Surfaces A: Physicochemical and Engineering Aspects*, 233(1), 39-42.
6. Grigoriev, D. O., Derkatch, S., Krägel, J., & Miller, R. (2007). Relationship between structure and rheological properties of mixed BSA/Tween 80 adsorption layers at the air/water interface. *Food Hydrocolloids*, 21(5), 823-830.
7. Tharapiwattananon, N., Scamehorn, J. F., Osuwan, S., Harwell, J. H., & Haller, K. J. (1996). Surfactant recovery from water using foam fractionation. *Separation Science and Technology*, 31(9), 1233-1258.
8. Boonyasuwat, S., Chavadej, S., Malakul, P., & Scamehorn, J. F. (2003). Anionic and cationic surfactant recovery from water using a multistage foam fractionator. *Chemical Engineering Journal*, 93(3), 241-252.
9. Ayorinde, F., Gelain, S. V., Johnson, J., & Wan, L. W. (2000). Analysis of some commercial polysorbate formulations using matrix-assisted laser desorption/ionization time-of-flight mass spectrometry. *Rapid Communications in Mass Spectrometry*, 14(22), 2116-2124.
10. Brown, L., Narsimhan, G., & Wankat, P. C. (1990). Foam fractionation of globular proteins. *Biotechnology and bioengineering*, 36(9), 947-959.
11. Fainerman, V. B., Lucassen-Reynders, E. H., & Miller, R. (1998). Adsorption of surfactants and proteins at fluid interfaces. *Colloids and Surfaces A: Physicochemical and Engineering Aspects*, 143(2), 141-165.

6. General conclusions and outlook

The process of molecular flotation, i.e. foam fractionation, is a very complex technological process. This thesis aims at contributing to a number of elements of this technology. These elements have been studied in detail, including single bubble formation processes in terms of bubble pressure and profile analysis tensiometry, including rising bubble velocity measurements, and foam formation, foam stabilization and foamate analysis experiments. As instrumentation the commercial bubble pressure tensiometer BPA1 and bubble profile analysis tensiometer PAT1 and some men-made set-ups were used. For bubble rising experiments, a laboratory instrument was used as described in section 4.2.3., based on the detailed description of hardware and software by Malysa et al. in [1,2]. For validation, the set-up was used for experiments with frequently studied surfactants and an excellent agreement was demonstrated (see section 5.2.1.). A third instrument, designed in our labs, was dedicated to the formation and characterization of foams, as it is described in section 4.2.5.1 In parallel, the commercial Foam Analyser DFA100 was applied for the characterization of different foams. Finally, a foam fractionation set-up was designed to produce and “harvest” foams under various process conditions. The enrichment effects in the foamate were analysed on the basis of rising bubble velocity profiles.

Proteins adsorb at liquid interfaces mainly in a diffusion controlled way. There were peculiarities observed in the tensiometry results for protein solution at particular bulk concentrations, the induction time and negative surface pressure. The induction time, which is the interval at which the adsorption of protein molecules does not lead to any measurable changes in the surface tension, decreases with the increase in bulk concentration. Due to changes in the surface activity of BLG at different pH and ionic strength the induction time dependencies differ from each other. Some peculiarities particularly at very low bulk concentrations are not yet understood. For protein solutions of small concentrations negative surface pressure values $\Pi(t)$ are measured at very short adsorption times, using the bubble pressure tensiometry. Negative surface pressure is synonym for an increase in surface tension with increasing amounts of adsorbed protein molecules. This effect of negative $\Pi(t)$ is a dynamic property and happens only at very short adsorption times. It was possible to explain this effect by a thermodynamic model via the interplay between the non-linear entropy of the interfacial layer and the changes in the required molar area of adsorbed protein molecules at

the surface. The effect was observed also for other proteins in literature, but it was mainly not explained or dedicated to surface charge effects. Probably a molecular dynamics simulation could help quantify the observed phenomena of negative $\Pi(t)$, however, for protein molecules the available simulation methods are not yet efficient enough.

Changes in the local velocity profile of rising bubbles are caused by the formation and structure of the dynamic adsorption layer at the surface of a bubble rising in a liquid. The adsorption flux to the bubble surface and desorption flux from the surface as well as the transport of adsorbed molecules along the surface layer and the effect of Marangoni flow in the adjacent liquid bulk phase are phenomena acting at the same time. The existing theoretical models can describe this complex situation so far only qualitatively.

The obtained results on the local velocity profile of air bubbles in solutions show how smallest amounts of BLG decelerate the bubble rising. At a fixed solution bulk concentration the height and location of the velocity maximum is characteristic for the surface activity of BLG as a function of pH and ionic strength. The addition of small amounts of surfactants (section 5.2.) is changing the velocity profile significantly. For non-ionic surfactants like $C_{12}DMPO$ the effect seems to be additive, i.e. a competition of BLG and the surfactant is observed. For the studied ionic surfactants SDS and DoTAB, the observed changes are explained by the formation and adsorption of protein-surfactant complexes. Anyhow the resulting local velocity profile for a bubble of a given size is a kind of fingerprint for the adsorbed layer at the bubble surface.

Foam experiments are comparatively easy to perform, however, the observed characteristics in terms of foamability and foam stability are difficult to be correlated with parameters of the stabilizers' adsorption layers. Also in the present work, no simple correlations could be found. The reason for these difficulties may be seen in the complexity of foam and the large variety of destabilization mechanisms. While foamability seems to correlate rather well with the adsorption kinetics of the foaming agent, supposed the substance allows forming a foam in general, the stability of single foam lamellae and of a real foam cannot be set into a clear relationship with surface layer properties.

The foamability and foam stability experiments performed with two different set-ups demonstrate that there is no direct correlation between adsorption activity of the BLG and the foam parameters. With the available knowledge it is not possible to explain why the foam stability of BLG at the same solution concentration is larger at pH 3 and 7 instead of for pH 3,

which is the isoelectric point. This finding is in line with the rising bubble characteristics where also the data for pH 3 are deviating from the expected behavior.

A great challenge for future work is the further deepening of understanding of the rising bubble process, i.e. new approaches for a quantitative computational fluid dynamics simulation which allows a direct link between the hydrodynamic flow field around a rising bubble of different dimension and the transport to, from and at the bubble surface.

The experiment with rising bubbles seems to have a great potential for shining light into the dynamics of adsorption layers. The presented experiments with protein solutions demonstrate that there are differences between the properties of dynamic and equilibrium adsorption layers. As one of the possible explanations, the kinetics of conformational changes is responsible for these differences. Hence, rising bubbles are a potential candidate for elucidating the kinetics of conformational changes at interfaces. In addition, the impact of surfactants on the rising bubble velocity profile depends strongly on the rate of adsorption and desorption. Hence, based on rising bubble experiments it seems feasible to get access to the rate constants of adsorption and desorption, as other experiments provide only information on the ratio of the two parameters.

Also relationships between foam properties and the adsorption layer behaviour of the respective foaming agents and foam stabilizers are still pending. As it was shown in the presented thesis, the structure and properties of surface layers formed under dynamic conditions are pretty much different from those at equilibrium, although the solution compositions in both cases are identical. This is due to the different adsorption kinetics of the contributing components and it can also be caused by the kinetics of conformational changes when proteins are involved as foaming agents.

There is still no clear picture for the solution's pH effect on the contribution of proteins on adsorption and foaming properties. Although it is generally accepted that proteins are most hydrophobic at their isoelectric point, in particular the dynamic adsorption layer and foam properties do not show maximum values. Obviously the conformational changes are responsible for this discrepancy, i.e. the process of adaptation of protein molecules to different environments like surface layers.

The enrichment of a component from an aqueous solution in foam and finally harvested from a foamate is possible only under certain conditions. Most important here is the ratio between the number of molecules in the solution bulk and at the interface. This ratio is a measure of the surface activity of this compound. If we assume a Langmuir isotherm $\Gamma = \Gamma_{\infty} \frac{c}{a + c}$ as a

rough model for the adsorption of a protein, the ratio Γ_{∞} / a is a good measure for the surface activity of this protein. To get a remarkable enrichment of the compound in the foam, the value of $\Gamma \times A$ must be of the order of $c \times V$, where Γ is the amount adsorbed at the effective surface A from a solution bulk having the volume V and the concentration c . As an example we could assume foam with typical foam bubbles of the size of 2.5 mm in diameter. If we further assume a foam volume of 5 cm³ on top of a solution column of $V = 10$ cm³, the foam volume corresponds to an effective area A of roughly 500 bubbles \times 0.2 cm², in total $A = 100$ cm². To fulfill the condition $\Gamma \times A > c \times V$ we get $c < \Gamma A / V$. Taking the data for A and V of the given example, and $\Gamma = \Gamma_{\infty} / 2 = 10^{-10}$ mol/cm² for the adsorbed amount we obtain for the concentration $c < 10^{-6}$ mol/l below which a reasonable enrichment can be expected. Note, for proteins a surface concentration of 10^{-10} mol/l is rather large so that the concentration limit is to be found much below the given concentration limit.

There is also a concentration limit due to the required rate of adsorption kinetics. Although the enrichment is the better the lower the bulk concentration of the compound is, the efficiency of the amount in the foamate becomes less. Also the minimum concentration at which foam can be formed represents a clear constrain and must be considered in practical applications.

There is also a minimum travel length required for slow adsorbing molecules to reach the bubble surface. Note, the lower is the concentration of the compound, the longer is the time required to get molecules adsorbed at the bubble surface. In order to have the required adsorption time, the foam column can be chosen longer. A longer travel path for the bubble also improved the selectivity of the enrichment because the adsorption of the competing molecules in the adsorption layer becomes more advantageous when the slower adsorbing molecules have sufficient time to replace the faster adsorbing compounds.

Addition of flotation supporting molecules is another option to modify proteins to make them attach stronger to the rising bubble. According to what we know about the increasing adsorption activity of protein/surfactant complexes, ionic surfactants at an optimum concentration are the best candidates for such a process, while the addition of nonionic surfactants typically replace proteins from the interface.

For harvesting foam layers which exist only over transient period of time a caterpillar system could be useful to collect systematically the foamate before it disappears due to insufficient foam stability.

References

1. Krzan, M., & Malysa, K. (2002). Profiles of local velocities of bubbles in n-butanol, n-hexanol and n-nonanol solutions. *Colloids and Surfaces A: Physicochemical and Engineering Aspects*, 207(1), 279-291.
2. Krzan, M., Lunkenheimer, K., & Malysa, K. (2004). On the influence of the surfactant's polar group on the local and terminal velocities of bubbles. *Colloids and Surfaces A: Physicochemical and Engineering Aspects*, 250(1), 431-441.

7. Acknowledgments

I would like to thank my supervisor Dr. Reinhard Miller for providing me generous and kind support during my PhD. Also I would like to extend my gratitude to Dr. Georgi Gochev who has mentored and given me advises in both science and life. Dr. Cécile Gehin-Delval has provided a great care and support over all these years for which I am ever grateful for. My thanks are also dedicated to her for always being available during her busy schedule and organizing all the requirements during my visit in Lausanne. I would like to thank Dr. Martin Leser and Dr. Deniz Zeynel Gunes for their interest in this project and their intuitive discussions about the experiments.

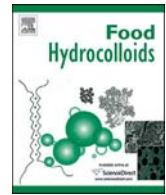
My special thanks are to Sabine Sigmund for her patience with all our colleagues and regulating our lab. I would also like to thank Inga Retzlaff for helping in doing experiments with foams and for creating a positive atmosphere in our group. Jooyoung Won has been my office mate all these years often challenging me at every level and at the same time taking care for which I am thankful. I thank Narges, Mohsen, Marzieh who extended their support whenever needed. I thank Dr. Jürgen Krägel who first introduced me to interfacial shear rheology and trained me to perform proper experiments. I would also like to thank Dr. Rainer Wüstneck for his loving and caring attitude towards our group.

Andreas Kretzschmar and Jeff Janiszewski from our workshops at MPIKG have greatly helped in building the experimental setups and their services are gratefully acknowledged.

This project was supported by Nestle Research Center, Lausanne, Switzerland and SINTERFACE Technologies, Berlin, Germany and is gratefully acknowledged. I also thank the MPI of Colloids and Interfaces for providing all the necessary conditions for nurturing young scientists.

8. Appendices

8.1.



Evidence of negative surface pressure induced by β -lactoglobulin and β -casein at water/air interface



V. Ulaganathan^{a,*}, V.B. Fainerman^b, G. Gochev^a, E.V. Aksenenko^c, D.Z. Gunes^d,
C. Gehin-Delval^d, R. Miller^a

^aMax-Planck-Institut für Kolloid- und Grenzflächenforschung, 14424 Potsdam, Germany

^bDonetsk Medical University, 16 Ilych Avenue, 83003 Donetsk, Ukraine

^cInstitute of Colloid Chemistry and Chemistry of Water, 42 Vernadsky Avenue, 03680 Kyiv (Kiev), Ukraine

^dNestlé Research Center, CH-1000 Lausanne 26, Switzerland

ARTICLE INFO

Article history:

Received 12 June 2012

Accepted 28 March 2013

Keywords:

Dynamic surface tensions
Bubble pressure tensiometry
 β -lactoglobulin
pH effect
Negative surface pressure
Thermodynamic model

ABSTRACT

Protein adsorption is one of the most complex and intriguing phenomenon in interfacial science. This phenomenon has been addressed in this paper for a short time range using maximum bubble pressure tensiometer. This study presents the issue of negative surface pressure of proteins which has been much of a speculation, with the thermodynamic model. Here β -lactoglobulin has been studied at different pHs and the experimental results agree with the theoretical model presented.

© 2013 Elsevier Ltd. All rights reserved.

1. Introduction

Proteins are macromolecules occurring in the nature which carry many biological functions. Their properties are subject of study for decades owing to their complexity in their structural configurations. The hydroxyl or amine groups of amino acids are ionized depending upon the pH giving rise to different charges on protein as the pKa values of amino acids vary. Therefore it is known that at isoelectric point the net charge of protein is zero as the number of positively and negatively charged amino acids are equal (Dickinson & McClements, 1996).

The proteins undergo structural changes orienting the hydrophobic parts towards the interface while adsorbing, so it requires some time for this unfolding process. Therefore the reduction interfacial tension is slower compared to the surfactant molecules. Unlike the surfactant molecules which has adsorption and desorption processes taking place simultaneously the proteins has irreversible adsorption which makes them unique in interfacial science. Thus the proteins attract interest in many applications in food, pharmaceutical industries due to these unique properties

(Brent, 2011; Dickinson, 1999; Graham & Phillips, 1979; Izmailova, Yampolskaya, & Tulovskaya, 1999; Miller et al., 2000).

Often in surface tension measurements of protein solutions there is an initial period of time during which the dynamic surface tension does not change remarkably. This so-called induction time is required for the protein to change its conformation and establish at the interface and it has been observed experimentally at low concentrations of certain proteins (Beverung, Radke, & Blanch, 1999; Erickson, Sundaram, & Stebe, 2000; Miller, Policova, Sedev, & Neumann, 1993; Wüstneck et al., 1996). Also theoretical models have been proposed to describe explain this induction time (Fainerman & Miller, 2005; Miller, Aksenenko, Fainerman, & Pison, 2001). Damodaran and Song (1988) have shown that the folded – unfolded states of a protein affect greatly its surface activity. Wierenga, Meinders, Egmond, Voragen, and de Jongh (2003) proved that chemically modified proteins expose their hydrophobic parts at the interface which could influence the corresponding induction time. Therefore, this lag time or induction time can be attributed to the rate of protein unfolding at the interface while exposing its hydrophobic parts towards the interface. Depending on whether the interface is water/air or water/oil, the induction time for a protein varies. At the water/oil interface the induction times are lesser and one reason for this could be the greater affinity of the hydrophobic parts of the protein to the oil (Beverung et al.,

* Corresponding author. Tel.: +49 17669921428.

E-mail address: Vamseekrishna.Ulaganathan@mpikg.mpg.de (V. Ulaganathan).

1999). Another reason for such difference is the charge at the interface offering attractive or repulsive interactions to protein molecules carrying a net charge (Sengupta, Razumovsky, & Damodaran, 1999). If both, the interface and the proteins, carry the same charge this would create an electrostatic energy barrier as in case of phosvitin at neutral pH (net charge -184) which showed highest induction time at the water/air interface compared to the ones at lower pH (Damodaran & Xu, 1996). In addition, there has been some speculation in the literature about the possible initial increase in surface tension, i.e. a negative surface pressure, for certain proteins at low concentrations during the induction time. This effect has been accounted to electrostatic charge effects which contribute to an increase in interaction energy between the water molecules at the interface and can cause an increase in surface tension (Chen, Prokop, Susnar, & Neumann, 1998; Damodaran & Xu, 1996; Wüstneck et al., 1996; Xu & Damodaran, 1992, 1993).

Therefore, in this paper we present the investigation of induction times of β -lactoglobulin at higher concentrations, increase in surface tension during those times and its dependence on the pH. We interpreted these results with thermodynamic model of protein adsorption which shows that negative surface pressure occurs at lower bulk protein concentrations.

2. Materials & methods

β -lactoglobulin (BLG) and β -casein (BCS) were purchased from Sigma–Aldrich (90% pure). The stock solutions were prepared by dissolving the protein in respective buffer along with 4 times by weight of activated charcoal. The solution is stirred for 20 min and rested for 10 min and then centrifuged to remove the activated charcoal in the solution.

For stock solutions of at pH 7, an equimolar mixture of 10 mM Na_2HPO_4 and NaH_2PO_4 was used as buffer, whereas for solution of BLG at pH 6.2, 10 mM NaH_2PO_4 solution was adjusted with HCl. In case of pH 8 and 9 we used a 10 mM Na_2HPO_4 and adjusted the pH with NaOH such that we got same ionic strength for all cases. The pH close to isoelectric point (~ 5.3) wasn't chosen as precipitation was observed at higher concentrations.

The maximum bubble pressure tensiometer BPA-1S (SINTERFACE Technologies, Berlin) was used for the experiments. The principle of this method was described in detail elsewhere (Fainerman & Miller, 2004). In short, a bubble is formed at the tip of a capillary and the maximum pressure inside the bubble is reached when bubble radius is equal to radius r_{cap} of the capillary. The pressure as a function of time $P(t)$ is recorded by the instrument and the maximum values are converted into surface tension by via the Laplace equation, $\gamma = P r_{\text{cap}} f/2$, where f is a correction factor. Different gas flow rates give different time periods of adsorption, and hence a dependence of surface tension on the adsorption time. Note, the used BPA-1S allows measurements down to 100 μs adsorption time. However, in the range up to about 10 ms, a respective correction of hydrodynamic and aerodynamic effects is required to obtain correct surface tension values (Fainerman, Mys, Makievski, & Miller, 2004). Therefore, we cut the data at very short times off to avoid the risk that unwanted effects change the dynamic surface tensions.

3. Results

It is seen in the graphs for BLG that close to the surface tension of water which is around 72.2 mN/m at room temperature ($\sim 25^\circ\text{C}$), the curves for the different concentrations start to diverge indicating the adsorption process taking place from this point. This time period is the induction time and with techniques like drop profile analysis tensiometry the induction times (if longer than 1 s)

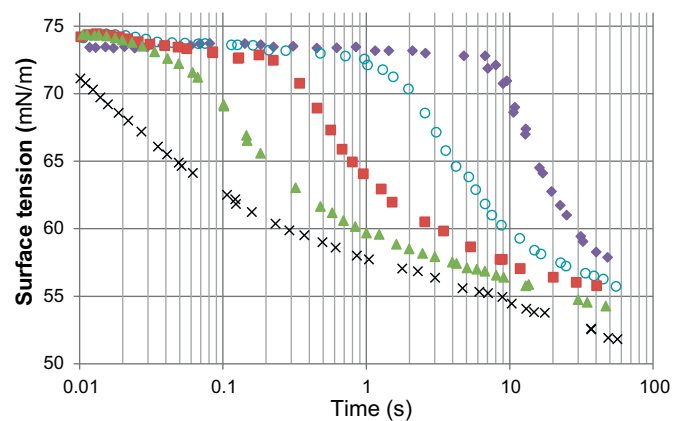


Fig. 1. Dynamic surface tension of β -casein solutions at pH 7 for concentrations: (\blacklozenge) 2×10^{-6} , (\circ) 5×10^{-6} , (\blacksquare) 10^{-5} , (\blacktriangle) 2×10^{-5} , (\times) 5×10^{-5} mol/L.

were quantified for different proteins at low concentrations (Beverung et al., 1999; Erickson et al., 2000). In our studies with a maximum bubble pressure tensiometer we can determine not only the induction times (less than 1 s) of proteins at higher concentrations, but also negative surface pressure values induced by the adsorption of protein molecules. Fig. 1 shows certain increases in surface tension at 0.01 s for five concentrations of BCS at pH 7.

From Figs. 2, 3 and 4 one could find that the surface tension values at 0.01 s for BLG does not depend on the concentration; however, the pH has an influence on it.

Fig. 5 shows that for the same BLG concentration the surface activity increases with pH. This could be due to a partial unfolding of the protein molecule with increasing pH which would bring changes in its tertiary structure and expose the non-polar parts making them to adsorb more actively (Fang & Dalgleish, 1997).

In Fig. 6 it is shown that the negative values of surface pressure (here the surface tension of pure water is considered as 72.2 mN/m) increases linearly with pH. Here, the net charge above its isoelectric point would be negative and, therefore, would linearly increase with the pH. The change in the net charges could induce changes in the molecular conformation and hence its molar area at the interface.

4. Discussion

It was shown in (Chen, Lahooti, Policova, Cabrerizo-Vílchez, & Neumann, 1996) that at small concentrations of protein solutions

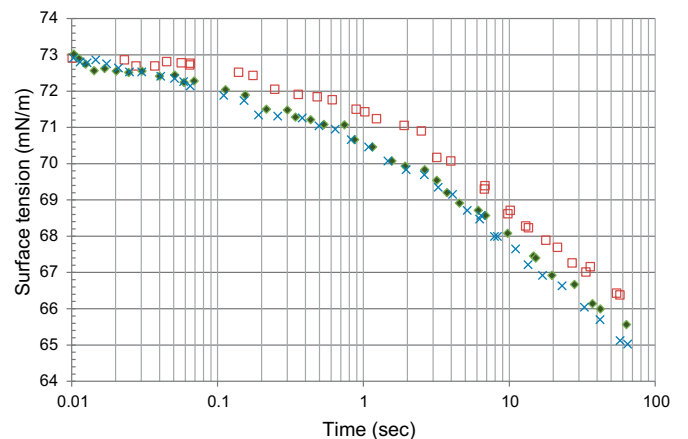


Fig. 2. Dynamic surface tension of BLG solutions at pH 6.2 for different concentrations: (\square) 5×10^{-5} mol/L, (\blacklozenge) 1×10^{-4} mol/L, (\times) 2×10^{-4} mol/L.

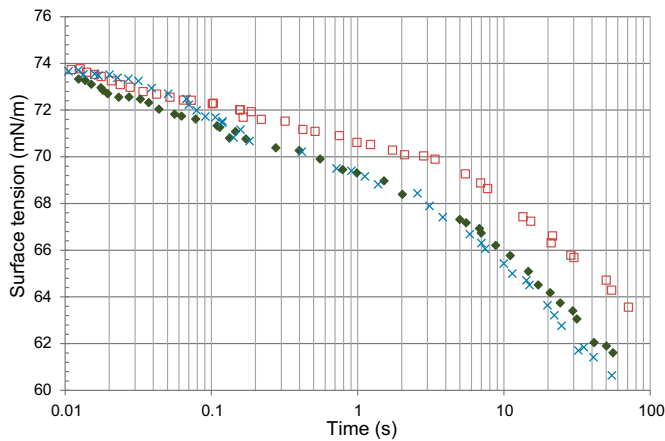


Fig. 3. Dynamic surface tension of BLG solutions at pH 8 for different concentrations: (□) 5×10^{-5} mol/L, (◆) 1×10^{-4} mol/L, (×) 2×10^{-4} mol/L.

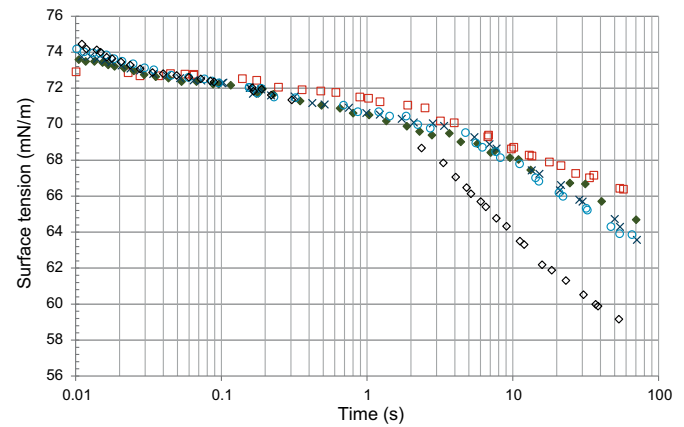


Fig. 5. Dynamic surface tension of BLG solutions at a concentration of 5×10^{-5} mol/L and different pHs (□) 6.2, (▲) 7, (×) 8, (○) 8.4 and (◇) 9.

(human serum albumin in the range of 10^{-9} – 10^{-8} mol/L) the surface pressure Π measured using the drop profile method becomes negative. Values of -2 mN/m to -3 mN/m were measured. In these experiments the solution drop was aged during 7 h. In other publications referred to in the study (Chen et al., 1996), negative Π values for diluted solutions of organic compounds were reported. However, the data of other studies reported in (Fainerman, Lucassen-Reynders, & Miller, 2003) yield zero Π values for HSA in the same concentration range. For BCS the equilibrium Π values in the concentration range of 10^{-10} to 10^{-8} mol/L as measured using the Du Noüy ring method were also shown to be zero (Wüstneck et al., 1996). To explain this essential discrepancy between the experimental results, we consider here a theoretical model for protein solutions described in (Fainerman et al., 2003).

Assuming that protein molecules can adsorb in n states of different molar area ω , varying between a maximum ω_{\max} and a minimum area ω_{\min} , the following equation of state is obtained (Fainerman et al., 2003):

$$-\frac{\Pi\omega_0}{RT} = \ln(1 - \theta) + \theta(1 - \omega_0/\omega) + a\theta^2. \quad (1)$$

The following symbols are used here: Π is the surface pressure, R is the gas law constant, T is the absolute temperature, a is the intermolecular interaction parameter, ω_0 is the molar area of the

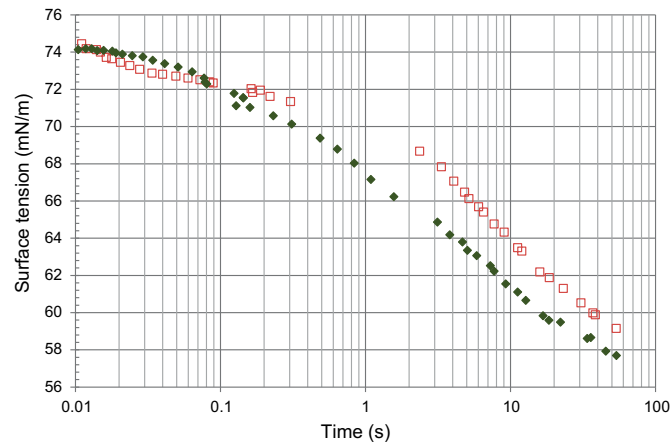


Fig. 4. Dynamic surface tension of BLG solutions at pH 9 for different concentrations: (□) 5×10^{-5} mol/L, (◆) 1×10^{-4} mol/L.

solvent and the area occupied by one segment of the protein molecule (the area increment), $\Gamma = \sum_{i=1}^n \Gamma_i$ is the total adsorption of proteins in all n states ($1 \leq i \leq n$). The total surface coverage by protein molecules is given by $\theta = \omega\Gamma = \sum_{i=1}^n \omega_i\Gamma_i$, while ω is the average molar area of adsorbed protein molecule, and $\omega_i = \omega_1 + (i - 1)\omega_0$ is the molar area in state i , assuming $\omega_1 = \omega_{\min}$, $\omega_{\max} = \omega_1 + (n - 1)\omega_0$. Additional equations for this model (adsorption isotherms for each state of adsorbed molecules and poly-layer adsorption isotherm) were also derived in (Fainerman et al., 2003). There is also a modification of the theory which assumes the aggregation of protein molecules and a limiting elasticity of composite adsorption layer in the post-critical concentration range which was presented in (Wüstneck et al., 2012).

It is seen from Eq. (1) that a positive value of the constant a (non-ideality of enthalpy) corresponds to an attraction between the adsorbed molecules which leads to a decrease of Π . The non-ideality of entropy (the second term in the right hand side of Eq. (1)) also results in a decrease of surface pressure. In physical terms, the intermolecular attraction could be related to the formation of temporary aggregates (dimers or trimers), resulting in a decreased number of kinetic entities in the adsorbed layer.

The influence of the electric charge of adsorbed molecules of protein or ionic surfactant, which remains unaccounted for in the

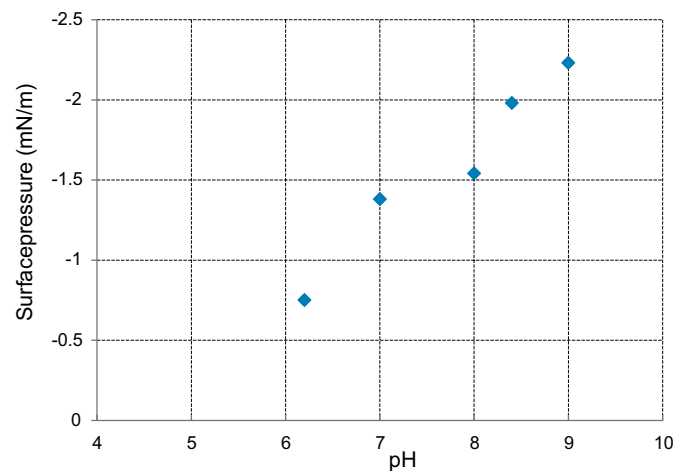


Fig. 6. Negative surface pressure values at 0.01 s surface age for BLG solutions at a concentration of 5×10^{-5} mol/L as a function of pH; the surface tension of pure water at room temperature was considered 72.2 mN/m.

present model, results in additional terms in the equation of state, which could increase the surface pressure (Fang & Dalgleish, 1997). However, this is not exactly the case. If no bulk charge separation takes place, and oppositely charged ions are located at the interface (two-dimensional electrolyte solution model), the Coulomb interaction leads to a certain arrangement of the ions. In this case an additional contribution to the surface pressure $\Delta\Pi$ also exists as was shown by Muller and Derjaguin (Chen et al., 1996). This contribution, however, is negative, and its value is lower than that for the case of a diffuse double layer.

For protein molecules $\omega_0 \ll \omega$; therefore the second term in the right hand side of Eq. (1) which corresponds to the non-ideality of mixing of molecules of different size, is approximately equal to θ . Consequently, the first and second terms in the right hand side of Eq. (1) compensate each other. Therefore, at very low protein concentrations (and, hence, low surface coverage), the values of Π calculated from Eq. (1) for $a > 0.5$ are negative. Fig. 7 illustrates the dependence of Π on concentration for BCS at pH 7 as calculated from Eq. (1). The experimental data are taken from (Fainerman & Miller, 2004) and the used model parameters are almost identical to those given in (Fainerman & Miller, 2004), in particular $a = 1.4$. It is seen that, with increasing c , the surface tension initially exhibits a decrease of almost to -3 mN/m, and becomes higher at larger concentrations. The fact that the range of negative Π values exists as shown in Fig. 7 contradicts the experimental results obtained in (Wüstneck et al., 1996) and indicates that the model developed in (Fainerman et al., 2003) is deficient in the range of extremely low concentrations (or adsorptions). In our published studies on protein solutions the Π value at equilibrium conditions was always assumed to be non-negative, which follows from the condition of thermodynamic stability in adsorption layers of usual surfactant solutions and insoluble monolayers (Fainerman & Vollhardt, 2003): $d\Pi/d\Gamma \geq 0$. However, it is possible that for very low bulk protein concentrations the thermodynamic equilibrium remains unattained, as was shown e.g. in Chen et al. (1996).

Fig. 1 illustrates the dynamic surface tension values in BCS solutions at pH 7 and high solution concentrations as measured by maximum bubble pressure method. The concentrations of studied solutions essentially exceed the critical concentration 3×10^{-8} mol/L (cf. Fig. 7). It is clearly seen from Fig. 1 that in the short time range the surface tension of the solutions is higher than that of the buffer (72.2 mN/m); in particular, for the solution with the concentration of 2×10^{-5} mol/L the maximum surface pressure is ca. 76 mN/m which yields $\Pi = -3.5$ mN/m.

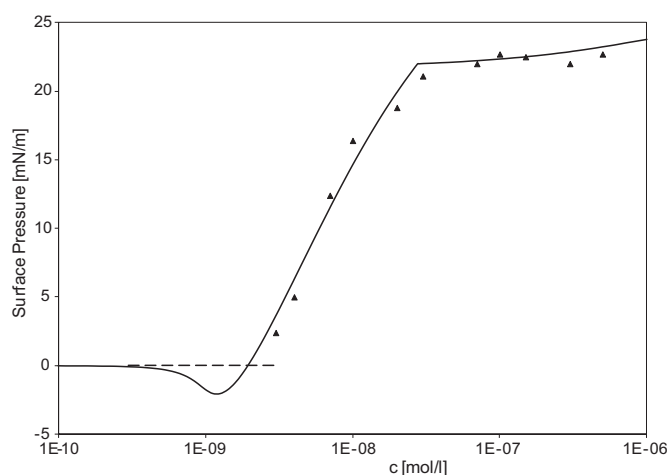


Fig. 7. Surface pressure Π as a function of protein concentration as calculated from Eq. (1).

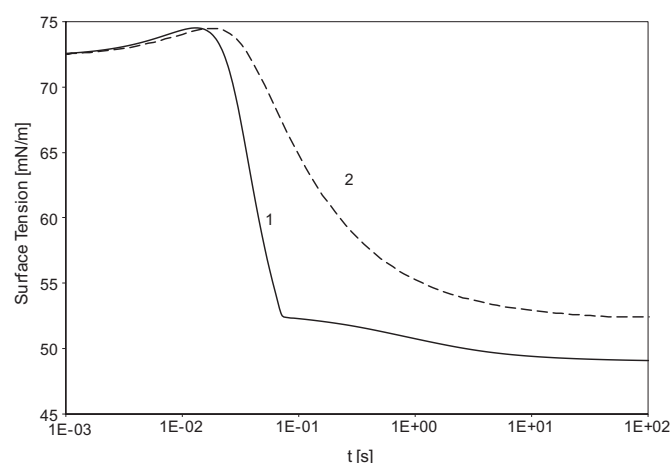


Fig. 8. Surface tension γ as a function of time, calculated for a diffusion controlled adsorption process with a diffusion coefficient of $D = 10^{-6}$ cm²/s and Eq. (1); the curves 1 and 2 refer to different sets of model parameters (see text).

The dynamic surface tension values of the solution with the same concentration (2×10^{-5} mol/L) calculated from the model Eq. (1) using the software described in (Fainerman et al., 2009) is shown in Fig. 8. Curve 1 was obtained for the same parameter values as the equilibrium curve shown in Fig. 7, calculated with a protein diffusion coefficient of 10^{-6} cm²/s. The maximum in the theoretical curve is located in the same time range as that in Fig. 1, while at larger times the theory predicts a much faster decrease of surface tension than that observed in the experiment. This discrepancy could possibly be ascribed to the fact that at such high post-critical concentrations of BCS (three orders of magnitude higher than the critical value), in addition to the diffusion, other processes take place, e.g. the disintegration of bulk and surface complexes. This could result in the decrease of the adsorption activity of the protein, which in turn decreases the adsorption activity constant by a factor of 1000. This yields the values shown by curve 2 in Fig. 8, which exhibits good agreement with the experiment.

Another explanation for negative Π values for the protein solutions in dynamic conditions could also be proposed. It is quite possible that the time range is too short for the formation of the electric double layer. In such a case the model for 2D electrolyte solutions proposed in (Muller & Derjaguin, 1977) is applicable, which predicts negative Π values.

However, with these theoretical models it is hard to assume a reason for increase in negative surface pressure values with increasing pH (as shown in the Fig. 6). We only know that pH induces the molecular confirmation which in turn affects the interfacial tension of proteins but the effect on non-ideal thermodynamic properties is unknown. Nevertheless, the model would at least provide us an insight for this complex phenomenon of protein adsorption.

5. Conclusion

The process of adsorption of proteins at the water/air interface at small surface coverage is clearly dominated by a transition of adsorbed molecules with large surface area demand to smaller molar area. This can be described very well by a thermodynamic model described in detail in (Fainerman et al., 2003). On its basis is seems obvious that there can be surface states with negative surface pressure, which in equilibrium conditions are of course unstable. However, in dynamic conditions, as a transient situation, such situations with negative surface pressure may exist.

By measuring the dynamic surface tensions with the methods of maximum bubble pressure it is possible to gain such transient adsorption data at rather short adsorption times. It turns out that the negative surface pressure values can very reproducibly be measured, as we have shown here for β -casein and BLG. The absolute values for the increased surface tension depend on the concentration and the pH of the solutions. The location and amount of the maxima in the dynamic surface course are in quite good agreement with simulations using the known thermodynamic model presented above.

In the past this observed unexpected phenomenon was discussed in various ways Chen et al. (1998) for example tried to explain it mainly by charge effects of the adsorbed protein. By the present work it seems clear that it is more the interplay between the non-ideality of entropy, which leads to a decrease in surface tension, and changes in the molar area of adsorbed protein molecules in the adsorption layer that causes the observed phenomenon of the 2D pressure passing through a minimum with negative values in a certain time range. One can expect that this explanation also holds for the same phenomena observed in literature for other protein systems.

Acknowledgements

The work was performed in the framework of the DFG SPP 1506 (Mi418/18-1) and the project PASTA of ESA, and financially supported by a PhD grant (VU) by Nestlé Research.

References

- Beverung, C. J., Radke, C. J., & Blanch, H. W. (1999). Protein adsorption at the oil/water interface: characterization of adsorption kinetics by dynamic interfacial tension measurements. *Biophysical Chemistry*, 81, 59–80.
- Brent, M. S. (2011). Rheological properties of protein films. *Current Opinion in Colloid & Interface Science*, 16, 27–35.
- Chen, P., Lahooti, S., Policova, Z., Cabrerizo-Vilchez, M. A., & Neumann, A. W. (1996). Concentration dependence of the film pressure of human serum albumin at the water/decane interface. *Colloids and Surfaces B: Biointerfaces*, 6, 279–289.
- Chen, P., Prokop, R. M., Susnar, S. S., Neumann, A. W. (1998). Interfacial tensions of protein solutions using axisymmetric drop shape analysis. In D. Möbius, R. Miller (Eds.), *Proteins at liquid interfaces* (pp. ix, 498). Amsterdam, The Netherlands and New York: Elsevier.
- Damodaran, S., & Song, K. B. (1988). Kinetics of adsorption of proteins at interfaces: role of protein conformation in diffusional adsorption. *Biochimica et Biophysica Acta (BBA) – Protein Structure and Molecular Enzymology*, 954, 253–264.
- Damodaran, S., & Xu, S. (1996). The role of electrostatic forces in anomalous adsorption behavior of phosvitin at the air/water interface. *Journal of Colloid and Interface Science*, 178, 426–435.
- Dickinson, E. (1999). Adsorbed protein layers at fluid interfaces: interactions, structure and surface rheology. *Colloids and Surfaces B: Biointerfaces*, 15, 161–176.
- Dickinson, E., McClements, D.J. (1996). *Advances in food colloids* (1st ed.). London and New York: Blackie Academic & Professional.
- Erickson, J. S., Sundaram, S., & Stebe, K. J. (2000). Evidence that the induction time in the surface pressure evolution of lysozyme solutions is caused by a surface phase transition. *Langmuir*, 16, 5072–5078.
- Fainerman, V. B., Lucassen-Reynders, E. H., & Miller, R. (2003). Description of the adsorption behaviour of proteins at water/fluid interfaces in the framework of a two-dimensional solution model. *Advances in Colloid and Interface Science*, 106, 237–259.
- Fainerman, V. B., Lylyk, S. V., Aksenenko, E. V., Liggieri, L., Makievski, A. V., Petkov, J. T., et al. (2009). Adsorption layer characteristics of triton surfactants: part 2. Dynamic surface tension and adsorption. *Colloids and Surfaces A: Physicochemical and Engineering Aspects*, 334, 8–15.
- Fainerman, V. B., & Miller, R. (2004). Maximum bubble pressure tensiometry—an analysis of experimental constraints. *Advances in Colloid and Interface Science*, 108–109, 287–301.
- Fainerman, V. B., & Miller, R. (2005). Equilibrium and dynamic characteristics of protein adsorption layers at gas-liquid interfaces: theoretical and experimental data. *Colloid Journal*, 67, 393–404.
- Fainerman, V. B., Mys, V. D., Makievski, A. V., & Miller, R. (2004). Correction for the aerodynamic resistance and viscosity in maximum bubble pressure tensiometry. *Langmuir*, 20, 1721–1723.
- Fainerman, B., & Vollhardt, D. (2003). Equation of state for monolayers under consideration of the two-dimensional compressibility in the condensed state. *The Journal of Physical Chemistry B*, 107, 3098–3100.
- Fang, Y., & Dalglish, D. G. (1997). Conformation of β -lactoglobulin studied by FTIR: effect of pH, temperature, and adsorption to the oil–water interface. *Journal of Colloid and Interface Science*, 196, 292–298.
- Graham, D. E., & Phillips, M. C. (1979). Proteins at liquid interfaces: I. Kinetics of adsorption and surface denaturation. *Journal of Colloid and Interface Science*, 70, 403–414.
- Izmailova, V. N., Yampolskaya, G. P., & Tulovskaya, Z. D. (1999). Development of the Rehinder's concept on structure-mechanical barrier in stability of dispersions stabilized with proteins. *Colloids and Surfaces A: Physicochemical and Engineering Aspects*, 160, 89–106.
- Miller, R., Aksenenko, E. V., Fainerman, V. B., & Pison, U. (2001). Kinetics of adsorption of globular proteins at liquid/fluid interfaces. *Colloids and Surfaces A: Physicochemical and Engineering Aspects*, 183–185, 381–390.
- Miller, R., Fainerman, V. B., Makievski, A. V., Krägel, J., Grigoriev, D. O., Kazakov, V. N., et al. (2000). Dynamics of protein and mixed protein/surfactant adsorption layers at the water/fluid interface. *Advances in Colloid and Interface Science*, 86, 39–82.
- Miller, R., Policova, Z., Sedev, R., & Neumann, A. W. (1993). Relaxation behaviour of human albumin adsorbed at the solution/air interface. *Colloids and Surfaces A: Physicochemical and Engineering Aspects*, 76, 179–185.
- Muller, V. M., & Derjaguin, B. V. (1977). Theory of a “two-dimensional electrolyte solution”. *Journal of Colloid and Interface Science*, 61, 361–364.
- Sengupta, T., Razumovsky, L., & Damodaran, S. (1999). Energetics of protein–interface interactions and its effect on protein adsorption. *Langmuir*, 15, 6991–7001.
- Wierenga, P. A., Meinders, M. B. J., Egmond, M. R., Voragen, F. A. G. J., & de Jongh, H. H. J. (2003). Protein exposed hydrophobicity reduces the kinetic barrier for adsorption of ovalbumin to the air–water interface. *Langmuir*, 19, 8964–8970.
- Wüstneck, R., Fainerman, V. B., Aksenenko, E. V., Kotsmar, C., Pradines, V., Krägel, J., et al. (2012). Surface dilatational behavior of β -casein at the solution/air interface at different pH values. *Colloids and Surfaces A: Physicochemical and Engineering Aspects*, 404, 17–24.
- Wüstneck, R., Krägel, J., Miller, R., Fainerman, V. B., Wilde, P. J., Sarker, D. K., et al. (1996). Dynamic surface tension and adsorption properties of β -casein and β -lactoglobulin. *Food Hydrocolloids*, 10, 395–405.
- Xu, S., & Damodaran, S. (1992). The role of chemical potential in the adsorption of lysozyme at the air–water interface. *Langmuir*, 8, 2021–2027.
- Xu, S., & Damodaran, S. (1993). Comparative adsorption of native and denatured egg-white, human, and T4 phage lysozymes at the air–water interface. *Journal of Colloid and Interface Science*, 159, 124–133.

8.2.



Contents lists available at ScienceDirect

Colloids and Surfaces A: Physicochemical and Engineering Aspects

journal homepage: www.elsevier.com/locate/colsurfa

Influence of β -lactoglobulin and its surfactant mixtures on velocity of the rising bubbles



V. Ulaganathan^{a,*}, M. Krzan^b, M. Lotfi^{a,c}, S.S. Dukhin^d, V.I. Kovalchuk^e,
A. Javadi^{a,f}, D.Z. Gunes^g, C. Gehin-Delval^g, K. Malysa^b, R. Miller^a

^a Max-Planck-Institut für Kolloid- und Grenzflächenforschung, 14424 Potsdam, Germany

^b Jerzy Haber Institute of Catalysis and Surface Chemistry Polish Academy of Sciences, Niezapominajek 8, 30-239 Cracow, Poland

^c Sharif University of Technology, Teheran, Iran

^d Department of Civil and Environment Engineering, New Jersey Institute of Technology, University Heights, Newark, NJ 07102, USA

^e Institute of Biocolloid Chemistry, Vernadsky str. 42, 03142 Kiev, Ukraine

^f Chemical Engineering Department, University of Tehran, Tehran, Iran

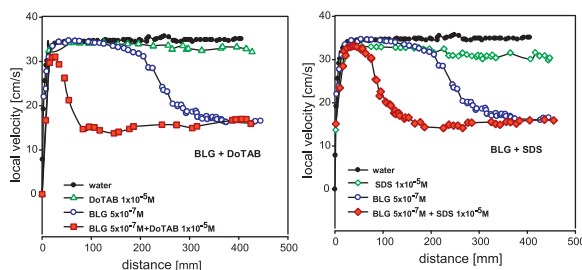
^g Nestlé Research Center, CH-1000 Lausanne 26, Switzerland

HIGHLIGHTS

- β -Lactoglobulin alone and mixed with different surfactants were studied.
- The local velocity profiles of rising bubbles in these solutions were analyzed.
- Addition of ionic surfactants to protein solutions caused strong retardation in velocity.
- Mixture of protein and nonionic surfactant had only additive effect.
- Ionic strength of the solution had an effect on the surface activity of the formed complexes.

GRAPHICAL ABSTRACT

The addition of smallest amounts of ionic surfactants to solutions of β -lactoglobulin leads to a strong retardation of the rising bubble velocity, which can be explained by the high surface activity of the complexes formed between BLG and the surfactants.



ARTICLE INFO

Article history:

Received 19 December 2013

Received in revised form 11 April 2014

Accepted 13 April 2014

Available online 24 April 2014

Keywords:

Dynamic adsorption layer

Rising bubble velocity

BLG adsorption

Mixed BLG/surfactant adsorption

SDS

DoTAB

Non-ionic surfactant

Diffusion controlled adsorption

ABSTRACT

The rising velocity of air bubbles in surfactant solutions is a sensitive measure for the formation of a dynamic adsorption layer (DAL) at the bubble surface. Due to a certain surface coverage by adsorbed species the bubble surface starts to become immobilized and the rising velocity is retarded. There is a large difference in the retardation effect in presence of the protein β -lactoglobulin (BLG) alone and its mixed solutions with surfactants. In presence of added surfactants BLG forms complexes, which adsorb and retard the bubble rising velocity according to their respective surface activity and adsorption kinetics. While the nonionic surfactant C_{12} DMPO does not show significant increase in retardation effects as compared to BLG alone, the ionic surfactants SDS and DoTAB form highly surface active complexes and change the rising velocity much stronger.

© 2014 Elsevier B.V. All rights reserved.

* Corresponding author. Tel.: +49 17669921428.

E-mail address: Vamseekrishna.Ulaganathan@mpikg.mpg.de (V. Ulaganathan).

1. Introduction

Mixtures of proteins and surfactants are widely studied due to their major industrial applications in food processing (from sponginess of bread to proper consistency of mayonnaise), pharmacology, or formulations for hair and body cosmetics, such as shampoos and creams. The formation and stabilization of foams and emulsions depend on the interfacial properties of these mixtures, i.e. the variations of interfacial tension, the bulk and surface rheological behaviour, and the adsorption dynamics, which can be drastically different as compared to those of the single components [1]. From a physical point of view, surfactants and proteins adsorb at interfaces, reducing the respective interfacial tension. While low molecular weight surfactants in most formulations are responsible for foam/emulsion formation thanks to a quick adsorption at the bubble/drop surface, the high-molecular weight proteins stabilize them on longer time scales, forming elastic and often electrically charged interfacial networks [2]. Different methods like dynamic and equilibrium surface tension measurements, dilational and shear rheology, ellipsometry, etc., were used to understand the adsorbed layers of proteins and their mixtures with surfactants [1,3–8]. Interactions of proteins with ionic surfactants such as the anionic sodium dodecyl sulfate (SDS) or cationic cetyl trimethyl ammonium bromide (CTAB) have been described in detail in literature [5]. It was clearly shown that proteins interact with ionic surfactants which lead to formation of complexes. Even in the case when the net charge of the protein and the charge of the surfactant are both negative (or positive), there are local counter charges available on the protein chain so that an electrostatic interaction with the surfactants is possible. After charge compensation due to the binding of ionic surfactants, with increasing surfactant concentration the protein/surfactant complexes start to interact with further surfactant molecules mostly via hydrophobic interaction. In protein solutions containing non-ionic surfactants a complex formation happens exclusively via hydrophobic interactions. A general overview on complex formation between proteins and different types of surfactants was given in [9].

The motion of bubbles in a liquid is strongly affected by the adsorption of surface-active species at the bubble surface and, therefore, has been used as a sensitive tool for investigating the adsorption layer formation in surfactant solutions under dynamic conditions. As proteins also adsorb at liquid/gas interfaces, measurements of the rising bubble velocity in solutions of protein and protein–surfactant mixtures can provide information about their influence on the formation of adsorption layers under dynamic conditions. Generally, the presence of an adsorbed layer retards the mobility of a bubble surface [10–13] and, thereby, the velocity of the rising bubble can be lowered by more than 50% [13–15]. When a bubble grows at the tip of a capillary immersed in a surfactant solution an adsorption layer is formed over the entire bubble surface. The degree of adsorption coverage over the bubble surface in the moment of bubble detachment is determined by the surfactant surface activity and its bulk concentration, the adsorption kinetics and the rate of bubble growth (bubble surface expansion). At low surfactant concentrations the adsorption coverage can be lower than at equilibrium, however, it is a uniform coverage [13,15]. After bubble detachment a non-uniform distribution of surfactants along the bubble surface (dynamic structure of the adsorption layer – DAL) starts to develop [10,12–16], as a result of the viscous drag exerted by the continuous liquid medium on the bubble surface. The formation of a DAL over the surface of a rising bubble means that the adsorption coverage tends to a minimum at the upstream pole of the moving bubble, while at the rear pole it becomes higher than the equilibrium value. This gradient of surface concentration corresponds to a surface tension gradient which causes a reduction of the fluidity of the bubble surface (Marangoni effect). In turn, the

immobilization of the bubble surface leads to an increase of the hydrodynamic drag exerted by the liquid on the bubble surface so that the velocity of the bubble decreases. When the bubble moved with a constant (terminal) velocity (steady state conditions) it is an indication that the dynamic architecture of the adsorption layer (DAL) has been established. In solutions of classical surfactants the time-scale of the DAL establishment over the surface of a rising bubble depends on the surfactant type and its solution bulk concentration [14–20]. It was shown in [21,22] that also in solutions of the protein bovine serum albumin (BSA) the velocity of a rising bubble can be lowered significantly as the result of protein adsorption at the bubble surface. However, as far as we know, there is no investigation on bubble motion in protein–surfactant mixtures and this is the topic of this paper.

The present manuscript deals with the investigation of rising air bubbles in solutions containing the protein β -lactoglobulin (BLG), one of the three surfactants SDS, DoTAB, C₁₂DMPO, or respective protein/surfactant mixtures at different mixing ratios. We measured the velocity profiles of air bubbles as a function of the distance from the origin or alternatively of the rising time, and discuss qualitatively the differences observed for pure BLG and its mixtures with an ionic or a non-ionic surfactant. The velocity profiles are discussed in terms of adsorbed amounts and their impact on the immobilization of the surface of a rising bubble.

2. Experimental method

The bubble rising velocity profiles were determined in a glass square column of cross section area 40 × 40 mm and 50 cm height. A capillary with an inner diameter of 0.075 mm fitted to the column bottom was used to form single bubbles at a controlled time intervals. The time of bubble formation (t_f) at the capillary tip was 1.6 sec and the bubble diameter in distilled water was 1.48 ± 0.01 mm. A digital camera (MotiCam) and a stroboscope illumination were used to record images of rising bubbles. The special software ImageJ was used to analyze the video recordings. More details about the experimental set-up and the data analysis procedure can be found elsewhere [14–17]. The reagents used were dodecyl trimethyl ammonium bromide (DoTAB) and sodium dodecyl sulfate (SDS) both purchased from Fluka (Switzerland). The non-ionic surfactant dodecyl dimethyl phosphine oxide (C₁₂DMPO) was synthesized in our lab following the protocol given in [23]. BLG was purchased from Sigma–Aldrich (90% pure). The stock solutions were prepared by dissolving the protein in Milli-Q water used for the preparation of the solutions had a surface tension of 72.4 mN/m at 22 °C and a conductivity 0.05 μ S/cm. All experiments were carried out at room temperature of 22 °C, and the pH of all studied solutions was 6.2.

3. Results

The velocity of the bubble is determined from the capillary tip till the top level of liquid at regular intervals. This gives us the velocities at regular distances from the capillary tip, which when plotted against the distance or time gives us local velocity profile (LVP).

Fig. 1 presents sequences of images of bubbles rising in BLG solutions of different concentrations. All photos were recorded at an identical distance of 100 mm from the capillary orifice. As the pictures were recorded at an identical frequency of the stroboscopic illumination (100 Hz), a smaller distance between subsequent positions of the rising bubble illustrate clearly that the bubble velocity decreases with increasing BLG concentration. Note also, that the shape deformation of the bubbles also decreases with increasing BLG concentration.

Quantitative data on the influence of the BLG concentration on the bubble motion are presented in Fig. 2 as the dependences of

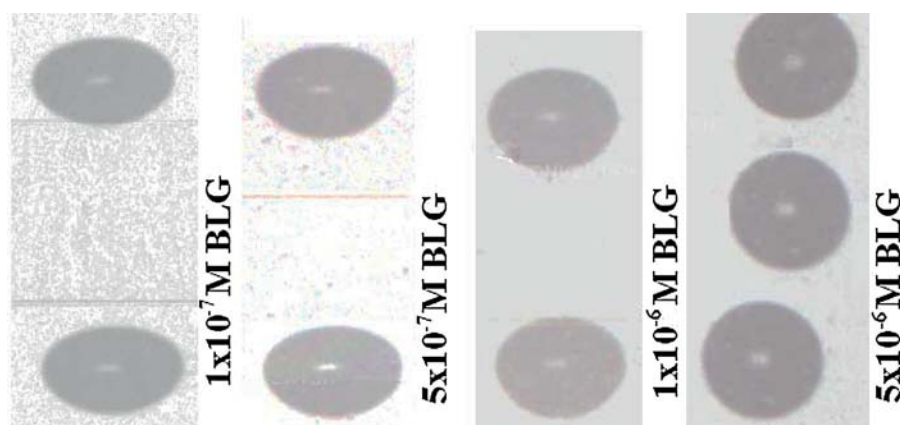


Fig. 1. Sequences of photos of air bubbles, rising in BLG solutions of different concentrations; the frequency of the stroboscopic lamp was 100 Hz; all images were recorded at a distance $L = 100$ mm from the capillary orifice.

the bubble local velocity, U_L , on the distance from the capillary tip. As seen there, in all BLG solutions the bubbles accelerated rapidly after detachment and profiles of their local velocity were strongly dependent on the solution concentration. For the lowest BLG concentration of 10^{-7} M the bubble velocity profile was identical to that in distilled water, i.e. after the acceleration stage the bubble attained its terminal velocity. At higher BLG concentrations the velocity profiles are different, but similar as observed in dilute solutions of classical surfactants [14–17]. This means, that the acceleration stage is followed by a stage of monotonic decrease of the bubble local velocity which then levels off at the terminal velocity. It can be observed in Fig. 2 that the height, width, and position of the maximum vary with the BLG concentration. The velocity maximum is shifted towards shorter distances, and its height and width decrease with increasing BLG concentration. However, the “plateau” values of the terminal velocity are practically identical, $U_T = 15.3 \pm 0.3$ cm/s, for BLG concentrations $c \geq 5 \times 10^{-7}$ M.

Figs. 3 and 4 present the local velocity profiles (LVP) in binary solutions of BLG mixed either with a non-ionic (Fig. 3) or an ionic (Fig. 4) surfactant. As can be observed the general features of the bubble velocity profiles for the mixed protein–surfactant solutions are similar to those observed in BLG solutions, i.e. after the acceleration stage, there is a maximum followed by the velocity decrease till a constant (terminal) velocity is attained. Note, please, that in mixed BLG–surfactant solutions the terminal bubble velocity was also ca. 15.3 cm/s. The influence of the non-ionic surfactant C_{12} DMPO was, however, quite different from that of the cationic (DoTAB) and

anionic (SDS) surfactant, respectively (see Figs. 3 and 4). A comparison of the velocity profiles in single solutions of C_{12} DMPO and BLG presented in Fig. 3 shows that at identical bulk concentrations the bubble velocity profiles are very similar. Moreover, the bubble velocity profile in mixed solution of 5×10^{-7} M BLG + 5×10^{-7} M C_{12} DMPO is practically identical to that in a 10^{-6} M BLG solution. For the studied ionic surfactants much higher concentrations were needed (see Fig. 4) to lower the bubble rising velocity, despite the fact that the hydrocarbon chain length is identical for all used surfactants. The reason of these differences is rather obvious and can easily be explained – the surface activity of the non-ionic C_{12} DMPO is much higher than of the ionic counter-partners.

The most striking and interesting effect was observed for the mixed solutions of BLG with the cationic DoTAB (Fig. 4A) and anionic SDS (Fig. 4B) surfactants, respectively. As seen the local bubble velocity in mixed solutions of 5×10^{-7} M BLG + 10^{-5} M DoTAB and 5×10^{-7} M BLG + 10^{-5} M SDS was much stronger changed than in the pure protein solutions at the corresponding two concentrations of 5×10^{-7} M and 10^{-6} M BLG. Note, in solutions with a concentration of 10^{-5} M either for SDS or for DoTAB the bubble velocity profiles are not affected at all (see Fig. 4). The fact that these small amounts of ionic surfactants added to the protein solution had such a large influence on the bubble velocity profiles can be caused by formation of BLG–SDS and BLG–DoTAB complexes in the bulk, which are much stronger surface active than the original protein [5]. The significant narrowing and shift

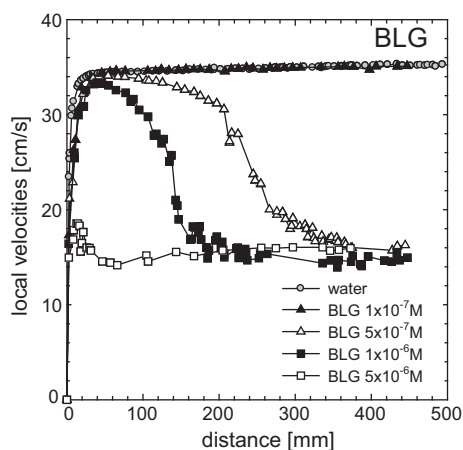


Fig. 2. Local velocity of air bubbles, rising in BLG solutions, as a function of the distance from the capillary orifice.

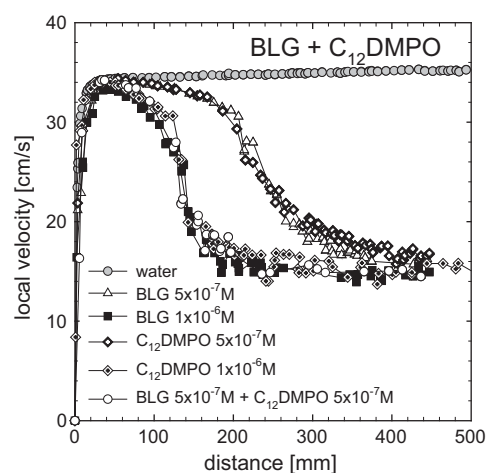


Fig. 3. Local velocity of air bubbles, rising in solutions of BLG, C_{12} DMPO and 1:1 mixtures as a function of the distance from the capillary orifice.

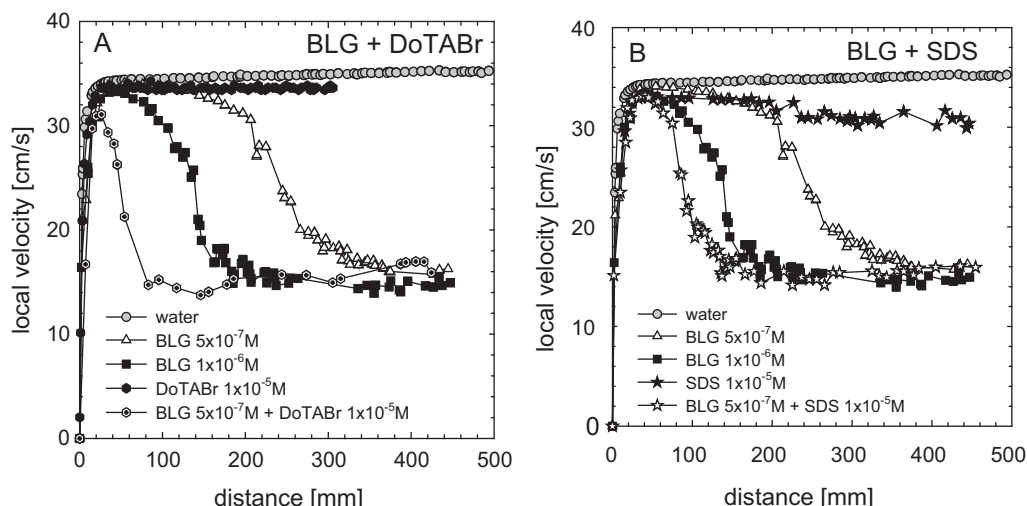


Fig. 4. Local velocity of air bubbles, rising in solutions of BLG, DoTAB (A), SDS (B) and their mixtures, as a function of distance from the capillary tip.

of the velocity maximum, and the faster attainment of the terminal velocity ($U_T = 15.3 \pm 0.3$ cm/s), indicate that the surface of the rising bubbles in mixed BLG-SDS and BLG-DoTAB solutions was faster immobilized, i.e. at a shorter distance and therefore after a shorter time of bubble motion. It can, however, also be the result of an increased kinetic coefficient and therefore an acceleration of the adsorption process, as will be discussed further below.

4. Discussion

The influence of concentration of a protein on the local velocity profile (LVP), which may be formulated based on the results presented in Figs. 2–4, follow the regularities very similar to those revealed in earlier measurements for example with some medium chain alcohols [15]. These regularities will be explained qualitatively below. However, a valuable novelty was discovered from experiments with mixed protein–surfactant solutions which we will discuss separately.

4.1. General regularities of LVPs in individual protein solutions

The local velocity profiles of bubbles rising in surfactant solutions are determined largely by the solution concentration [17]. Generally two types of LVP can be distinguished. The first type is usually observed at relatively low solution concentrations and consists of three distinct stages: (i) a rapid initial acceleration of the bubble, (ii) attainment of a maximum velocity with its subsequent monotonous decrease, and (iii) rising with a constant (terminal) velocity. The second type of profiles, observed at high concentrations and in pure water, consists of only the stages (i) and (iii). The bubble terminal velocity is maximal in pure water and decreases rapidly with surfactant concentrations until a certain critical concentration is reached. Above this critical concentration the minimal terminal velocity V_{term}^{min} is reached which is almost independent of concentration. For high Reynolds numbers ($Re > 1$), this low terminal velocity is more than two times smaller than that in pure water. The bubble velocity decrease is caused by the retardation of the surface due to Marangoni effects, and, therefore, the velocity cannot be lower than the velocity of a solid sphere with the same dimension and the same Archimedes force. This explains the cessation of retardation growth above a certain characteristic concentration C_c , corresponding to an almost complete surface immobilization.

The surfactant molecules, adsorbed at the bubble surface, are swept down and form a so-called rear stagnant cap (RSC). The

surface tension gradient, built up within this zone, retards the bubble surface. The size of the RSC, usually characterized by the angle ψ measured from the rear stagnant point to the upper pole, increases with increasing concentration. The current state of the theory allows describing the dependence of rising bubble velocity on ψ , while ψ depends on the adsorption isotherm and kinetic coefficients of adsorption of the respective surface active compound. The onset of the minimum rising velocity at high Re was described by numerical simulations [24]. These simulations show that the angle ψ amounts to about 120° , which means that any further increase in concentration and, accordingly, any increase of ψ within the range 120 – 180° does not lead to a further decrease in the rising velocity. The identical values of the minimal terminal velocity V_{term}^{min} shown in Figs. 2–4 for different concentrations $C > C_c$ and different surface active compounds is the manifestation of the achievement of the RSC angle $\psi \geq 120^\circ$.

A quantitative data analysis, including the formation of DAL, is presently not possible, as there is no theory that allows correlating the formation of a DAL with the velocity profile of a rising bubble, which remains the purpose of future theoretical work. Therefore, we can present only a semi-quantitative data analysis here.

In the present study the time of bubble growth at the capillary tip (t_f) was almost identical and of the order of 1.6 s. Thus, for a semi-quantitative comparison of the contribution of the two stages – bubble growth and bubble rising – to the accumulation of adsorbate at the surface, we require information about the time elapsed from the moment of bubble detachment. This information can be obtained from Figs. 5 and 6 showing the same local velocities as in Figs. 2 and 4 but here as functions of time, t_m , measured from the moment of bubble detachment.

For $C \ll C_c$ the amount of the accumulated adsorbate in the moment of bubble detachment from the capillary tip is less than the amount M_s , required for the formation of a RSC with $\psi = 120^\circ$. This means, that the bubble rises (after the acceleration stage) with a velocity $V(C) > V_{term}^{min}$ and, correspondingly, the whole LVP is located above V_{term}^{min} . In addition to the solute mass M_{gr} , accumulated during the bubble growth, the solute accumulates due to adsorption during the time of bubble rising. This amount, M_{ac} , together with M_{gr} , determines the dimension of RSC, the bubble retardation and, consequently, its velocity which is smaller than the terminal velocity to be found in super-clean water V_{term}^{max} . Hence, we have the situation of

$$V_{term}^{min} < V(C) < V_{term}^{max} \quad (1)$$

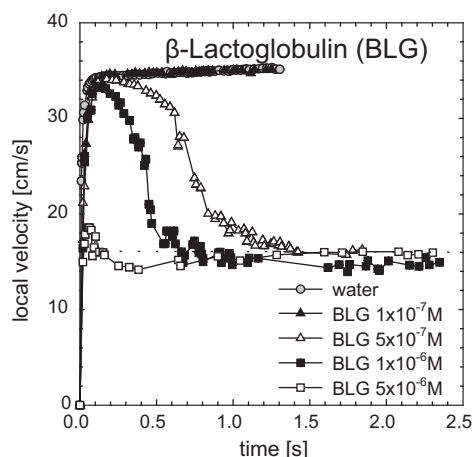


Fig. 5. Local velocity of air bubbles in BLG solutions as functions of time; $t=0$ denotes the moment of bubble detachment from the capillary tip.

Let us consider first the case of a low concentration $C < C_c$. At such a concentration the amount adsorbed during bubble formation/growth is not sufficient to provide a noticeable retardation. But even at such a low concentration, the velocity retardation may be visualized with the use of a column of much larger height which will show a stage of decelerated rising after the stage of accelerated rising with a clear maximum in the LVP. With increasing concentration, the slope of deceleration becomes visible first, while the decrease in the height of the velocity maximum becomes measurable only at a further concentration increase. These features are seen in Figs. 3 and 4 and the corresponding Figs. 5 and 6.

The regularities of both stages, acceleration and deceleration, determine the position and height of the maximum. The necessity to account for acceleration makes the theory for a maximum more complicated than the theory of the deceleration stage. Taking this into account for a certain solute, it looks reasonable to introduce the term *low concentration* for that family of LVP which have a maximum close to V_{term}^{max} and, consequently, do not affect the independent interpretation of the descending parts of LVP. The existence of a measurable maximum corresponds to an *intermediate region* of concentrations. The height of the maximum decreases with increasing concentration C , and it disappears when C is above a certain value C_m . At any higher concentration there is only a transition from accelerated rising velocity to the minimal terminal velocity V_{term}^{min} .

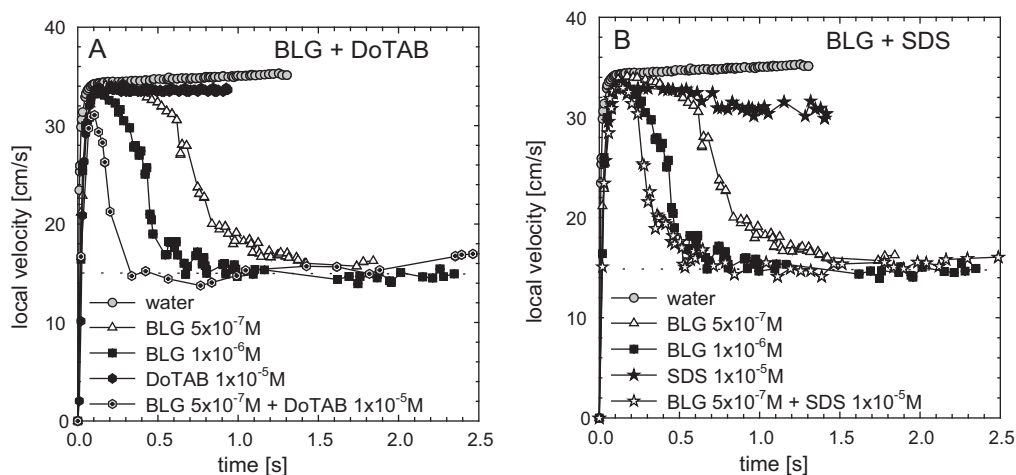


Fig. 6. Local velocity of air bubbles in BLG + DoTAB (A) and BLG + SDS (B) solutions as functions of time; $t=0$ denotes the moment of bubble detachment from the capillary tip.

For decelerated rising at small concentrations, in a chosen time moment t , we know that for a larger concentration the adsorbed amount $M_{ad}(t)$ is also larger. Hence, the retardation increases and the velocity decreases with the increase in concentration. It means the descending branch of LVP is lower for higher concentrations. This regularity is seen in Figs. 2–4.

For kinetically limited adsorption processes the adsorption flux J_{ad} is proportional to the area S_m of the mobile portion, which is almost free of surfactant

$$J_{ad} = \beta C S_m(t) \quad (2)$$

where β is the kinetic coefficient of adsorption. As proteins practically do not desorb from the surface we can neglect the desorption flux in Eq. (2). The viscous flow of the liquid compresses the adsorption layer within RSC. It is known that the area occupied by protein molecules can change under the action of lateral pressures. However, the analysis of the rheological surface properties of BLG adsorption layers shows that, within the surface pressures interval between 0 and 13 mN/m, the average molar area ω of BLG molecules changes only slightly and amounts to about 10^5 to 1.1×10^5 m²/mole [25]. With this the kinetic equation for RSC growth can be written as

$$\frac{1}{\omega} \frac{dS_{RSC}}{dt} = \beta C (S - S_{RSC}(t)) \quad (3)$$

where $S_{RSC} = S - S_m$ is the area of the rear stagnant cap and S is the total bubble surface area. The solution of Eq. (3) is

$$S_{RSC}(t) = S [1 - \exp(-\omega \beta C t)] \quad (4)$$

with the characteristic time for the growth of the RSC

$$t_{ad} \sim (\omega \beta C)^{-1} \quad (5)$$

This characteristic time decreases with increasing concentration in agreement with the data shown in Figs. 2–4.

Eqs. (3) and (4) are derived under the assumption that the solute transport is controlled by the transfer between the sublayer and the bubble surface. For a diffusion controlled transport of molecules towards the sublayer and to the mobile bubble surface we can use the approximation

$$J_{dif} = D \frac{\partial C}{\partial x} \approx D \frac{C}{\delta} \quad (6)$$

where δ is the thickness of the diffusion layer, D is the diffusion coefficient, while the concentration within the sublayer in

comparison to C is small and can be disregarded. An equation for δ can be found in [10]

$$\delta = \sqrt{\frac{4\pi}{9} \frac{a\sqrt{2+\cos\theta}}{Pe^{0.5}(1+\cos\theta)}} \quad (7)$$

where, $Pe = 2av/D = Re \times Pr$ is the Peclet number, $Re = 2aV/\nu$, $Pr = \nu/D$ is the Prandtl number, a is the bubble radius, θ is the angle measured from the leading pole of the bubble, and $\nu = 10^{-6} \text{ m}^2/\text{s}$ is the kinematic viscosity of water. As for surfactants $D \sim 10^{-10} \text{ m}^2/\text{s}$, we have $Pr \sim 10^4$, $Re \sim 500$ for rising bubbles, used in the present experiments. The Peclet number $Pe \sim 5 \times 10^6$ characterizes the ratio of the convective flux to the diffusion flux.

The angular dependence in Eq. (7) corresponds to the velocity distribution of the potential flow around a rising bubble as derived by Levich (cf. Chapter 8 in [10]) in absence of a RSC. When the RSC is rather small its influence on the velocity distribution and, consequently, on $\delta(\theta)$ is weak, which allows us to use Eq. (7). When the RSC is large, its influence on the velocity distribution increases to a certain degree. A similar problem was discussed in Chapter 5 in [13], where the hydrodynamic separation of a flow from the surface of a moving solid sphere was quantified. Schlichting [26] used the potential velocity distribution as first approximation for the velocity distribution far from the turbulent zone and revealed, that it is valid for $\theta < 30^\circ$. For the sake of simplicity, we will use here Levich's equation for the total flux. The expression for the density of the diffusion flux J_{dif} averaged over the bubble surface, obtained from Eq. (7), reads

$$J_{dif} = \frac{D}{a} Pe^{0.5} \sqrt{\frac{1}{3\pi}} C \cong \frac{D}{3a} Pe^{0.5} C \quad (8)$$

As both Eqs. (2) and (8) are characterized by a linear dependence on C , the equation for the kinetics of RSC growth, i.e. when it is controlled by diffusion, may be obtained by the replacement of βC in Eq. (4)

$$S_{RSC}(t) = S \left[1 - \exp\left(\frac{\omega Da^{-1} Pe^{0.5} C}{3} t\right) \right] \quad (9)$$

and

$$t_{dif} \sim \left(\frac{\omega Da^{-1} Pe^{0.5} C}{3}\right)^{-1} \quad (10)$$

Eq. (4) allows obtaining an expression for an easy to measure characteristic quantity, the time τ_{term} for the onset of the terminal velocity V_{term}^{min} . This time corresponds to $\psi = 120^\circ$ and S_{RSC} can be expressed through ψ .

$$S_{RSC} = \frac{S}{2} (1 - \cos \psi) \quad (11)$$

i.e. the time τ_{term} corresponds to $\psi = 120^\circ$ in Eq. (11). The combination of Eqs. (4) with (11) yields

$$\tau_{term} = \frac{1}{\omega\beta C} \ln \frac{2}{1 + \cos 120^\circ} \quad (12)$$

ψ is unknown for any moment of time with the exception for the moment, when the measured velocity $V(C,t)$ attains for the first time the minimal value V_{term}^{min} . For this moment we know that $\psi = 120^\circ$.

Combining Eqs. (11) and (9) one obtains a similar expression

$$\tau_{term} = \frac{3}{\omega Da^{-1} Pe^{0.5} C} \ln \frac{2}{1 + \cos 120^\circ} \quad (13)$$

which described the case of a diffusion controlled adsorption process.

4.2. Common regularities in LVPs formed in surfactant solutions and protein solutions.

Common LVP regularities are seen in Fig. 3. An almost identical LVP for the non-ionic surfactant C_{12} DMPO and the protein BLG is found when their molar concentrations are equal. They are reproduced for two concentrations, namely for $5 \times 10^{-7} \text{ M}$ and 10^{-6} M . This similarity of LVPs for the surfactant and the protein may be an indication that in the particular case of BLG adsorption layers there is not any significant intrinsic relaxation processes related to conformation changes of the protein molecules which can influence the rising of a bubble (at least within the considered time scale). Such behaviour is possible when the protein preserves its compact globular structure upon adsorption at the air/water interface. This supposition is in agreement with the fact that the average molar area ω of BLG molecules changes only slightly within the surface pressures interval between 0 and 15 mN/m as mentioned above. Additional indications that the globular proteins can preserve their tertiary structure in the course of adsorption in absence of denaturing agents can be found in a recent review [27].

In absence of any intrinsic relaxation processes the dynamics of protein adsorption may be described by the same diffusion-kinetic adsorption model, which is justified for surfactants (see Chapter 4 in [12]). With respect to diffusion controlled transport the similar dynamics can be expected when the difference in the values of ωD for a protein and for a surfactant may be not large. In contrast, a rather specific analysis is required for identical LVPs, when the transport is controlled by the solute transfer from the sublayer in the presence of an adsorption barrier. Then, a non-essential difference in the values of $\omega\beta$ for the protein and for the surfactant is required ($\omega_p\beta_p \approx \omega_s\beta_s$, p – protein, s – surfactant) to obtain the identity in their LVPs (Fig. 3). While in this particular case, the experimental proof of the model based on the kinetic coefficients α and β as valid for both surfactant and proteins is the most certain, there is no ground to doubt, that at least a class of proteins exists, the adsorption dynamics of which may be described by this simplest model. The prerequisites were discussed in Chapter 4 in [12], given by Eq. (4.80) derived for the kinetics of protein adsorption which is equivalent to Eqs. (4.32)–(4.34) valid for surfactants.

Not only the LVPs for BLG and C_{12} DMPO at the same concentrations are identical, also the LVP for their mixture at the same total concentration is also identical, which can be seen in Fig. 3. This additivity indicates that no essential interactions between the molecules in the mixture exist which may lead to the formation of a new compound, at least at these small concentrations. Would a new compound arise (such as a complex), its specific contribution to the dynamics of adsorption and desorption would violate the additivity.

4.3. Manifestation of protein–surfactant interaction in LVPs

Only a qualitative interpretation of LVPs for the protein mixtures with cationic (Fig. 4A) and anionic (Fig. 4B) surfactants can be made here. Despite the DoTAB alone at a concentration of two orders of magnitude higher than that of BLG does not remarkably affect the bubble rising velocity profile, for the mixed solution the bubble surface becomes much faster retarded than in each individual solution at the corresponding concentrations (Fig. 4A). A similar effect is observed also for mixed BLG-SDS solutions (Fig. 4B). This allows us to define a specific role of ionic surfactants in their mixtures with proteins [9].

It is well established that protein molecules in solutions can form complexes with ionic surfactant molecules due to Coulomb forces and hydrophobic interactions [9]. At relatively small surfactant concentrations the interaction between the protein and surfactant molecules is mainly due to Coulomb forces, resulting

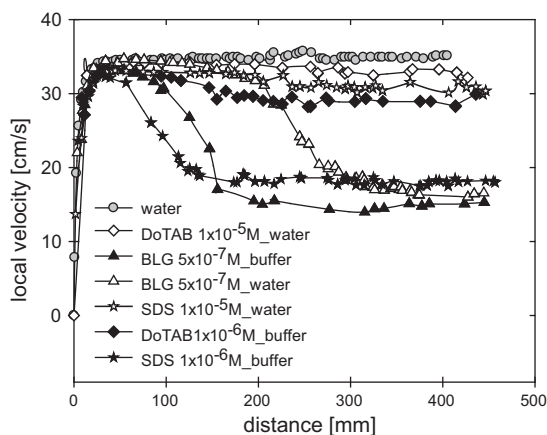


Fig. 7. Comparison of the velocity profiles of each component in buffer and pure water.

in the formation of complexes which are more hydrophobic than the original proteins. At larger concentrations the contribution of hydrophobic interaction increases and this leads to a subsequent hydrophilization of the complexes. In both cases the surface activity of the protein molecules can change significantly.

Usually protein molecules, except at very low and very high pH, show ionized groups of both signs, and, therefore the Coulomb interaction is possible with both cationic and anionic surfactants. Thus, higher surface activities for BLG-DoTAB and BLG-SDS complexes seem to be reasonable at low concentrations of the admixed ionic surfactants [5,9]. Therefore, the adsorption of the higher surface active BLG-DoTAB and BLG-SDS complexes can lead to a faster immobilization of the bubble surface.

Another consequence of the protein-surfactant complex formation can be its effect on the adsorption kinetics of the protein. The neutralization of some charges of the protein by surfactant ions may suppress to a certain degree the electrostatic repulsion arising between the double layer of the water-air interface and the approaching protein-surfactant complex. This interaction may be strong for a sufficiently large Debye radius κ^{-1} , in particular in the absence of buffer. The addition of electrolyte leads to a compression of the diffuse part of DL and to a decrease in electrostatic repulsion. Hence, in a buffer solution the electrostatic retardation of adsorption is suppressed and the adsorption rate increases. This assumption is supported by literature data concerning the effect of added salt on the kinetics of adsorption of polyelectrolytes and proteins [27]. As the adsorbate accumulation becomes faster due to the buffer, a shorter time $t_{term}^{exp}(C)$ is sufficient for the formation of a RSC, which causes rising with the terminal velocity V_{term}^{min} . Our results presented in Fig. 7 reveal that the bubble rising velocity decreases much faster when buffer is added to the protein or ionic surfactant solution. This, probably, confirms the mechanism of electrostatic retardation of adsorption of BLG or ionic surfactants and the suppression of the rising velocity in presence of a buffer.

On the other hand, a larger effect can be caused by an increase in the mean ion activities which depend on the buffer concentration [28,29]. For example, the mean ion activity for SDS $C^* = \sqrt{C_{SDS}C_{SDS+Na}}$ depends on the presence of sodium ions and, therefore, strongly increases when a buffer is added to the surfactant solution at a fixed surfactant concentration. This leads to a much higher adsorption of SDS [28,29]. The same effect should be observed for DoTAB in the presence of phosphate ions. Thus, the faster retardation of the rising velocity in SDS and DoTAB solutions in the presence of buffer (Fig. 7) can be the consequence of the increased mean ion activities or the combined effect of the decreased Debye length and increased mean ion

activities. The same effect can be expected for BLG in buffered solutions.

In absence of buffer the DoTAB-BLG complexes can be adsorbed faster than BLG alone due to the smaller net charge, which leads to a shorter time $t_{term}^{exp}(C)$ required for the onset of the angle $\psi = 120^\circ$ (Fig. 6A). Note, however, that a shorter time $t_{term}^{exp}(C)$ can be also the result of increasing hydrophobicity of the protein-surfactant complexes, as discussed above. Thus, additional studies are necessary to characterize more precisely the relative contribution of these two effects.

The notion of the adsorption rate constant β remains valid also in the case of adsorption retarded due to electrostatic repulsion. Naturally, in this case β is smaller than that in absence of repulsion

$$\beta_{ps} > \beta \quad (14)$$

The substitution of β_{ps} into Eq. (12) yields the time, required for the onset of the terminal velocity for solutions containing protein-surfactant complexes

$$t_{term}^{ps}(C) = \frac{1}{\omega\beta_{ps}C} \ln \frac{2}{1 + \cos 120^\circ} \quad (15)$$

and, according to Eq. (14), we have

$$t_{term}^{ps}(C) < \tau_{term} \quad (16)$$

in agreement with the results presented in Fig. 4A or 6A.

On a first glance, the electrostatic retardation of the adsorption rate and its suppression for protein-surfactant mixtures does not allow to quantitatively explain the results in Fig. 4A and B. Indeed, when the protein molecule has a negative net charge and some positive charges of BLG are neutralized by SDS, then the electrostatic repulsion and electrostatic retardation increase. This should lead to a conclusion opposite to Eq. (16) and that is in contradiction with the results in Fig. 4B. This controversy may be solved if we consider a change in the value of ω in Eq. (12). When RSC consists of charged protein molecules, the mean area ω per protein is the larger, the stronger the electrostatic repulsion between them is. A larger ω can compensate the decrease in β for BLG-SDS mixtures, according to Eq. (12). This assumption, however, requires additional experimental proofs.

Considering the effect of added ionic surfactants on bubble rising in protein solutions one has to take one more mechanism into account resulting from the possibility of unfolding of the protein by its interaction with surfactants. The data presented in [27] show, however, that there is a strong difference in BLG interaction with cationic and anionic surfactants—the globular structure of the protein can be destroyed in the presence of cationic surfactants (e.g. DTAB), but preserves in the presence of anionic surfactants (e.g. SDS). This depends probably on the possibility for the surfactant molecules to penetrate into the cavities of the globule which have an excess negative charge [27]. The data presented in Fig. 4 show a stronger effect on the bubble rising velocity by DoTAB as compared to SDS. This can be explained by the partial protein unfolding in the presence of DoTAB. However, it seems that the protein unfolding is possible when the surfactant concentration exceeds a critical level [27]. It is not clear whether the concentration used in the present study was sufficiently high to destroy the protein structure. Hence, again detailed investigations have to be performed to support or reject this possible impact.

5. Conclusions

The studies on rising air bubbles in aqueous solutions of BLG and its mixtures with the nonionic C_{12} DMPO, the anionic SDS and the cationic surfactant DoTAB demonstrate the sensitivity of this experimental tool for the presence of a DAL at the bubble surface. The additivity, observed in BLG- C_{12} DMPO mixtures, indicates that

there is no essential interaction between the molecules in the mixture leading to the formation of stable complexes, at least at small concentrations. This result may be also an indication that BLG preserves its globular structure at air–water interface and there are no significant intrinsic relaxation processes which can influence the rising of a bubble.

At low surfactant concentrations BLG forms complexes with SDS and DoTAB, respectively, which have a surface activity larger than that of the original BLG. The retardation effect on the rising bubble velocity is therefore stronger and leads quickly to the terminal velocity. This velocity refers to a bubble with a larger part of the bubble surface immobilized. A faster immobilization of the bubble surface can also be a consequence of an increased adsorption rate constant for BLG–DoTAB complexes or increased mean molar area per protein for BLG–SDS complexes.

These findings are in an excellent qualitative agreement with the rheological behaviour of mixed protein/surfactant adsorption layers, as discussed earlier for example in [7,9]. For future work it seems interesting to quantitatively compare the bubble rising characteristics in mixed protein/surfactant solutions with the dilational and shear visco-elasticity of the corresponding surface layers and the results of electrokinetic studies in order to understand the complex formation in the bulk and to see consequently what kind of mechanism governs the formation of the DAL.

Acknowledgements

The work was financially supported by the DFG (Mi418/20-2), by the Polish National Science Centre (grant no. 2011/01/B/ST8/03717) and by the Nestle Research Centre, Lausanne, Switzerland. The study is also related to the activity of the European network actions COST MP1106 and CM1101.

References

- [1] V. Pradines, V.B. Fainerman, E.V. Aksenenko, J. Krägel, R. Wüstneck, R. Miller, Adsorption of protein–surfactant complexes at the water/oil interface, *Langmuir* 27 (2011) 965–971.
- [2] C. Kotsmar, J. Krägel, V.I. Kovalchuk, E.V. Aksenenko, V.B. Fainerman, R. Miller, Dilational and shear rheology of mixed β -casein/surfactant adsorption layers, *J. Phys. Chem. B* 113 (2009) 103–113.
- [3] A.R. Mackie, A.P. Gunning, P.J. Wilde, V.J. Morris, Orogenic displacement of protein from the air/water interface by competitive adsorption, *J. Colloid Interface Sci.* 210 (1999) 157–166.
- [4] A.V. Makievski, G. Loglio, J. Krägel, R. Miller, V.B. Fainerman, A.W. Neumann, Adsorption of protein layers at the water/air interface as studied by axisymmetric drop and bubble shape analysis, *J. Phys. Chem. B* 103 (1999) 9557–9561.
- [5] R. Miller, V.B. Fainerman, A.V. Makievski, J. Krägel, D.O. Grigoriev, V.N. Kazakov, O.V. Sinyachenko, Dynamics of protein and mixed protein/surfactant adsorption layers at the water/fluid interface, *Adv. Colloid Interface Sci.* 86 (2000) 39–82.
- [6] V.S. Alahverdijeva, D.O. Grigoriev, V.B. Fainerman, E.V. Aksenenko, R. Miller, H. Möhwald, Competitive adsorption from mixed hen egg-white lysozyme/surfactant solutions at the air–water interface studied by tensiometry, ellipsometry, and surface dilational rheology, *J. Phys. Chem. B* 112 (2008) 2136–2143.
- [7] R. Miller, M.E. Leser, M. Michel, V.B. Fainerman, Surface dilational rheology of mixed β -lactoglobulin/surfactant layers at the air/water interface, *J. Phys. Chem. B* 109 (2005) 13327–13331.
- [8] M. Piotrowski, J. Lewandowska, K. Wojciechowski, Biosurfactant–protein mixtures quillaja bark saponin at water/air and water/oil interfaces in presence of β -lactoglobulin, *J. Phys. Chem. B* 116 (2012) 4843–4850.
- [9] Cs. Kotsmar, V. Pradines, V.S. Alahverdijeva, E.V. Aksenenko, V.B. Fainerman, V.I. Kovalchuk, J. Krägel, M.E. Leser, R. Miller, Thermodynamics, adsorption kinetics and rheology of mixed protein–surfactant interfacial layers, *Adv. Colloid Interface Sci.* 150 (2009) 41–54.
- [10] V.G. Levich, *Physicochemical Hydrodynamics*, Prentice–Hall, Englewood Cliffs, NJ, 1962.
- [11] R. Clift, J.R. Grace, N.E. Weber, *Bubbles, Drops and Particles*, Academic Press, New York, 1978 (Chapter 9).
- [12] S.S. Dukhin, G. Kretzschmar, R. Miller, *Dynamics of Adsorption at Liquid Interfaces. Theory, Experiments, Application*, Elsevier, Amsterdam, 1995.
- [13] S.S. Dukhin, R. Miller, G. Loglio, Physico-chemical hydrodynamics of rising bubble, in: D. Möbius, R. Müller (Eds.), *Drops and Bubbles in Interfacial Research*, Elsevier, New York, 1998, pp. 367–432.
- [14] K. Malysa, J. Zawala, M. Krzan, M. Krasowska, Bubbles rising in solutions; local and terminal velocities, shape variations and collisions with free surface, in: R. Miller, L. Liggieri (Eds.), *Bubble and Drops Interfaces*, Brill, Leiden–Boston, 2011, pp. 243–292.
- [15] M. Krzan, K. Malysa, Profiles of local velocities of bubbles in n-butanol, n-hexanol and n-nonanol solutions, *Colloids Surf. A* 207 (2002) 279–291.
- [16] M. Krzan, J. Zawala, K. Malysa, Development of steady state adsorption distribution over interface of a bubble rising in solutions of n-alkanols (C5, C8) and n-alkyl trimethyl ammonium bromides (C8, C12, C16), *Colloids Surf. A* 298 (2007) 42–51.
- [17] K. Malysa, M. Krasowska, M. Krzan, Influence of surface active substances on bubble motion and collision with various interfaces, *Adv. Colloid Interface Sci.* 114–115 (2005) 205–225.
- [18] C. Ybert, J.-M. di Meglio, Ascending air bubbles in solutions of surface active molecules: influence of desorption kinetics, *Eur. Phys. J. E* 3 (2000) 143–148.
- [19] Y. Zhang, J.A. Finch, A note on single bubble motion in surfactant solution, *J. Fluid Mech.* 429 (2001) 63–66.
- [20] Y. Zhang, J.B. McLaughlin, J.A. Finch, Bubble velocity profile and model of surfactant mass transfer to bubble surface, *Chem. Eng. Sci.* 56 (2001) 6605–6616.
- [21] C. Ybert, J.-M. di Meglio, Ascending air bubbles in protein solutions, *Eur. Phys. J. B* 4 (1998) 313–319.
- [22] J. Zawala, R. Todorov, A. Olszewska, D. Exerowa, K. Malysa, Influence of pH of the BSA solutions on velocity of the rising bubbles and stability of the thin liquid films and foams, *Adsorption* 16 (2010) 423–435.
- [23] K. Lunkenheimer, K. Haage, R. Miller, On the adsorption properties of surface-chemically pure aqueous solutions of n-alkyl-dimethyl and n-alkyl-diethyl phosphine oxides, *Colloids Surf.* 22 (1987) 215–224.
- [24] R. Bel Fdhila, P.C. Duineveld, The effect of surfactant on the rise of a spherical bubble at high Reynolds and Peclet numbers, *Phys. Fluids* 8 (1996) 310.
- [25] G. Gochev, I. Retzlaff, E.V. Aksenenko, V.B. Fainerman, R. Miller, Adsorption isotherm and equation of state for β -lactoglobulin layers at the air/water surface, *Colloids Surf. A* 422 (2013) 33–38.
- [26] H. Schlichting, *Boundary Layer Theory*, 6th ed., McGraw Hill, New York, 1968.
- [27] B.A. Noskov, Protein conformational transitions at the liquid–gas interface as studied by dilational surface rheology, *Adv. Colloid Interface Sci.* (2014), <http://dx.doi.org/10.1016/j.cis.2013.10.024>.
- [28] V.B. Fainerman, S.V. Lylyk, E.V. Aksenenko, J.T. Petkov, J. Yorke, R. Miller, Surface tension isotherms, adsorption dynamics and dilational visco-elasticity of sodium dodecyl sulphate, *Colloid Surf. A* 354 (2010) 8–15.
- [29] V.B. Fainerman, S.V. Lylyk, N.M. Kovalchuk, V.I. Kovalchuk, E.V. Aksenenko, J.T. Petkov, R. Miller, Effect of water hardness on surface tension and dilational visco-elasticity of sodium dodecyl sulphate solutions, *J. Colloid Interface Sci.* 377 (2012) 1–6.